噴霧熱分解法による
機能性微粒子の性状および形態の評価と制御
（研究課題番号08650893）

平成 8 年度 ～ 平成 9 年度科学研究費補助金 (基盤研究 (C)(2))

研究成果報告書

平成10年3月

研究代表者　奥山　喜久夫
（広島大学・工学部・教授）

目次

平成8年度～平成9年度科学研究費補助金 (基盤研究 (C) (2))

1．研究課題番号　08650893

2．研究課題　噴霧熱分解法による機能性微粒子の性状および形態の評価と制御

3．研究代表者　奥山喜久夫（広島大学・工学部・教授）

4．研究分担者　なし

5．研究経費

平成8年度	1400千
平成9年度	800千
計	2200千

6．研究発表

（1）学会誌等

(i) 奥山、Lenggoro、田上、玉城、 峠
静電噴霧熱分解法による金属硫化物超微粒子の製造
粉体工学会誌, 33 (3), 26-32, 1996.

(ii) Okuyama, K., Lenggoro, I. W., Tagami, N., Tamaki, S. and Tohge, N.
Preparation of ZnS and CdS fine particles with different particle sizes by a spray-pyrolysis method.
Journal of Materials Science, 32 (5), 1229-1237, 1997

(iii) Lenggoro, I. W. and Okuyama, K.
Preparation of nanometer-sized zinc sulfide particle by electrospray pyrolysis
Journal of Aerosol Science, 28, S351-S352, 1997

(iv) Lenggoro, I. W., Kang, Y. C., Komiya, T., Okuyama, K. and Tohge, N.
Preparation of submicron copper sulfide particles by spray pyrolysis.
Japanese Journal of Applied Physics, 37 (3A), L228-L290, 1998

(v) I. W. Lenggoro、奥山喜久夫
噴霧熱分解法による微粒子の製造
微粒化, 6 (13), 9-13, 1997

(vi) I. W. Lenggoro、奥山喜久夫
静電噴霧法を用いた微粒子の製造
微粒化, 6 (14), 15-20, 1997

(vii) I. W. Lenggoro、奥山喜久夫
噴霧熱分解法による金属硫化物微粒子の製造
ケミカルエンジニヤリング, 42 (11), 24-28, 1997

(viii) I. W. Lenggoro、奥山喜久夫
静電噴霧法による微粒子の製造
静電気学会誌, 21 (6), 258-262, 1997

(2) 口頭発表

(i) I.W.Lenggoro, K.Okuyama
Preparation of nanometer-sized zinc sulfide particles
by electrospray pyrolysis
1997 European Aerosol Conference, Hamburg, Germany,
15-19 September 1997

(ii) I.W.Lenggoro, K.Okuyama, S. Tamaki, and N.Tohge.
Preparation and characteristics of fine metal sulfide particles
by spray pyrolysis
1996 Japan-U.S. Joint Workshop on Nanoparticle
Synthesis and Applications
Mechanical Engineering Lab, AIST-MITI Research Center,
Tsukuba, Oct 28 - Nov 1, 1996

(iii) I.W.Lenggoro, N.Tagami, K.Okuyama, S.Tamaki, and N.Tohge
The morphology and composition of fine metal sulfide particles prepared
by spray pyrolysis
The American Association for Aerosol Research 1996 Annual Conference,
Orlando, Florida, USA, 14-18 October 1996

(iv) Lenggoro、奥山、玉城、 峠
静電噴霧熱分解法による金属硫化物微粒子の製造"
第29回化学工学秋季大会, 同志社大学, 1996年9月

(v) Lenggoro、奥山、玉城、 峠
噴霧熱分解法による金属硫化物微粒子の製造と性状の評価
第13回エアロゾル科学・技術討論会, 金沢, 1996年8月

(vi) Lenggoro、奥山、田上、玉城、 峠
噴霧熱分解法による金属硫化物微粒子の形態変化の評価
化学工学会第61年会, 名古屋大学, 1996年4月

(vii) 奥山、Lenggoro、田上、玉城、 峠
静電噴霧熱分解法による金属硫化物微粒子の生成
静電気学会, 岡山大学, 1995年11月

(viii) 奥山、Lenggoro、田上、玉城、 峠
静電噴霧熱分解法による金属硫化物超微粒子の生成
第28回化学工学秋季大会, 北海道大学, 1995年9月

(ix) 奥山、Lenggoro、田上、玉城、 峠
静電噴霧熱分解法による金属硫化物超微粒子の生成
第31回粉体工学会夏期シンポジウム, 静岡, 1995年8月

7. 研究成果

7.1　噴霧熱分解法による微粒子製造

1. はじめに

機能性材料を応用したエレクトロニクスデバイスの開発を目指す上で、粒径、形態および結晶構造が制御された微粒子を連続的に、迅速に製造できるプロセスの開発が重要となっている。一般に微粒子の製造は、固相反応法、液相法、気相法などによって行われている。この解説では、液相法として分類されている噴霧熱分解法による微粒子の製造を2回に分けて、著者らの研究を中心に最近の研究を述べる。

噴霧熱分解法以外の液相法、固相法などで微粒子を製造する場合、均質で配向性の良いものを製造するためには、仮焼や粉粋を繰返すことが必要となり、その結果、不純物が混入したり微粒子化が困難となり、多くの操作を必要とするという欠点をもつ。これに対して、噴霧熱分解法では、分子レベルで十分に混合された原料溶液の噴霧による微小（ミクロンオーダー）液滴の熱分解により、化学量論的に制御された目的の微粒子を連続的に得ることができるという利点がある。各液滴が同じ量のプリカーサーからなっていると、この利点を利用して複合材料（アロイ）も比較的容易に設計して製造できる。さらに、装置がシンプルで反応時間が数秒と非常に短く、連続的に微粒子が製造でき、工業化への応用が期待される。噴霧熱分解法を用いて、酸化物、硫化物、金属、超伝導材料などの微粒子製造が行われてきた。その一例を表１に示す。

Table 1. 噴霧熱分解法で製造される微粒子の一例

微粒子	原料溶液粒径 組成のプリカーサー	(平均) [μm]	Ref. no.
ZnO	硝酸塩	0.3 - 1.0	1
ZrO_2	塩化物	1 - 3	2
Al_2O_3, BaO	硫／酢酸塩	0.5 - 1.5	3
TiO_2	イソプロポキシド	0.2-0.3	4
Y-Ba-Cu-O系	硝酸塩	-1	5
Bi-Ca-Sr-Cu-O系	硝酸塩	0.1 - 2	6
ZnO-TiO_2	硝酸塩	0.4 - 0.5	7
$CoAl_2O_4$	硫酸塩	-9	8
$CuCr_2O_4$	硝酸塩	0.015-0.12	8
$PbCr_2O_4$	硝酸塩	0.015-0.4	8
$CoFe_2O_4$	塩化物	0.02-0.17	8
$(Mn,Zn)Fe_2O_4$	塩化物	0.02-0.2	8
$BaO \cdot 6Fe_2O_3$	塩化物	0.02-0.18	8
ZnS, CdS	硝酸塩、チオ尿素	0.2 - 1.5	9
ZnS-CdS	硝酸塩、チオ尿素	0.3 - 1.5	10
Si_3N_4	ポリシラザン	0.38	11
C60/70-Rh	塩化物	0.02 - 0.1	12
Ag	硝酸塩	0.4 - 0.5	13
Pd	硝酸塩、塩化物	0.2	14

2. プロセスおよび装置

噴霧熱分解法による微粒子の製造プロセスでは、まず目的の固体粒子の金属塩などが溶けている原料溶液またはプリカーサーを噴霧（液滴化）し、キャリアガスによってその液滴を直接反応炉などの高温場に導入する。反応炉内では、液滴中の溶媒は蒸発し、液滴内のプリカーサーが周囲のガスとの反応または熱分解などにより、固体の微粒子となる。

噴霧熱分解法による微粒子の製造の代表的装置は、Fig.1 に示すような構成となる。主に、原料溶液を噴霧する噴霧器、キャリアガス、反応炉（管状加熱炉）、捕集器(例えば：静電型／熱泳動型捕集器、フィルター）からなっている。使用した反応炉は、長さ1mで、5つの加熱ゾーンからなっているので、必要に応じて、温度分布を設定することが可能となる。また、測定においては、浮遊したままで粒子の粒径分布を測定する on-line 測定機器（例えば：微分型静電分級器DMA、凝縮核計数器CNC[15]）や、粒子を捕集 (off-line) してからX-線回折または電子顕微鏡（SEM, TEM）の解析などが主に行われる。

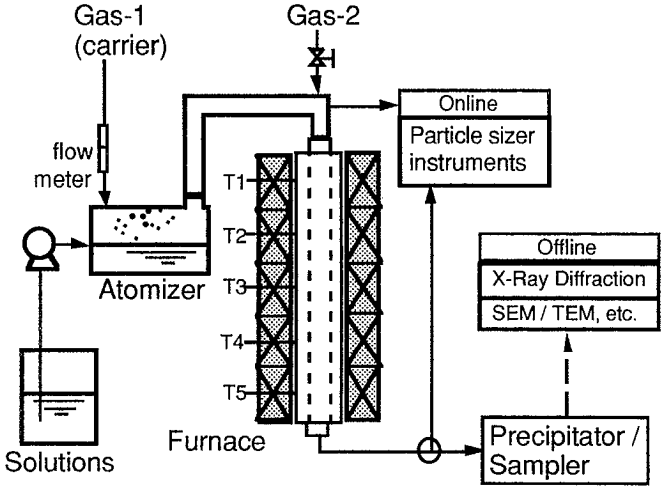

Fig.1 噴霧熱分解による粒子生成の装置

2.1 溶液の噴霧

本プロセスで、目的の微粒子材料の種類は、原料溶液によって決定される。最近、新しい原料溶液の開発も進んでいるが、幅広い材料の製造には、一般に各種の金属の塩化物、硝酸塩、酢酸塩などが広く用いられ、これらの溶液は比較的簡単に入手でき、しかも安価である。またこれらの溶質を、溶媒である純水またはアルコール類中に溶かして、噴霧液体とする。

2.2 懸濁液の噴霧

溶液とは別に、ポリスチレンラテックス粒子、シリカなどの固体粒子の懸濁液を噴霧させて粒子を含む液滴とし、液体を蒸発させて固体の粒子を発生させる方法もある[7]。この方法では、懸濁液の濃度が高くなると凝集粒子が生成したり、個数濃度が低下すると固体粒子の含まれていない液滴が生成し、液体が蒸発した後に残った不純物が粒子になることがある。したがって、懸濁液の粒子濃度を最適にし、安定剤などの溶解性物質の量をで

きるだけ低くしなければならない。

2.3 溶液の濃度

製造される微粒子の粒径 dp は、1個の液滴（密度 rs ）より 1 個の微粒子（密度 rp ）が生成されるとき、液滴の粒径 Dd と溶液の濃度 Cs により、

$$d_p = D_d\left(\frac{\rho_s C_s}{\rho_p}\right)^{\frac{1}{3}} \qquad (1)$$

で求められる。液滴が均一径でなく分布している場合には、この関係を液滴の各粒径に運用すると、微粒子の粒径分布が求まることになる。液滴の粒径 Dd を小さくしたり、溶液の濃度 Cs を低くすると粒径の小さい微粒子が得られる。ただし、この式には、蒸発などによる液滴表面での核発生、成長および破裂などが生じていない緩やかな蒸発による粒子の生成の場合に適用できる。

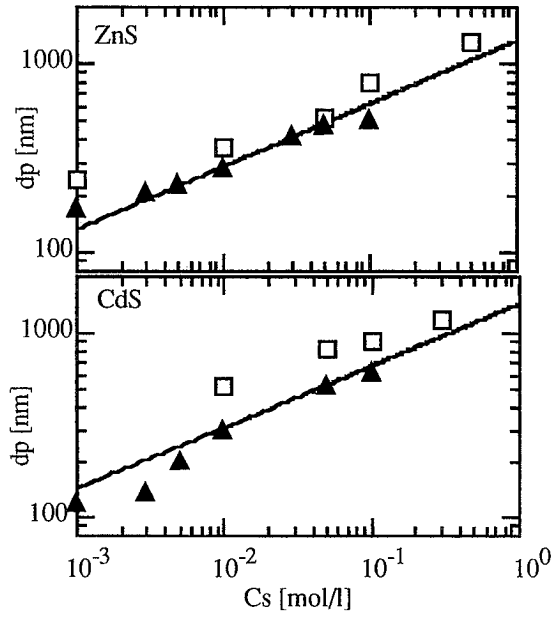

Fig.2 粒子径 dp の噴霧溶液濃度 Cs への依存性
（□はSEM/TEM、▲はDMA/CNCより測定した粒径、実線は式 (1)）（文献(9)より転載）

Fig. 2 に ZnS および CdS 粒子生成における粒子径の噴霧溶液濃度 Cs への依存性を示す。硝酸亜鉛$Zn(NO_3)_2$ または硝酸カドミウム$Cd(NO_3)_2$とチオ尿素 $(NH_2)_2CS$ を常温下で純水に溶かしたものを原料溶液とした（混合モル比：1:2）。固体粒子の粒径が溶液濃度 Cs の1/3 乗の関係になることがわかる [(9)]。

2.4 噴霧法

粒子径を制御できるひとつのパラメータとして、発生する液滴径の大きさおよび分布が重要となる。噴霧熱分解法において、液体（原料溶液）の微粒化にはいろいろな噴霧法が

用いられる（Table 2, Fig.3）。これらの、液滴の発生機構、液滴径、噴霧量（濃度）などの違いによって、噴霧熱分解法による生成粒子のサイズおよび形態も違ってくる。

Table 2.　噴霧法の比較

噴霧法	液滴径（平均） [μm]
加圧式	1 - 50
超音波	4 - 10
振動法	5 - 50
回転ディスク	20 - 100
静電気	0.5 - 10

加圧空気による噴霧法では、Fig.3.a のような簡単なタイプの他に、種々なタイプの装置が開発されている。一般に生成される液滴径は1～50μm程度である。超音波式は、ピエゾ電気結晶を利用したFig.3.b のような装置が代表的で、家庭用の加湿器としてもよく用いられる。超音波の振動数は2MHz付近が標準で、粒径4～10μmの液滴が発生する。ただし、時間とともに噴霧液の温度が上昇したり量が減るので、定常的な発生が望まれるときには工夫が必要である。振動法はFig.3.c に示すように穴径が10～20μmのオリフィスが振動子により振動し、そこへ一定の速度で供給されている液体が振動数に応じて一定量ずつ穴から放出され液滴となる。この方法は、5～50μmの範囲で、比較的そろった単文献(15)より転載）分散の液滴が発生される。遠心力による（回転ディスク）方法では、Fig.3.d のように回転している円板上に液を一定速度で落下させると、遠心力によってその液が微小液滴となって、20～100μmの範囲で液滴が生成される。

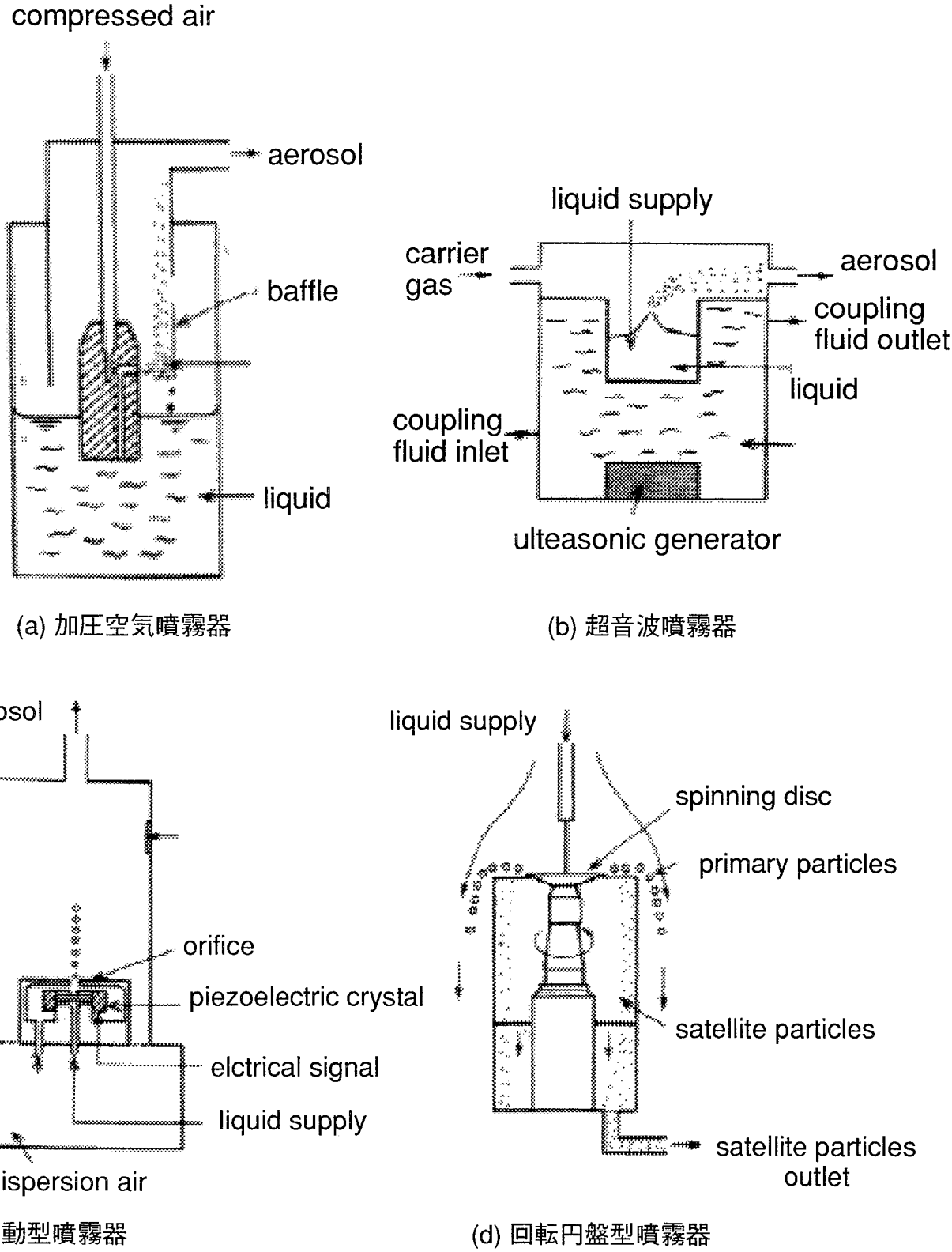

(a) 加圧空気噴霧器　(b) 超音波噴霧器

(c) 振動型噴霧器　(d) 回転円盤型噴霧器

Fig. 3 種々の噴霧法の例

3. 粒子形態の制御

噴霧熱分解法では、生成する粒子の形態および表面状態に影響を与えるパラメーターとして、溶液およびキャリアガスの種類、キャリアガス流量（溶媒の蒸発速度または高温場での滞留時間）、熱分解／反応炉温度（分布）などがあげられる。生成される粒子の形態は、中空の球、ポーラス、中の詰まった粒子、破砕された粒子などとなる。また、結晶構造により生成する粒子を分類すると、単結晶の凝集体および多結晶粒子となる。

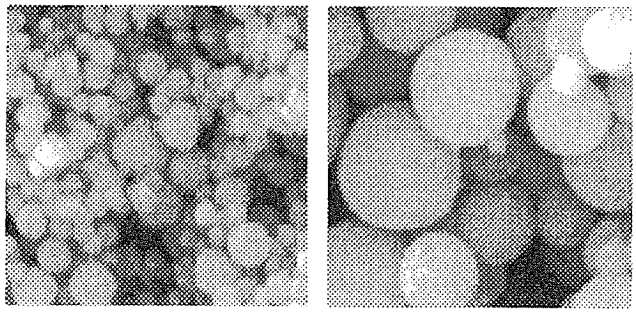

(a) (b)

Fig. 4 ZnS微粒子、原料溶液濃度：a) 0.001, b) 0.05 mol/l。（文献 (9) より転載）

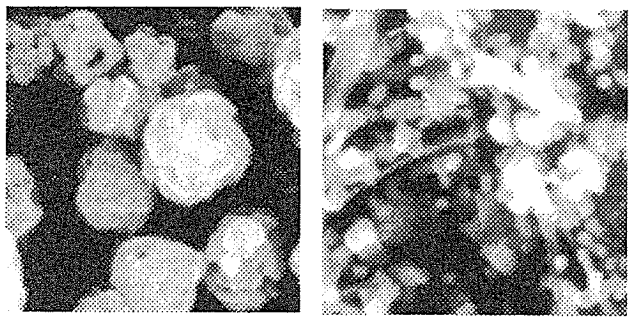

(a) (b)

Fig. 5 CdS 微粒子、反応炉温度：a) 700, b) 800℃、（文献 (16) より転載）

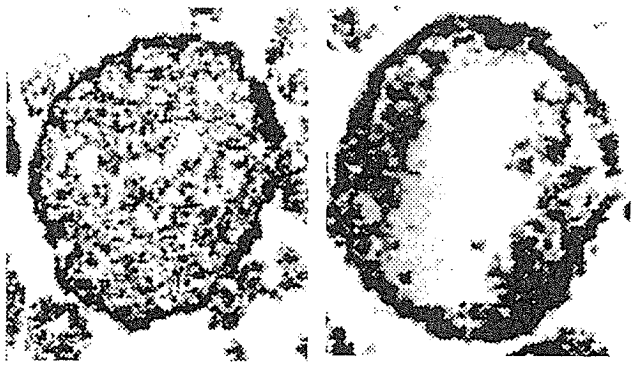

(a) (b)

Fig. 6 ZnO-TiO2複合微粒子（文献 (7) より転載）

Fig. 4（前節にも述べた粒子径における原料溶液濃度の依存性を参照）には、ZnS微粒子のような比較的表面が滑らかな粒子（nmオーダーの超微粒子の凝集体）も生成されているが、噴霧熱分解法では、プロセス中の加熱速度が非常に重要な因子となる。

加熱速度が速い場合、液滴の表面付近の蒸発が早く生じ、溶液の濃度が急激に高くなり過飽和となり、均一核生成により多くの核が発生し、多結晶の粒子となる。しかも、粒子の内部は、液の状態であるために、後の反応で生じたガスにより粒子が割れたり、ポーラスまたは中空粒子となる(Figs. 5.b, 6.b, 7.a)。

加熱速度が低い場合には、結晶サイズの大きい多結晶（Figs. 5.a, 6.a）もしくは単結晶に近い粒子が得られる。温度が粒子の融点以上と高い場合には、粒子は密度の高い中の詰まった球形粒子となりやすいが、冷却過程での結晶成長に方向性があると平らな粒子などが生成される(Fig. 7b)。Fig.8には、生成粒子の形態に関するプロセス中のメカニズムを簡単にまとめた。

以上の写真や結果などからも分かるように、粒子形態または粒子径を決定するのは、多くの複雑な現象に関係することがわかる。例えば、液滴の周囲へ溶媒が蒸発し、液滴表面の溶質濃度が高くなり、その濃度勾配によって液滴中心へ溶質の拡散がおこる。それから、反応または熱分解がおこり、固体粒子が生成されるという現象が考えられる。

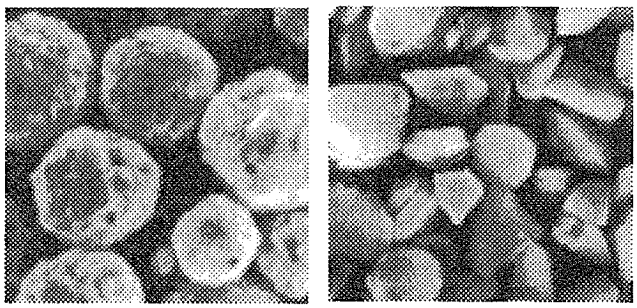

(a)　　(b)

Fig. 7 Bi-Ca-Sr-Cu-O系超伝導性微粒子、反応炉温度：
a) 800, b) 950℃、（文献 (6) より転載）

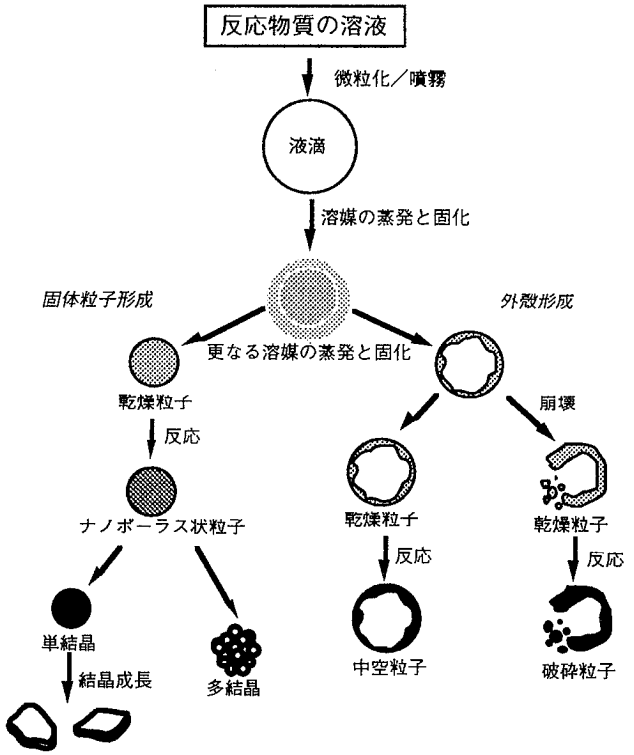

Fig.8 種々の粒子形態のメカニズム

4. モデル化

これらの現象のメカニズムは、ほとんど経験的な手法で研究されているが、液滴一粒子転換の理論／モデル化に関する研究も報告されている。

噴霧熱分解法のモデル化の研究は、噴霧乾燥法と重なることもあるが、高温場中の液滴の蒸発･固化に関するモデル化の研究がいくつかがある（例えば(17)-(19)）。
これらの研究では、溶媒の蒸発速度と中心への溶質の拡散速度の違いで、密に詰まった固体粒子もしくは中空粒子が生成されると報告されている。また、Jayanthiら[20]は液滴内の溶質分布における実験パラメーターの影響について報告している。一方、高温場中での多数の液滴の蒸発･固化を考慮したモデル化はほとんど行われていない[21]。

一般に、正確なモデル化または数値計算を行おうとしても、原料溶液中の溶解度と化学反応、固体化過程での核生成や結晶化などの情報を得るのが極めて困難である。したがって噴霧熱分解法の理論／モデル化の研究は、物性のわかった食塩などの非機能性微粒子を対象にした場合に限られている。

5. おわりに

噴霧熱分解法による微粒子材料の製造プロセスについて、粒子の生成過程、代表的な製造装置などについて述べた。生成される粒子のサイズおよび形態は、操作条件を変えることによりある程度制御が可能である。

しかし、微粒子製造における噴霧熱分解法のプロセスを評価または改善するには、生成粒子の形態や性状をプロセスと関連させ、理論的に解析する研究が重要となる。

引用文献

1. 大島賢太郎、傳慶一、奥山喜久夫、峠登、化学工論文集、18 (1992) 288
2. Zhang, S.C., Messing, G.L. and Borden, M., J. Am. Ceram. Soc., 73 (1990) 61-67
3. Zhang, S. and Messing, G.L., Ceramic Transactions, Vol. 12, Ceramic Powder Science III. Ed. Messing, Hirano and Hausner, Am. Ceram. Soc., Ohio, USA. (1990) 49-57
4. Ishizawa, H., Sakurai, N., Mizutani and Kato, M. Yogyo Kyokaishi, 93 (1985) 382
5. Tohge, N., Tatsumisago, M., Minami, T., Okuyama, K., Adachi, M. and Kousaka, Y. Jpn. J. Appl. Phys., 27 (1988) L1086
6. Tohge, N., Tatsumisago, M., Minami, T., Okuyama, K., Adachi, M. and Kousaka, Y., J. Am. Ceram. Soc., 74 (1991) 2112
7. Ohshima, K., Tsuto, K., Okuyama,K. and Tohge, N., Aerosol Sci. Tech., 19 (1993) 468
8. 粉体工学の基礎編集委員会、粉体工学の基礎、日刊工業新聞社、(1992)、26
9. Okuyama, K., Lenggoro, I.W., Tagami, N., Tamaki, S. and Tohge, N. J. Mat. Sci. (1997) 印刷中
10. Tamaki, S., Tohge, N., Tagami and N., Okuyama, K., J. Ceram. Soc., Jpn., 104 (1996) 137
11. Mizutani, N. and Liu, T.Q. ; ref 3を参照. pp59-73
12 Gurav, A.S., Duan, Z., Wang, L., Hampden-Smith, M.J., and Kodas, T.T. Chem. Mater.5 (1993) 214-216
13. 加藤昭夫、高山明彦、森満由紀子、日本化学会誌、12（1985）2342−2344
14. 車声雷、桜井修、篠崎和夫、水谷惟恭、日本セラミック協会学術論誌、104（1996）38−43
15. 奥山喜久夫、増田弘昭、諸岡成治、微粒子工学、オーム (1992)、78, 125, 129, 130
16. Tamaki, S., Tohge, N. and Okuyama, K. J. Mat. Sci. Lett., 14 (1995) 1388
17. Ranz, W.E., and Marshall, W.R., Jr. Chem. Eng. Prog. Part I 48 (1952) 141, Part II 48 (1952) 173.
18. Sano, Y., and Keey, R.B. Chem.Sci.37 (1982) 881
19. Leong, K.H. J. Aerosol Sci. 18 (1987a) 511
20. Jayanthi, G.V., Zhang, S.C., and Messing, G.L. Aerosol Sci. Technol., 19 (1993) 476-488.
21. Xiong, Y. and Kodas, T.T. J. Aerosol Sci.24 (1993) 893-908

7.2 Preparation of zinc sulfide and cadmium sulfide fine particles with different particle sizes by an ultrasonic spray pyrolysis

Preparation of zinc sulfide and cadmium sulfide fine particles with different particle sizes by an ultrasonic spray pyrolysis

1 Introduction

The particle preparation process in which submicrometer-sized particles are dispersed in the gas phase is called aerosol synthesis. Aerosol synthesis can be divided into the gas-to-particle conversion process and droplet-to-particle conversion process (Okuyama, 1988; Okuyama et al., 1991). The preparation of fine particles using aerosol processes has become an important techique in making carbon black, oxide ceramic and magnetic materials. The spray-pyrolysis method is a representative droplet-to-particle conversion process, which has following advantages: (i) the particles produced are spherical, (ii) the distribution of their diameters is uniform and controllable from micrometer to submicron meter, (iii) the purity of the products is high, and (iv) the process is continuous. This technique has been applied to the preparation of a variety of particles. Our laboratory has recently prepared several metal oxide particles such as high-Tc oxide superconductors in the Y-Ba-Cu-O and Bi-(Pb)-Ca-Sr-Cu-O systems, ZnO and ZnO-TiO_2 composites (Tohge et al., 1988; Tohge et al., 1989; Ohshima et al., 1992; Ohshima et al., 1993). In general, aqueous solutions of metal salts are used as solutions to be sprayed, and the pyrolyzed products are the particles of oxides.

On the other hand, thiourea forms complexes with a variety of metal salts in

aqueous and alcoholic solutions. These thiourea complexes can be thermally decomposed to form metal sulfides and thus solutions containing thiourea complexes are used to prepare metal sulfide films by the spray deposition process (chemical aerosol deposition technology: CADT) and dip-coating process (Feigelson et al., 1977; Rajaram et al., 1983; Richard et al., 1984; Krunks et al., 1986; Karanjai and Dasgupta, 1987). Thiourea complexes also have recently been applied to disperse sulfide particles of nanometer-size in silica glasses through the sol-gel process (Tohge et al., 1992; Tohge and Minami, 1992). In the previous study (Tohge et al., 1995; Tamaki et al., 1995) , we have confirmed the availability of spray-pyrolysis technique as a direct preparation process of fine powders of ZnS and CdS. In these studies, preparation conditions where ZnS and CdS particles were produced directly, were discussed without changing the concentration of starting solution. In the spray-pyrolysis process, the particle size and morphology can be changed depending on the heating temperature, the rate of solvent evaporation, and the concentration of starting solutions.

In this study, the formation of fine particles of ZnS and CdS with different particle sizes was investigated by changing the concentration of the aqueus solutions of the corresponding thiourea complexes and temperature profile in the reactor. The morphology and crystalline phase of metal sulfide particles were studied in terms of the preparation conditions and concentration of spraying solution. Namely, the particle size distributions were controlled by changing the concentration of spray solutions. The crystalline phases and fluorescence property of fine particles were examined as a function of particle size. The main goal was to demonstrate that the spray-pyrolysis method is an available and promising technique for the preparation of standard metal sulfide fine particles with different particle sizes.

2 Experimental procedure

The system used for the preparation of ZnS and CdS fine particles is schematically shown in fig.1. This spray-pyrolysis system, which was similar to the system used in a previous study (Tamaki et al., 1995) , consisted of an ultrasonic nebulizer, a reaction furnace and a electrostatic precipitator. The starting solution was atomized at the frequency of 1.75 MHz by an ultrasonic nebulizer (Omron Co., Model NE-U11B), which was cooled with running water and the level of the spray solution was kept constant, to ensure the constant rate of generation of droplets. The spray solution was prepared by dissolving proper amounts of $Zn(NO_3)_2$ or $Cd(NO_3)_2$ and thiourea $SC(NH_2)_2$ into ultrapure water. The concentrations of $Zn(NO_3)_2$ and $Cd(NO_3)_2$ were changed from 0.001 to 0.1mol/l, and from 0.01 to 0.3mol/l, respectively, while the molar ratio of $Zn(NO_3)_2$ and $Cd(NO_3)_2$ to thiourea was kept at 1:2, respectively (Tohge and Minami, 1992). The tubular furnace, or laminar flow aerosol reactor, used in the present study was a high-quality ceramic tube of 15 mm-inside diameter and about 1000 mm-long. The reaction furnace consisted of five independently-controlled heating zones, each 200 mm in length, separated by about 5 mm low-density insulation zones. The temperature of each heating zone was controlled to within 2°C with a temperature controller: T1, T2, T3, T4, and T5 indicate the wall temperatures at the middle of the each heating zone. The setting of five zones enables to provide desired temperature distribution.

In the present work, temperature profiles changed around 600°C in ZnS-preparation, and around 700°C in the case of CdS-preparation. The good crystallinity of ZnS and CdS particles can be formed at temperature profiles changed around 600°C and 700°C, respectivelly, as described in the previous studies (Tohge et al., 1995; Tamaki et al., 1995). The present work also investigated the effects of the temperature distribution on the crystalline phases and morphology of the particles. Fig. 2 shows

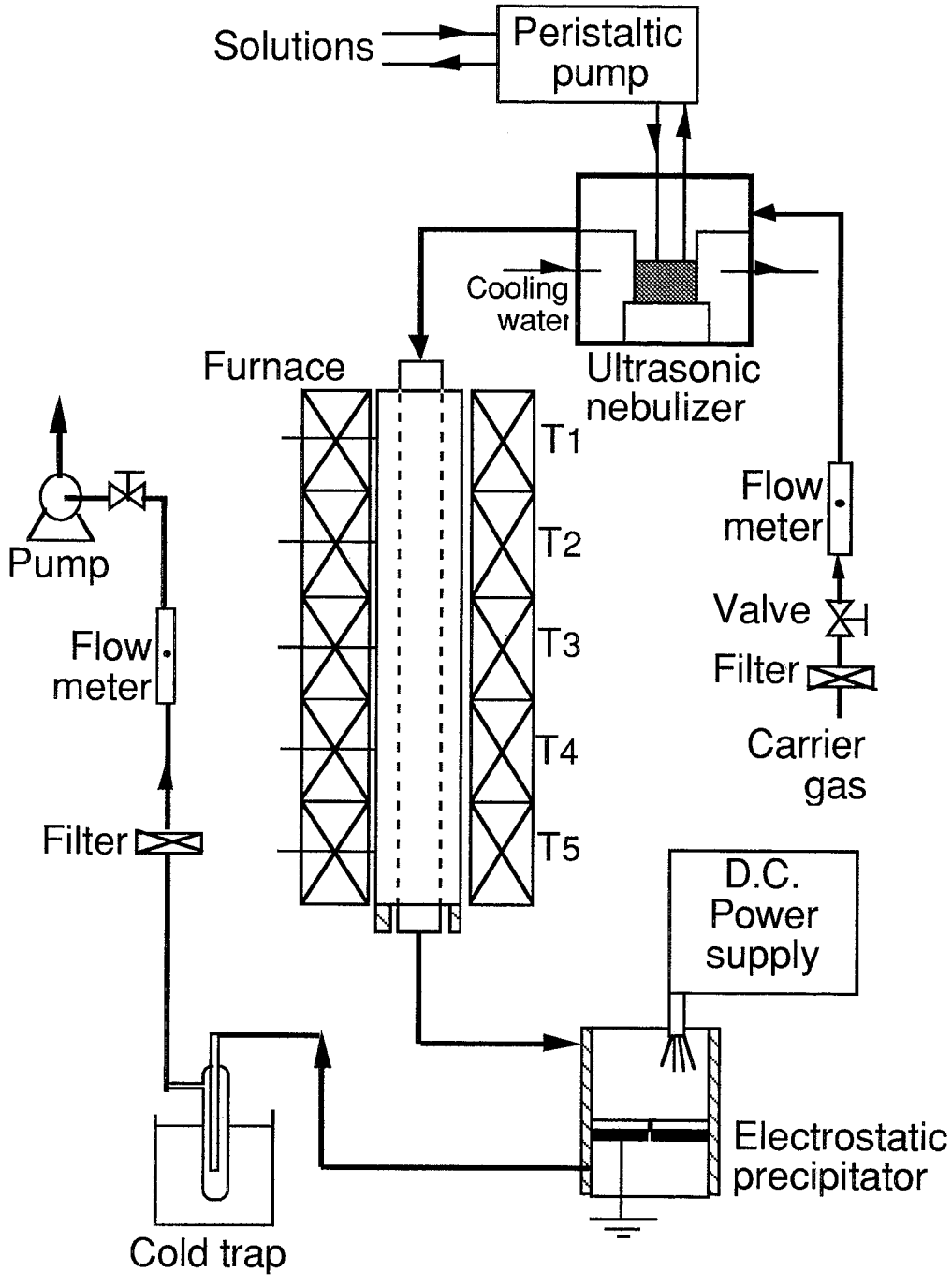

Fig. 1 Schematic presentation of the ultrasonic spray-pyrolysis system used in the present study.

the temperature profiles in the reactor for two typical cases, (a) constant and (b) increasing distributions.

The generated droplets were carried to the reaction furnace by N_2 gas, with the flow rate of 2.0 l/min, the corresponding residence time of a carrier gas in the furnace being estimated to be 5.3 s. The particles generated from the furnace exit were collected using an electrostatic precipitator, which was maintained at around 200°C, to avoid the condensation of water on the particles (Tohge et al., 1995) .

The particles obtained were examined by X-ray diffraction (CuKα, XRD, Rigaku-Denki Corp., model RINT 1000), scanning electron microscopy (SEM, JEOL Corp., model JSM-T100), respectively.

The fluorescence measurement system was composed from a N_2 laser (377nm in wavelength) as the excitation light source, a sample cell, a monochrometer, a photo multipier, a box-car integrator and a function generator as the supplier of code to laser and box-car integrator (Fig.3). An optical filter (UV36) was installed in a monochrometer to cut the excitation light reflecting from the sample cell. Each samples were spread on a nonfluorescent quartz plate with acetone, and after that, the samples were dried. These all equipments were setted inside a vessel in vacuum condition, and cooled down to 80±3K by a liquid Nitrogen.

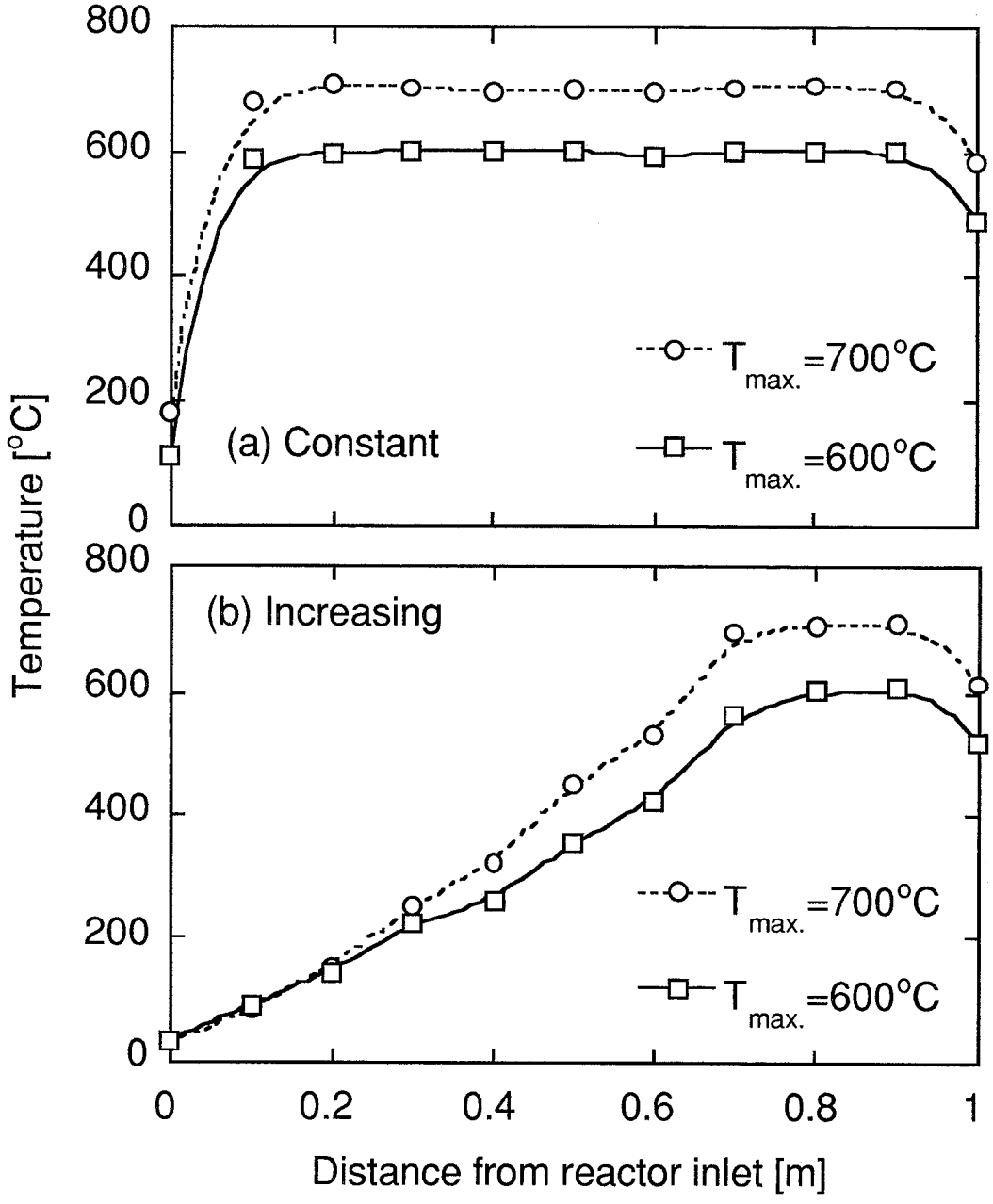

Fig. 2 Measured temperature profiles in the reaction furnace for two typical cases: (a) constant and (b) increasing temperature distributions.

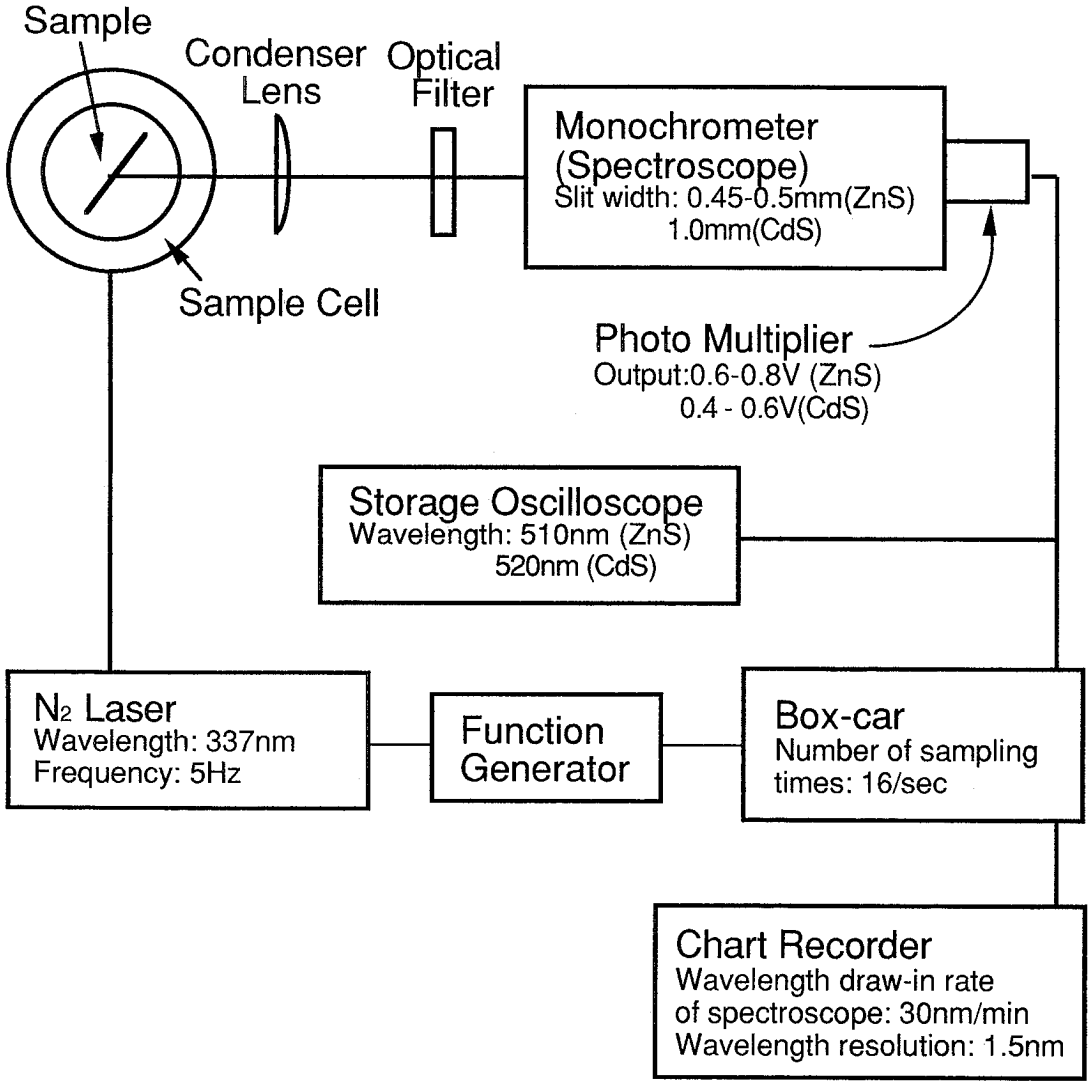

Fig. 3 System for the measurement of fluorescence of the particles

3 Results and discussion

3.1 Zinc sulfide particles preparation

Fig.4 shows X-ray diffraction patterns of the ZnS particles obtained from different solution concentrations at the constant temperature distribution of 600°C. The peaks assigned to the hexagonal phase of ZnS can be seen for all solution concentrations, but the peak height tends to decrease with the decrease in solution concentration, showing a decrease in crystallite size. In the pattern of particles generated at the concentration of metal nitrate of 0.05 and 0.1mol/l, their peaks show that ZnS particles of good crystallinity particles are formed.

Fig.5 shows SEM photographs of ZnS particles prepared under the same conditions as those in fig.4. As observed in the previous paper (Tohge et al., 1995), the surface of the particle is rather found to be smooth. As the concentration increases, it can be found that the particles sizes also increase. At the lowest concentration of 0.001mol/l, the prepared particles were necking each other, but at higher concentrations, particles seem to be separately formed. This shows that the particle size can be controlled by changing the concentration of starting solution.

Fig.6 shows the fluoresence spectral of the ZnS particles obtained by changing the solution concentration, 0.01, 0.05, and 0.5 mol/l. For all the particles, a rather broad emission peak is observable at around 475 nm. This emission can be ascribed to the electronic transition involving defect or impurity centers but not to the band transition, because the excitation energy (N_2 laser) used here was insufficient for the excitation of fundamental adsorption of ZnS. There are no changes of fluoresence spectra in these concentrations range. Thus, particles size did not affect the fluoresence spectra in this range.

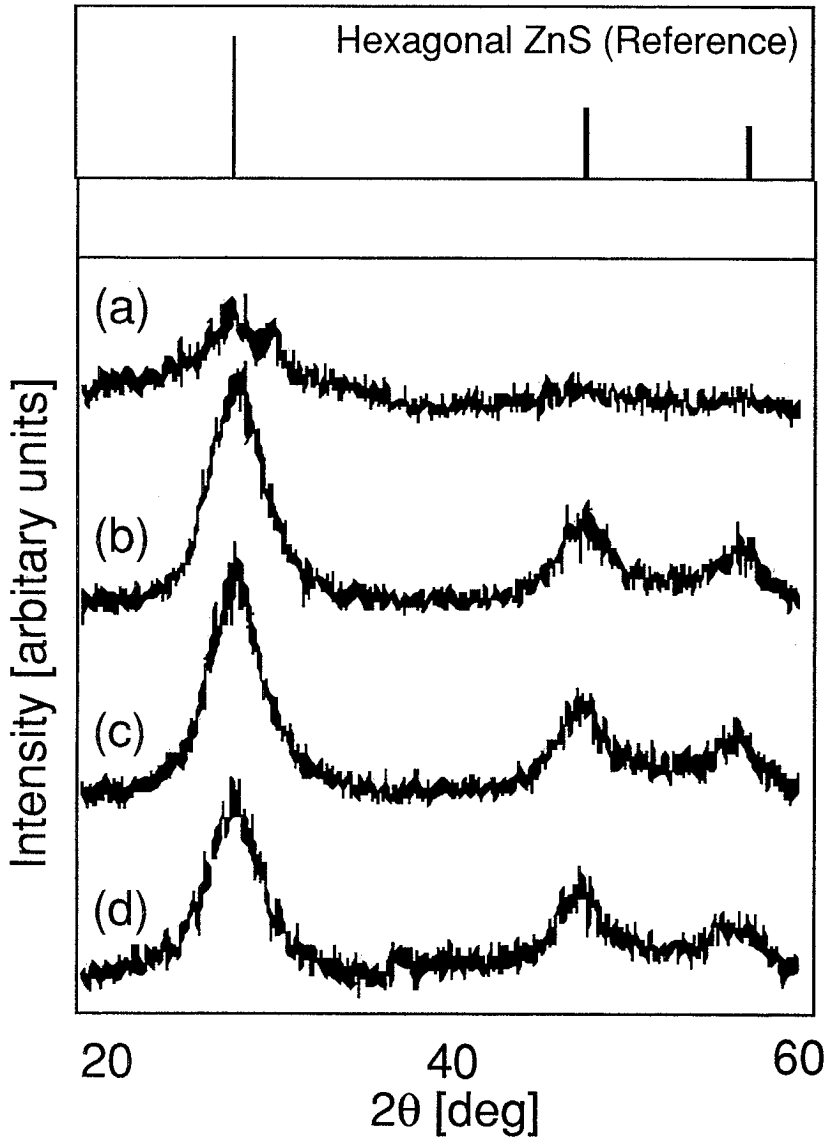

Fig.4. X-ray diffraction patterns of ZnS particles prepared at different starting-solution concentrations (Cs, mol/l); (a) 0.001, (b) 0.05, (c) 0.1, and (d) 0.5.

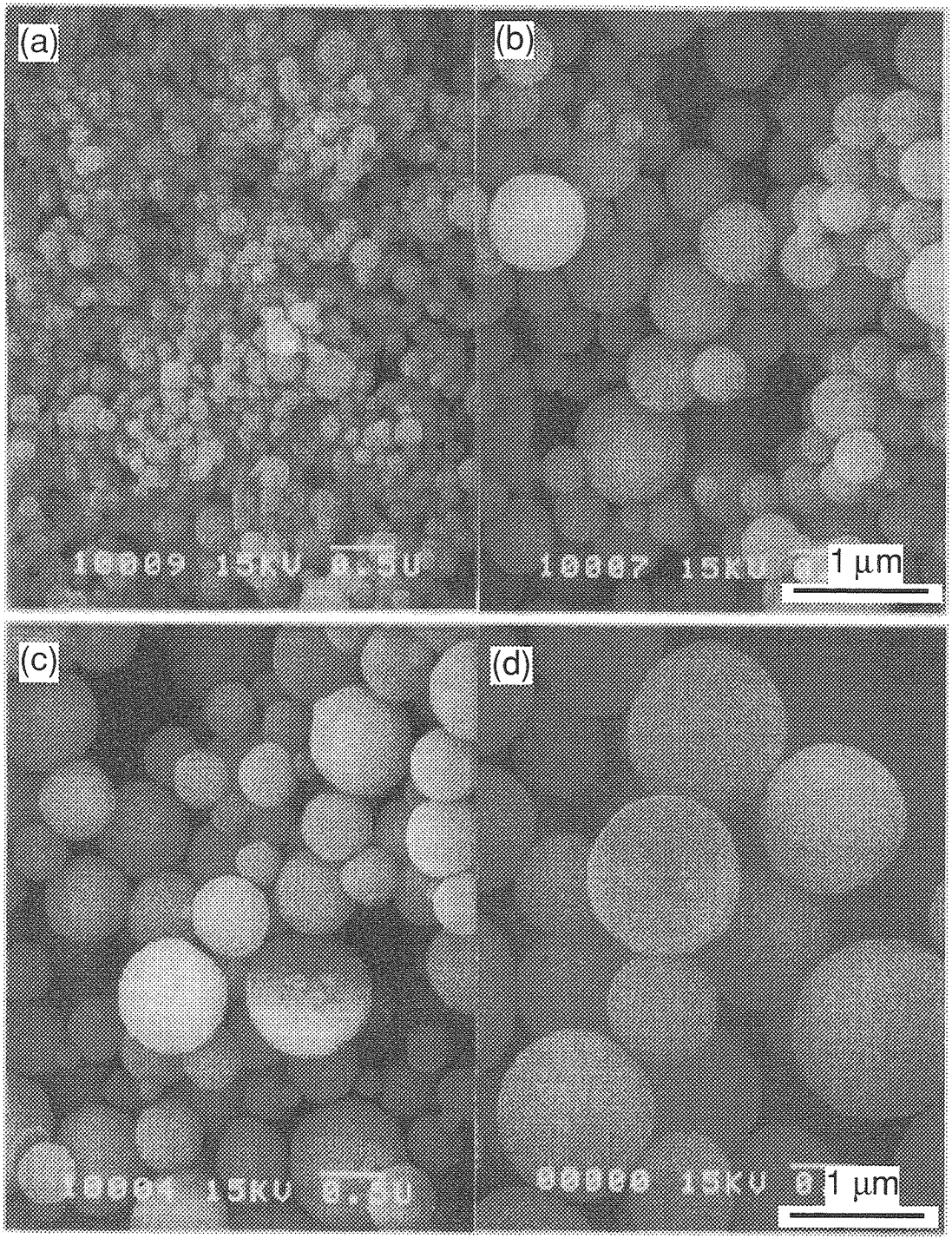

Fig.5. SEM photographs of ZnS particles prepared at different starting-solution concentrations (Cs, mol/l); (a) 0.01, (b) 0.05, (c) 0.1 and (d) 0.5.

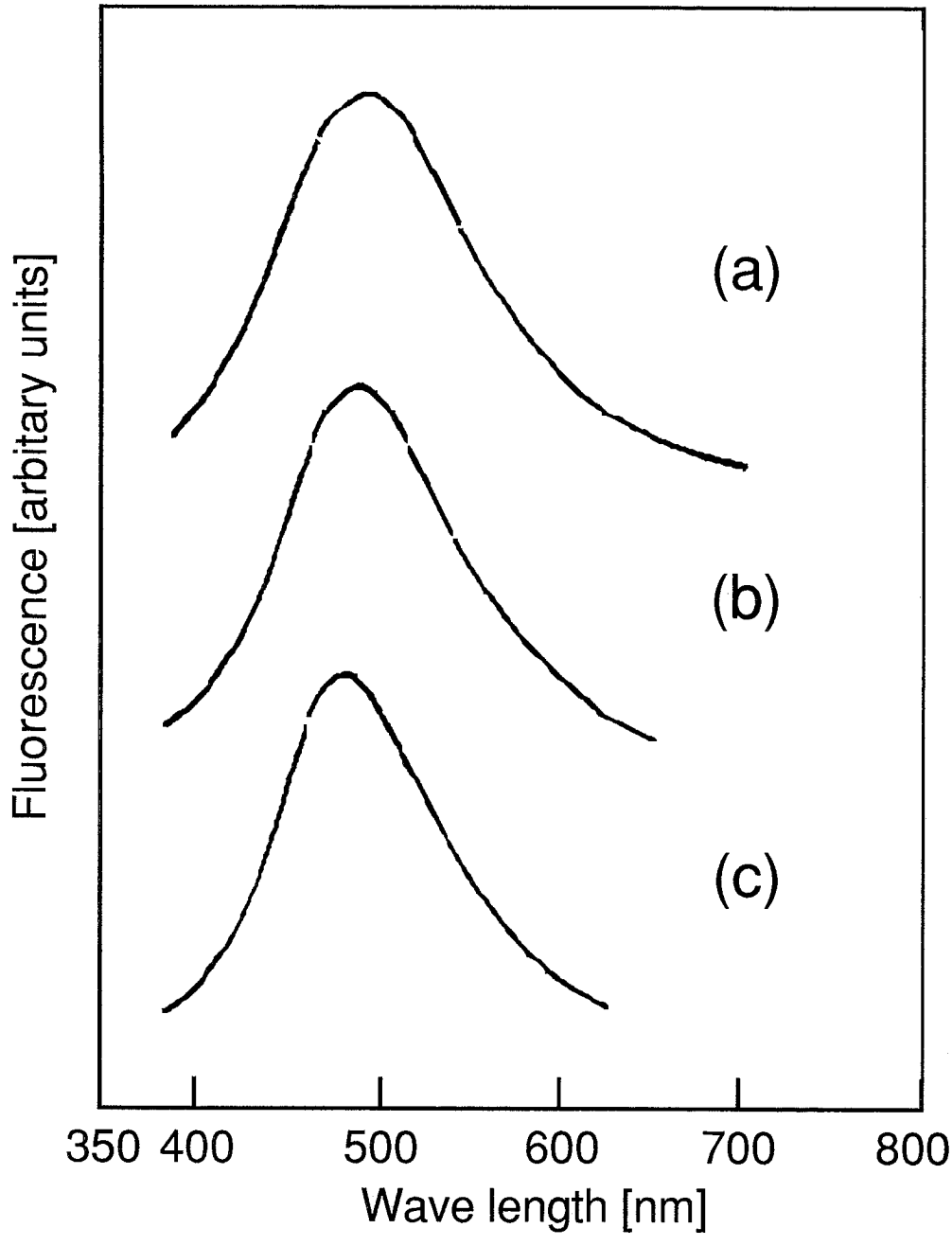

Fig.6 The relation between the fluoresence spectra of ZnS particle and the starting-solution concentrations (Cs, mol/l); (a) 0.01, (b) 0.05, and (c) 0.5.

3.2 Cadmium sulfide particles preparation

Fig.7 shows XRD patterns of particles prepared at 700°C from the different starting solutions: 0.01, 0.05, 0.1 and 0.3 mol/l. As examined for ZnS particles, the peaks assigned to the cubic phase of CdS can be seen for all solution concentration, but the peak height tends to decrease with the decrease in solution concentration showing a decrease in crystallite size. Fig.8 shows SEM photographs of CdS particles prepared at different concentrations. CdS particles have rough surface due to the growth of crystallite in the particles, whereas the surface of ZnS was smooth. The rough surface is originated from primary particles which aggregated each other. It shows that both aggregation and primary particle sizes become larger with increasing solution concentrations.

Fig.9 shows the fluorescence spectra of the CdS particles obtained by changing the solution concentration, 0.01, 0.05, and 0.5 mol/l. These particles show a sharp emission peak at around 500 nm, which is very close to the band gap of CdS. As ZnS particles, there are no changes of fluorescence spectra in these concentrations range, indicating that CdS particles size did not affect the fluoresence spectral.

3.3 The effects of the temperature distribution on the characteristics of the particles

In the increasing temperature distribution, the temperatures were set so that the particles were subjected to the gradual evaporation and subsequent nucleation in the liquid-to-particle conversion process.

In the present work, the effects of the temperature distribution on the crystalline phases and morphology of the particles were expected. We prepared the ZnS and CdS particles under the temperature profiles of the reactor furnace for two typical cases described in fig.2, respectivelly. The X-ray diffraction patterns and SEM photographs of the particles obtained at two cases of reactor temperature distributions were shown in fig.10 and fig.11.

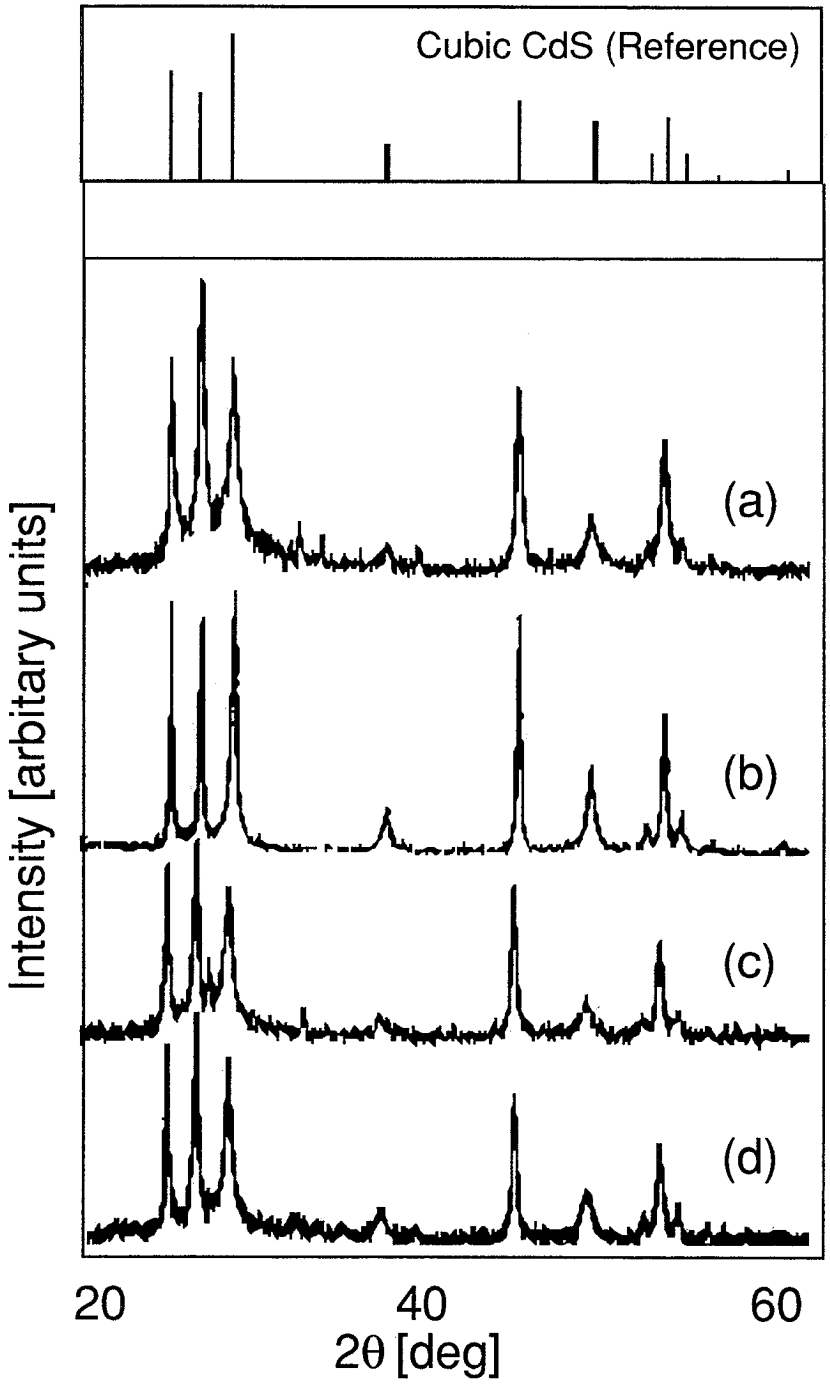

Fig.7 X-ray diffraction patterns of CdS particles prepared at different starting-solution concentrations (Cs, mol/l); (a) 0.01, (b) 0.05, (c) 0.1, and (d) 0.3.

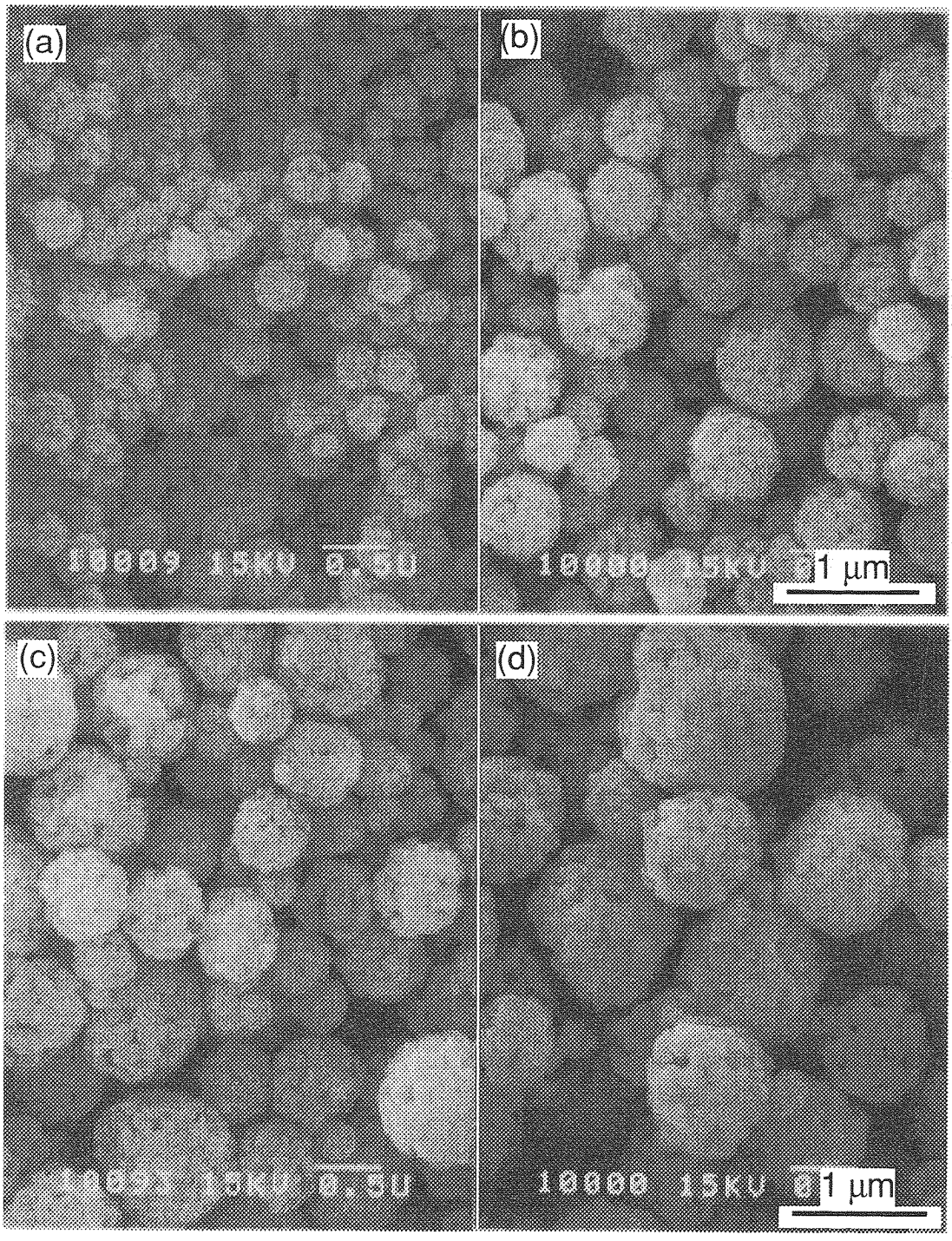

Fig.8 SEM photographs of CdS particles prepared at different starting-solution concentrations (Cs, mol/l); (a) 0.01, (b) 0.05.(c) 0.1, (d) 0.3.

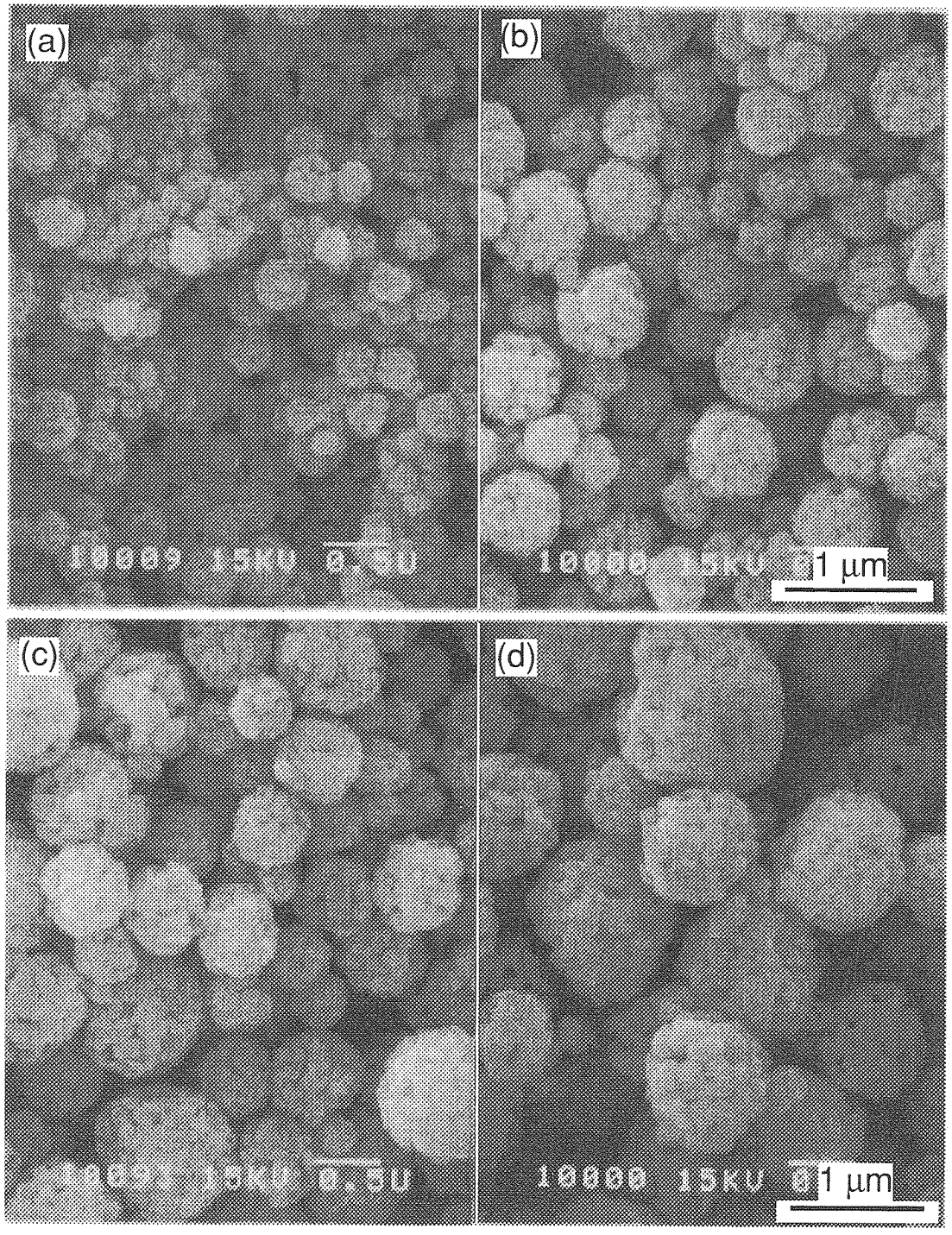

Fig.8 SEM photographs of CdS particles prepared at different starting-solution concentrations (Cs, mol/l); (a) 0.01, (b) 0.05.(c) 0.1, (d) 0.3.

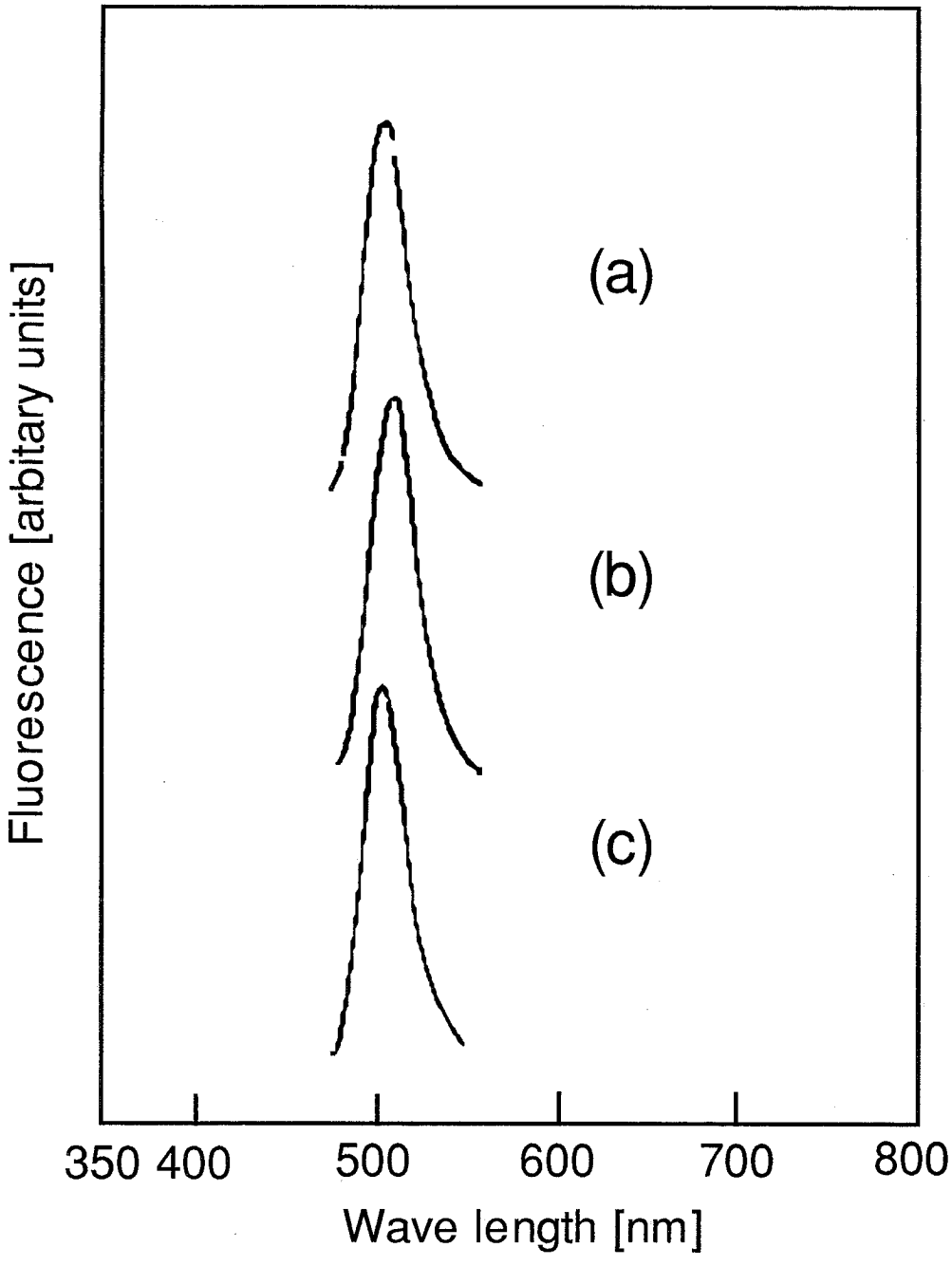

Fig.9. The relation between the fluoresence spectra of CdS particle and the starting-solution concentrations (Cs, mol/l); (a) 0.01, (b) 0.05, and (c) 0.5.

The X-ray diffraction patterns and SEM photographs of the particles obtained at increasing reactor temperature distributions showed the trends similar to the characteristics of the particles prepared at constant reactor temperature. But the SEM photographs of the CdS particles (Fig.11 (b) showed a morphological change. Comparing with the particles obtained at increasing temperature, at constant reactor temperature distributions, sintered like primary particles of CdS were observed. More studies are needed to investigate the effects of temperature distribution of the reactor furnace, since only the crystalline phases and morphology of the particles were examined in this work.

3.4 Relation between particle size and concentration of metal nitrate

The relation between the droplet size and the solid particle size was discussed by Zhang and Messing (1990) , and by Pluym et al.(1993) .

Now, assuming that one droplet changed into one dense spherical particle inside the reaction furnace. The final volume mean diameter of the solid fine particles, d_p, can be given by the following equation, derived from the mass balance of the system.

$$d_p^3 = (M D_d^3 C_s) / 1000 \rho_p \qquad (1)$$

where C_s is the concentration of the solution in mol/l, M is the molecular weight, ρ_p is the theoretical density of ZnS and CdS, and D_d is the volume mean diameter of solution droplets. For ZnS, ρ_p is known to be 4.09 $g.cm^{-3}$ and M is 97.46 and for CdS, ρ_p is reported to be 4.80 $g.cm^{-3}$, and M is 144.47. Accordingly, equation (1) can be written as

ZnS : $$d_p = 0.288 D_d C_s^{1/3} \qquad (2)$$

CdS : $$d_p = 0.311 D_d C_s^{1/3} \qquad (3)$$

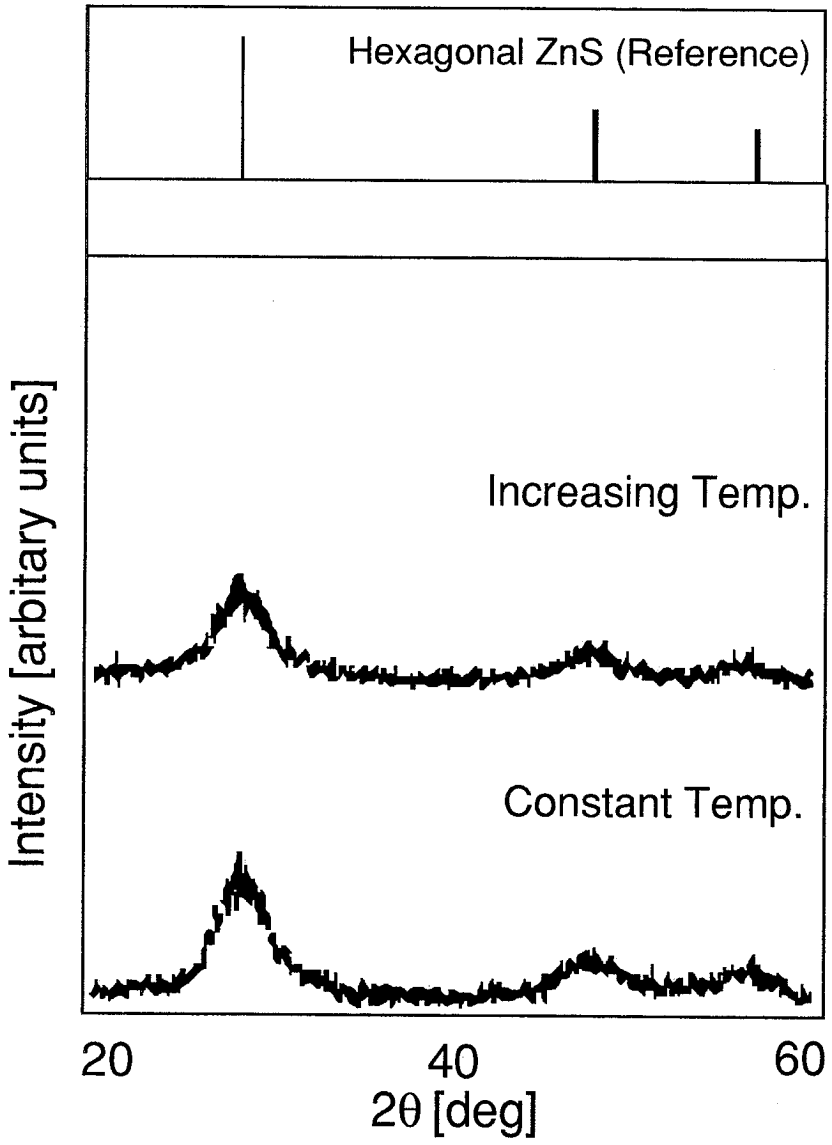

Fig.10 X-ray diffraction patterns of particles prepared at constant and increasing temperature distribution. (a) ZnS particles.

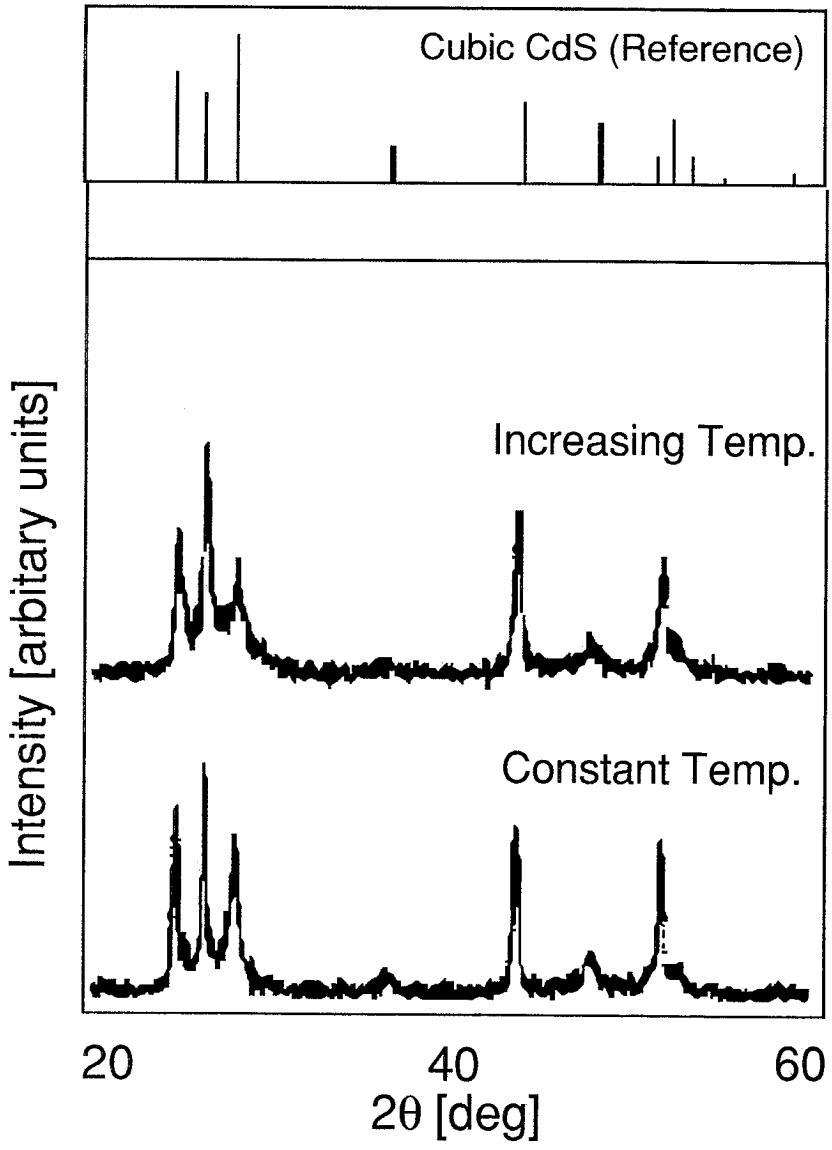

Fig.10 (continued) (b) CdS particles.

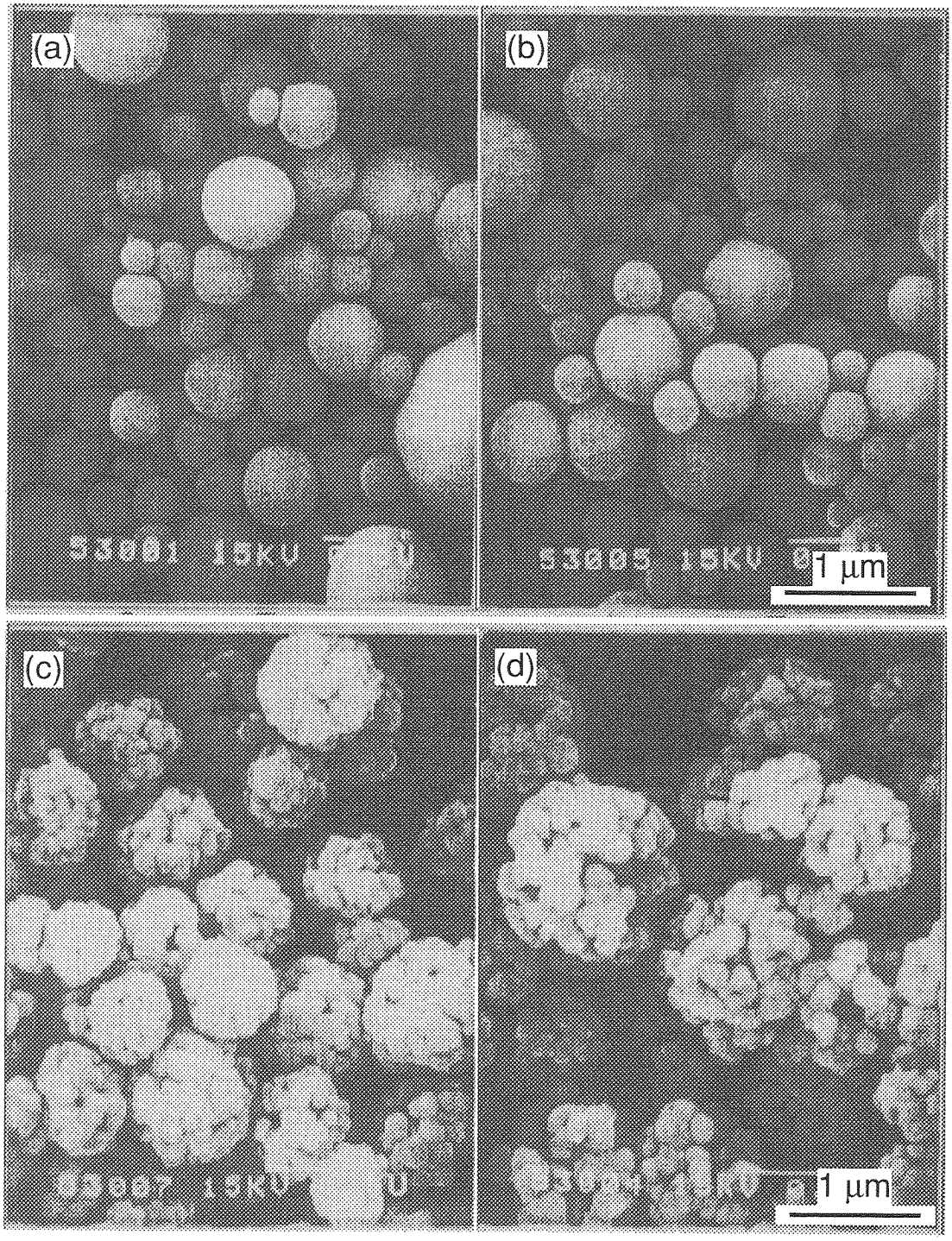

Fig.11 SEM photographs of ZnS (a,b) and CdS (c,d) particles prepared at constant (a,c) and increasing (b,d) temperature distribution. Solution concentrations are 0.05 mol/l.

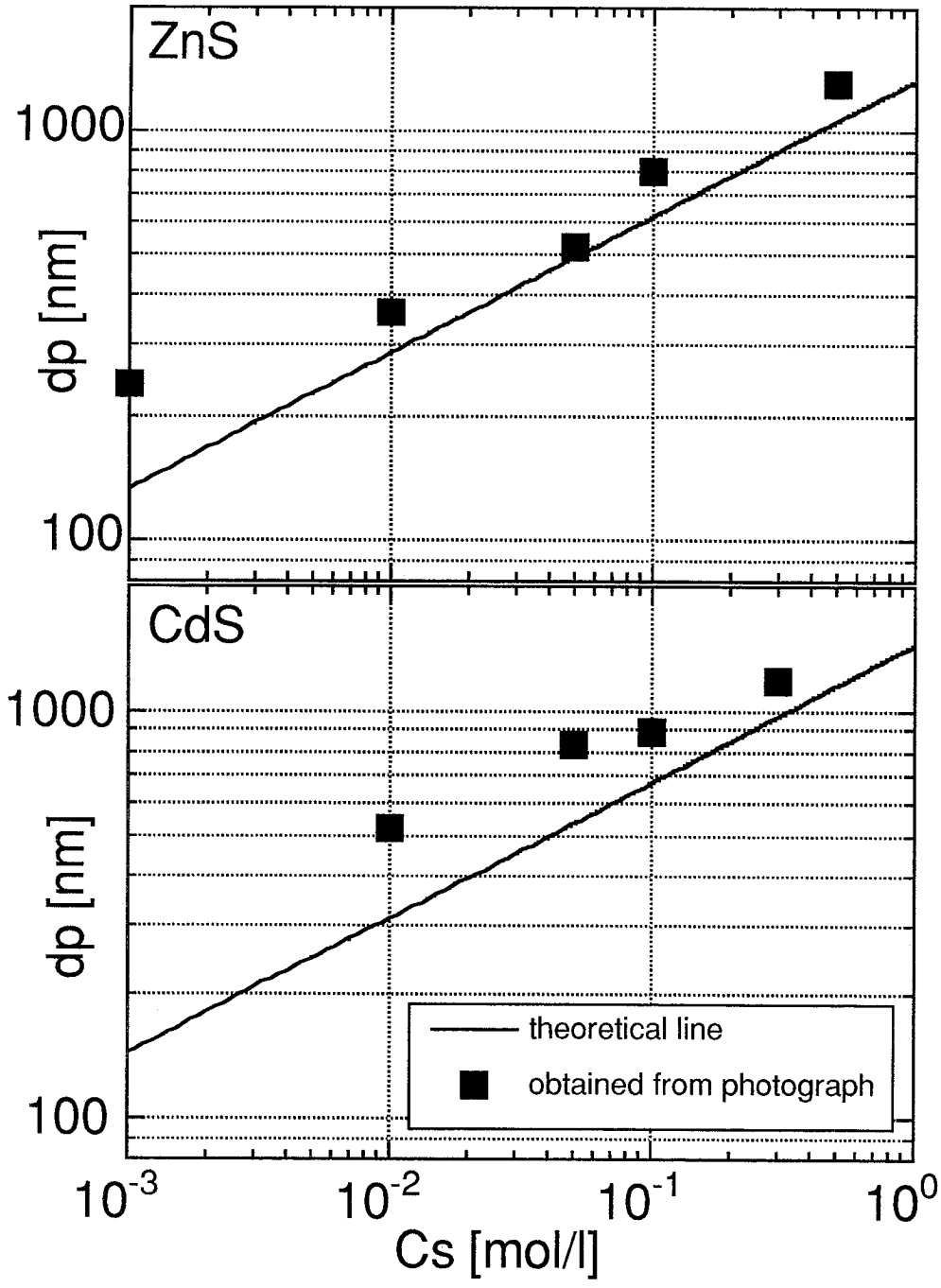

Fig. 12 The relation between the mean volume diameter (dp) of ZnS and CdS particle and the starting-solution concentrations (Cs).

Fig.12 shows the changes in the volume mean diameter of ZnS and CdS particles formed dp, with the concentration of the starting aqueous solution, Cs. Fig.13 shows a volume mean diameter distribution of atomized water droplets using an ultrasonic nebulizer; this was measured by a light-scattering particle-size analyser (Malvern Instruments Corp., Mastersize DPF). Dn is the number concentration in the size range, and N is the total particle number concentration. The volume mean diameter of water droplets was 4.56 micrometer. The droplet size distribution did not change for the concentration range of metal nitrate in the solution used in this experiment. The solid lines in fig.12 are equation (1).

ZnS particles size agrees quite well with the theoretical results. CdS particles size was comparatively shown to be bigger than the theoretical particles size. It is due to the existence of primary particles that construct the aggregated particles of CdS. From the tendency of fig.12 that particles size obtained by the experiment differs from the theoretical one, especially at low concentration of start solution, we also consider that inside the reactor, the evaporation rate of low concentrations droplets are larger than the ones of high concentrations, therefore low concentrations particles trend to be aggregation.

4 Summary

Fine particles of ZnS and CdS with different sizes were prepared by an ultrasonic spray-pyrolysis technique using various concentrations of the starting solutions. It was observed that both ZnS and CdS particles were spherical, but CdS was the aggregation particle constructing from the primary particles, whereas the surface of ZnS particle was smooth. As the concentrations increase, it can be found that both ZnS and CdS particle sizes also increase. The effects of the temperature distribution on the crystalline phases and morphology of the particles obtained were investigated and a morphological change was shown in the case of CdS particles. This

study also indicated that the changing the concentrations of starting solutions did not affect the fluorescence spectra of the particles.

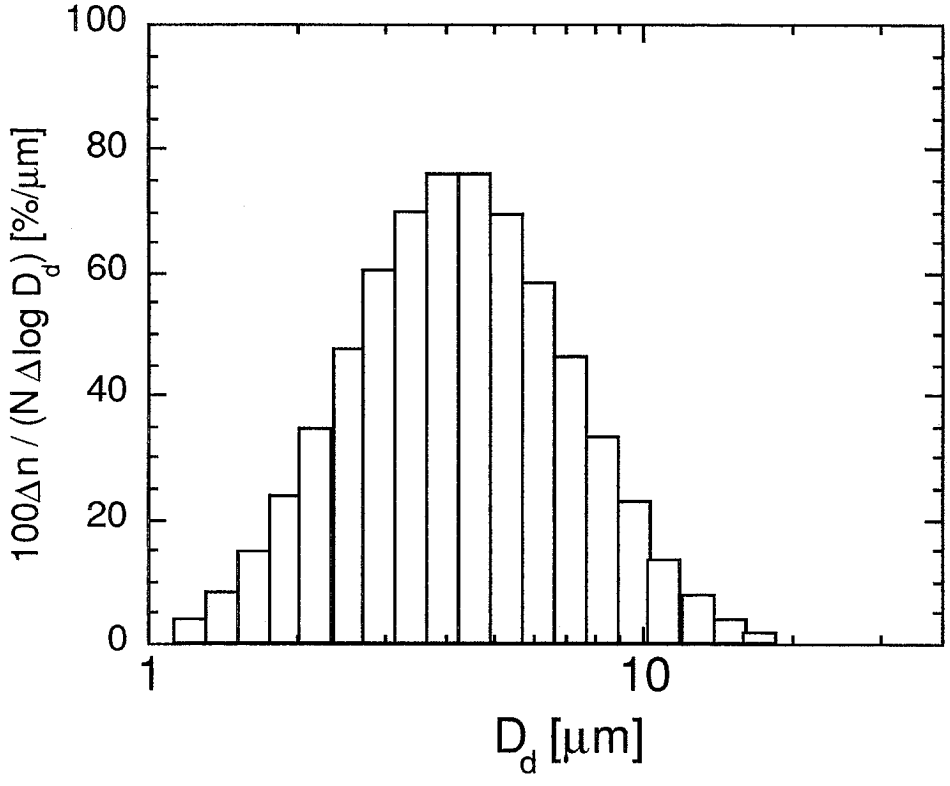

Fig.13 Size distribution of droplets using an ultrasonic nebulizer (see notation in the text).

5 References

Feigelson, R. S., N'Diaye, A., Yih-Yin, S. and Bube, R. H. (1977) *J. Appl. Phys.*, 48, 3162.

Karanjai, M. K. and D. Dasgupta, D. (1987) *Thin Solid Films*, 155, 309.

Krunks, M., Mellikov E. and Sork, E. (1986) *Thin Solid Films*, 145, 105.

Ohshima, K., Tsuto, K., Okuyama K. and Tohge, N. (1992) *Kagaku Kogaku Ronbunshu*, 18, 288.

Ohshima, K., Tsuto, K., Okuyama K. and Tohge, N. (1993) *Aerosol Sci. Technol.*, 19, 468.

Okuyama, K. (1988) *J. Aerosol Sci.*, 22, S7.

Okuyama, K., Oshima K. and Tsuto K. (1991) *KONA Powder Particles*, 9, 79.

Pluym, T. C., Lyons, S. W., Powell, Q. H., Gurav, A. S., Kodas, T. T., Wang, L. M. and Glicksman H. D. (1993) *Mater. Res. Bull.*, 28, 369.

Rajaram, P., Thangaraj, R., Sharma, A. K., Raza, A. and Agnihotri, O. P. (1983) *Thin Solid Films*, 100, 111.

Richard, D., El-korashy, A. M., Stirn, R. J. and Karulkar, P. C. (1984) *J. Vac. Sci. Technol.*, A 2, 332.

Tamaki, S., Tohge N. and Okuyama, K. (1995) *J. Mater. Sci. Lett.*, 14, 1388.

Tohge, N. and Minami, T. (1992) *SPIE Proc. Sol-Gel Optics II*, 1758, 587.

Tohge, N., Asuka, M. and Minami, T. (1992) *J. Non-Cryst. Solids*, 147, 652.

Tohge, N., Tamaki, S. and Okuyama, K. (1995) *Jpn. J. Appl. Phys.*, 34, L207.

Tohge, N., Tatsumisago, M., Minami, T., Okuyama, K., Adachi, M. and Kousaka, K. (1988) *Jpn. J. Appl. Phys.*, 27, L1086.

Tohge, N., Tatsumisago, M., Minami, T., Okuyama, K., Arai, K. and Kousaka, K. (1989) *Jpn. J. Appl. Phys.*, 28, L1175.

Zhang, S. C. and Messing, G. L. (1990) in "*Ceramic Powder Science III*" (Messing, G. L., Hirano, S.-I., and Hausner, H. Ed.) American Ceramic Society, Westerville, p.49.

7.3 Formation of submicron copper sulfide particles by an ultrasonic spray pyrolysis

Formation of submicron copper sulfide particles by an ultrasonic spray pyrolysis

1 Introduction

The application of fine particles as advanced materials is depended on their size, morphology and chemical property. Among the continuous techniques to prepare submicron particles, spray pyrolysis is the most suitable one that has advantages as the high purity and the uniformity in size and composition of the prepared particles. In the process, the starting solution is atomized into droplets, subsequently solvent evaporation and pyrolysis in the droplets occur in a heated zone and the solid particles are formed. In our previous studies (Tohge et al.,1995; Okuyama et al., 1997), spray pyrolysis was utilized as a promising method for the preparation of zinc sulfide and cadmium sulfide fine particles. The crystalline phases and fluorescence properties of these fine particles were examined as a function of particle size, which was controlled by changing the concentration of spray solutions (Okuyama et al., 1997).

The study of copper sulfides Cu_xS (x = 1 - 2) especially in a form of thin films, is of interest due to numerous technological application in the achievement of solar cells (Boer, 1977; Nair et al., 1993). At room temperature range, Cu_xS is known to exist in five stable phases (Loferski et al., 1979), with x = 1 (covellite), 1.75 (anilite), 1.8 (digenite), 1.95 (djurleite), and 2 (chalcolite). Various techniques are generally employed to prepare Cu_xS thin films. Using spray pyrolysis, the formation of Cu_xS thin films has been investigated for x > 1 (Vedel et al., 1980) and recently for x = 1

(Krunks et al., 1997; Nascu et al., 1997). In these studies, the crystalline phase and the optical properties of the thin films were discussed without considering the morphology.

For a better understanding of the formation of copper sulfide particles and their possible application in the thin films, this paper reports, for the first time, the formation of spherical and solid submicron copper sulfide particles by spray pyrolysis. The effects of experimental parameters on the crystalline phase and morphology of particles were studied.

2 Experimental procedure

Spray solutions were prepared by dissolving appropriate amounts of thiourea ($SC(NH_2)_2$) and copper nitrate trihydrate ($Cu(NO_3)_2 \cdot H_2O$) into distilled water. The molar ratio of the metal nitrate to thiourea was varied from 1:1 to 1:5. The concentrations of metal nitrate in the solution were changed from 0.01 to 0.05 mol/l. We did not investigate the solutions with Cu:S ratio over 1:5 and the concentration over 0.05 mol/l, due to the limit of solubility (around 0.03 wt %). The precipitate appeared in the solution during 2 h up to 8 h, depending on the concentration of the solution and molar ratio of Cu:S. Using the precursors of $CuCl_2$ and thiourea, Krunks et al. (1997) also reported the appearance of the precipitate and the change in solution's color at higher concentrated solutions (0.1-0.2 mol/l).

A typical experimental setup presented in our previous study (Okuyama et al., 1997) was used. The system consisted of an ultrasonic nebulizer, a tubular furnace, and an electrostatic precipitator. The 1000 mm-length furnace of 13 mm diameter consisted of five independently-controlled heating zones enables us to provide desired temperature distribution. In the present work, the temperature distribution was set to 'constant profile' (Okuyama et al., 1997). The furnace temperature (Tf) was maintained at 200-900°C. The lowest temperature of 200°C was chosen because it was

reported that CuS phase films were deposited at temperature higher than 200°C (Nascu et al., 1997) and 220°C (Krunks, 1997) by spray pyrolysis of aqueous solutions containing thiourea.

Droplets generated by ultrasonic nebulizer were transported to the tubular furnace using nitrogen as a carrier gas, with the flow rate of 0.5, 1.0 and 2.0 l/min. The corresponding residence time of a carrier gas in the furnace was estimated to be 10, 5 and 2.5 s, respectively. The particles generated from the furnace exit were collected using an electrostatic precipitator, which was maintained at around 150°C, to avoid the condensation of water on the particles (Okuyama et al., 1997). The particles obtained were examined by X-ray diffraction (XRD, CuKα, Rigaku-Denki Corp., model RINT 1000) and scanning electron microscopy (SEM, JEOL Corp., model JSM-T100).

3 Results and discussion

First, the effects of the pyrolysis temperature (furnace temperature, T_f) on the crystalline phases of particles prepared are studied. Figs. 1 and 2 show X-ray diffraction patterns of the particles prepared with the gas flow rate of 2.0 l/min and the solution concentration of 0.05 mol/l. Fig.3 shows the relation between Cu:S molar ratio and the temperature on the formation of the single CuS phase, which is shown by a shadowed area (symbols O).

For Cu:S molar ratio of 1:2 and T_f = 200°C (fig.1(c)) and 300°C, the particles are the single covellite phase copper sulfide with hexagonal structure. Using the molar ratio of 1:5, the single covellite phase particles can be prepared at a relatively wide temperature range, from 200 up to 600°C (figs. 2(b, c, d)). The upper limit value of 600°C is somewhat high and has not been reported in the preparation of CuS thin films by spray pyrolysis (Krunks et al., 1997; Nascu et al., 1997)

The results indicate that in the sulfur-rich side, the single crystalline phase can be

obtained at the higher temperature. Particles prepared at the outside shadowed area (symbols Δ) contain the mixed phase of $Cu_{1.8}S$ (digenite) and CuS (covellite). The formation of the mixed stable phases of $Cu_{1.96}S$ and CuS was reported in thin films prepared by metal-organic chemical vapor deposition (Nomura et al., 1996). However, after CuS phase was formed, the formations of CuS_xO_y phase films were also reported at temperatures of 410 (Krunks et al., 1997) and 250°C (Nair et al., 1993), probably due to the use of air atmosphere that leads to the easier oxidation.

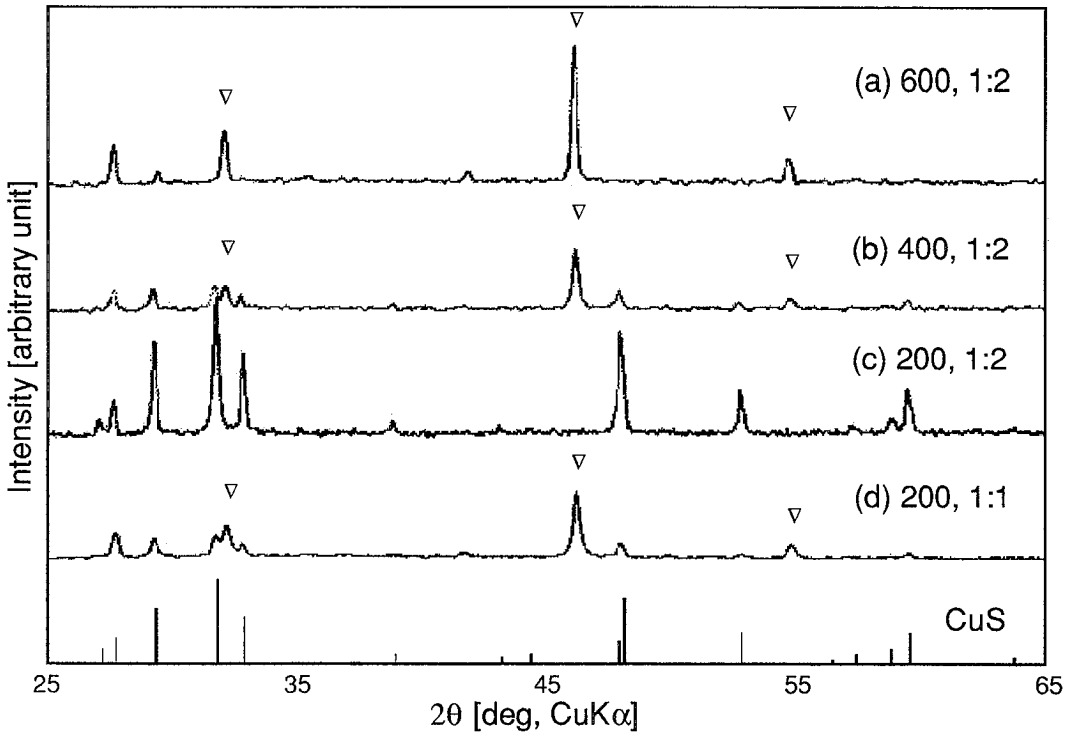

Fig. 1 XRD patterns of the copper sulfide particles prepared. Experimental conditions: Cu:S molar ratio 1:2 (a-c) and 1:1 (d), solution concentration 0.05 mol/l, and carrier gas flow rate 2.0 l/min. Furnace temperature (°C) as follows: (a) 600, (b) 400, (c, d) 200. Symbols ∇ represent $Cu_{1.8}S$ phase.

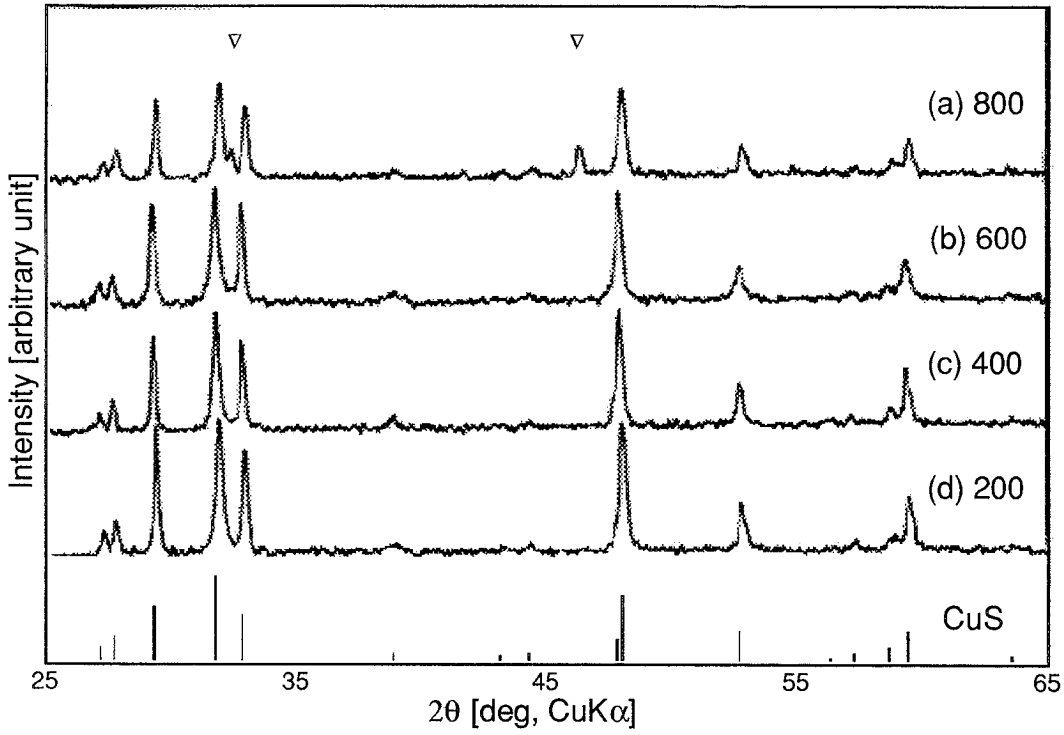

Fig. 2 XRD patterns. Experimental conditions: Cu:S molar ratio 1:5, solution concentration 0.05 mol/l, and carrier gas flow rate 2.0 l/min. Furnace temperature (°C) as follows: (a) 800, (b) 600, (c) 400, and (d) 200. Symbols ∇ represent $Cu_{1.8}S$ phase.

For Cu:S = 1:2, CuS particles prepared at the lower temperature have stronger crystalline peaks than those of higher temperatures. From the calculation of crystallite sizes (d_c) using Scherrer's equation, it can be shown that d_c of CuS prepared at T_f = 200°C (39 nm) is somewhat larger than that of T_f = 300°C (20 nm). The XRD peaks assigned to the single covellite phase are also obtained when, (i) the residence time is changed from 2.5 to 10 s, and (ii) the solution concentration is changed from 0.05 to 0.01 mol/l, in the case of Cu:S ratio of 1:2 and T_f = 200°C. However, the particles prepared from 0.01 mol/l solution showed lower crystallinity (d_c = 23 nm) compared with that of 0.05 mol/l (d_c = 39 nm). Also, a slight decrease in the crystallite size (d_c

= 34 nm) is found by prolonging the residence time (the flow rate of 0.5 l/min). This can be ascribed that increasing the temperature or prolonging the residence the time will drive the Cu_xS (x is not 1) phase to grow.

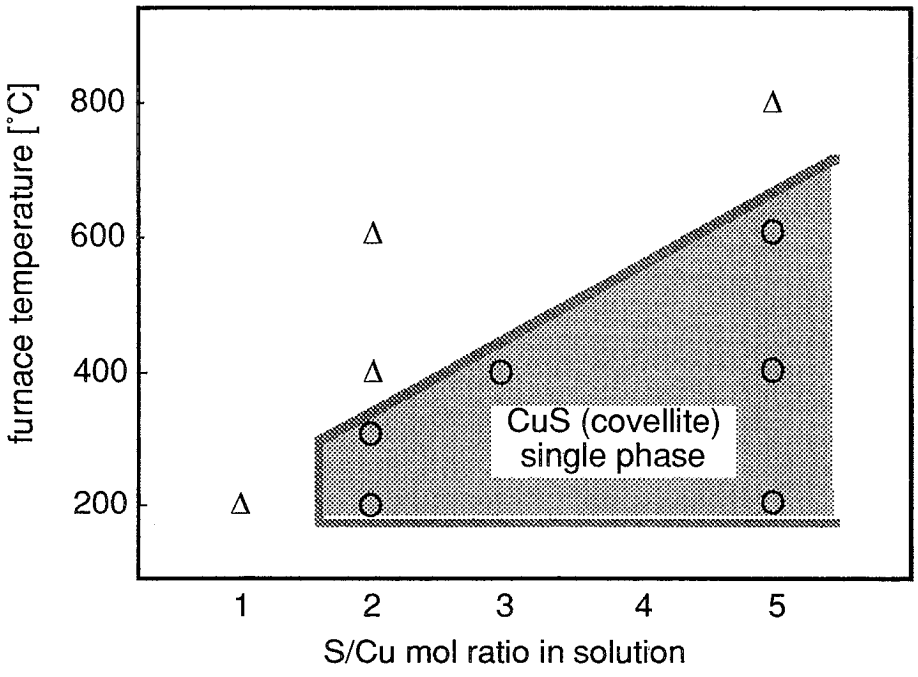

Fig.3 Relation of the crystalline phase of particles prepared with temperature and precursor composition. Solution concentration 0.05 mol/l and carrier gas flow rate 2.0 l/min. Symbols Δ and O represent $Cu_{1.8}S$ and CuS phase, respectively.

Figs. 4 and 5 show SEM photographs of CuS (covellite) particles prepared in this study. Fig.4 shows the morphology of the particles prepared from the solution with Cu:S molar ratio of 1:2 and 1:5 with the solution concentration of 0.05 mol/l and the carrier gas flow rate of 2.0 l/min at different furnace temperatures. For T_f = 200°C (fig. 4(a)), the particles seem to be necked together, which is probably due to the

existence of the liquid phase or unreacted precursor inside the particles, even when the particles have already been converted to CuS. The effect of the temperature on the morphology is clearly shown in fig.4(b), where at T_f = 300°C and 400°C (not shown), the particles are spherical and separately formed. The formation of spherical particles reflects one feature of spray pyrolysis.

Figs.4(c) and 4(d) show the different morphology of CuS particles prepared at Cu:S = 1:5, where the particles do not form separately, even when the higher temperature of 600°C was used. This is due to the effect of sulfur content on some processes that occurred during the formation of the particles, such as solvent evaporation and solute precipitation.

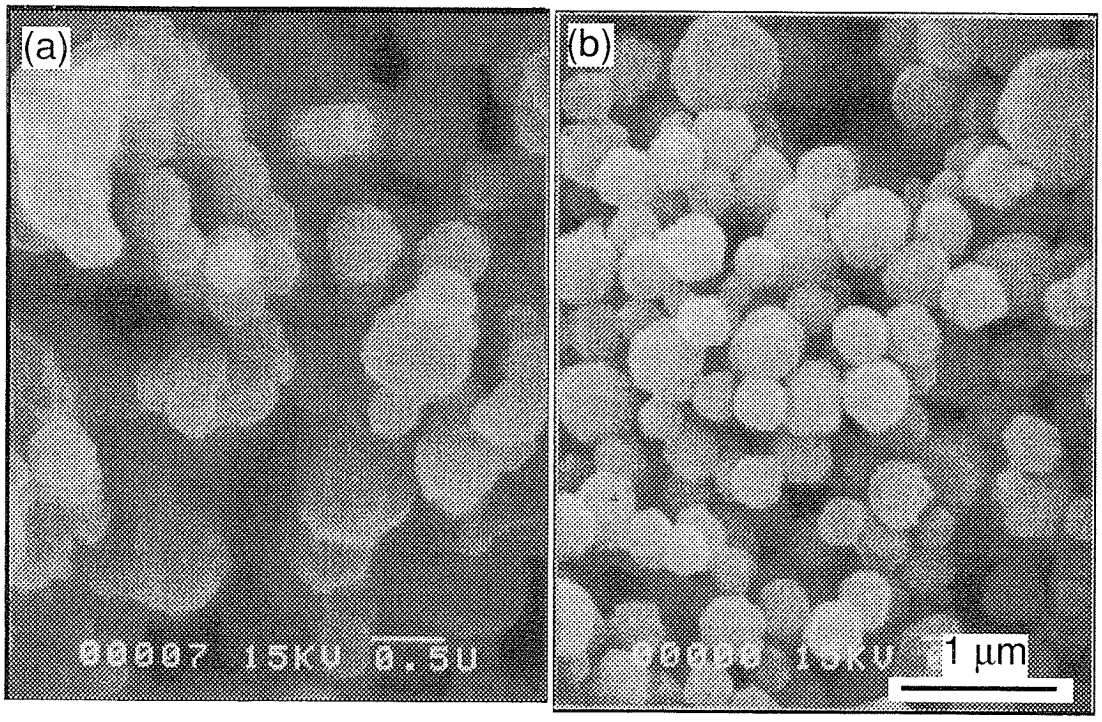

Fig.4 SEM photographs of CuS particles prepared. Experimental conditions: solution concentration 0.05 mol/l and carrier gas flow rate 2.0 l/min. Cu:S molar ratio and furnace temperature(°C) as follows: (a) 1:2, 200; (b) 1:2, 300.

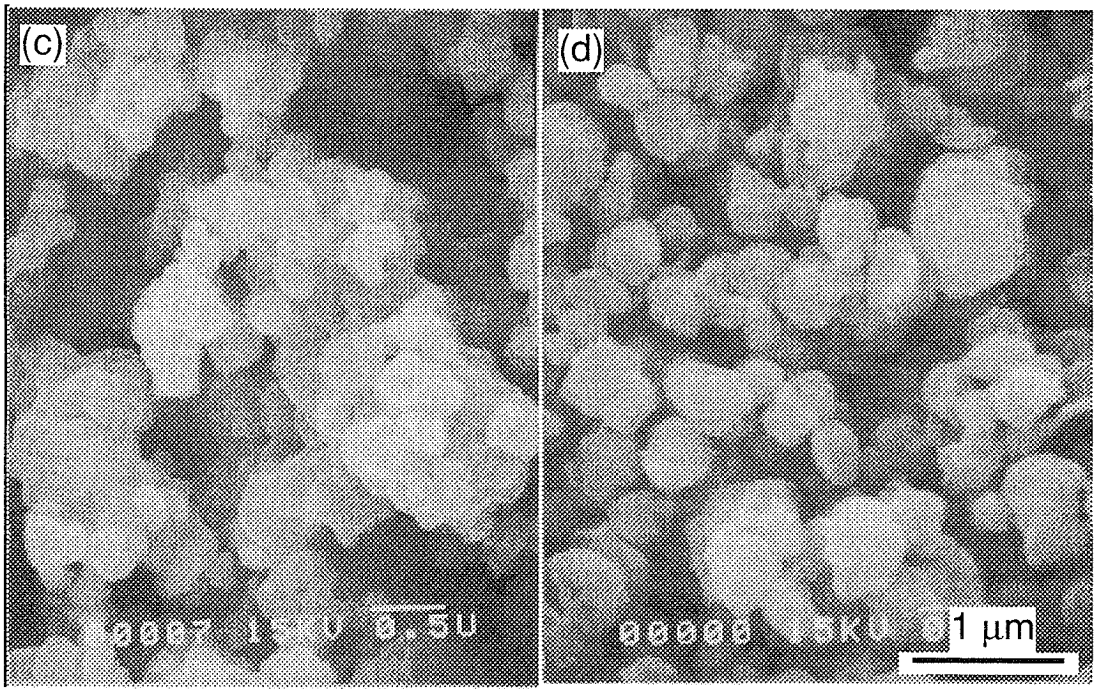

Fig.4 (continued) Cu:S molar ratio and furnace temperature(°C): (c) 1:5, 200; and (d) 1:5, 600.

Fig.5(a) shows that the particles prepared at the longer residence time are separately formed, compared with those prepared at the short residence time of 2.5 s (fig.4(a)). It is shown that particles prepared at the residence time of 10 s, are similar to those prepared at T_f = 300°C with the residence time of 2.5 s (fig.4(b)).

Fig.5(b) shows the particles prepared at the lower solution concentration of 0.01 mol/l, Cu:S = 1:2 and flow rate of 1.0 mol/l. As the solution concentration decreases, it can be observed that the particle size also decreases. In this study, we use only two solution concentrations, due to their solubility problems. However, the results show that spray pyrolyzed particle size can be controlled by changing the solution concentration.

By assuming that one droplet changes into one dense spherical particle, the

volume mean diameter of product particle, d_p^*, can be given by the following equation.

$$d_p^{*3} = (M D_d^3 C_s) / 1000 \rho_p \qquad (1)$$

where C_s is the solution concentration in mol/l, M is the molecular weight, ρ_p is the theoretical density in g/cm^3, and D_d is the volume mean diameter of solution droplets. For CuS with M = 95.65 and ρ_p = 4.09 g/cm^3, equation (1) can be written as

$$d_p^* = 0.274 D_d C_s^{1/3} \qquad (2)$$

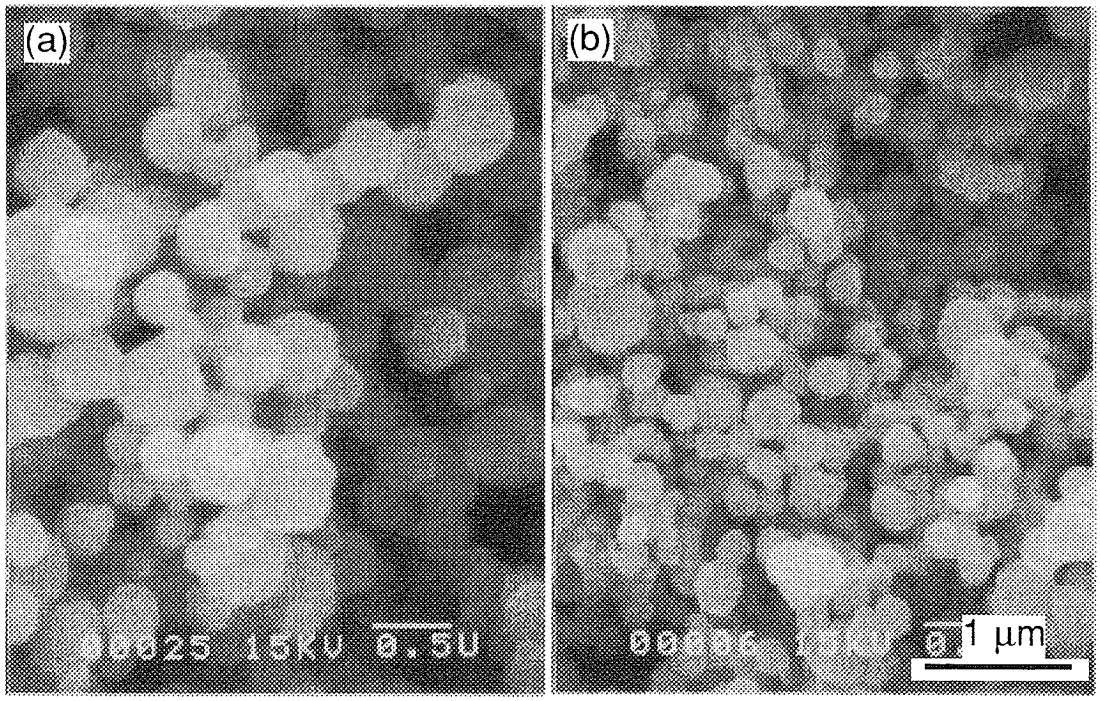

Fig.5 SEM photographs of CuS particles prepared. Experimental conditions: Cu:S molar ratio 1:2 and furnace temperature 200°C. Solution concentration (mol/l) and carrier gas flow rate (l/min) as follows: (a) 0.05, 0.5 and (b) 0.01, 1.

Table 1 Relationship between the solution concentration C_s and the volume mean diameter of CuS particles, experimental (d_p) and calculated by eq. (2) (d_p*).

C_s (mol/l)	d_p (μm)	d_p* (μm)	Error (%)
0.05	0.430	0.461	7.20
0.01	0.271	0.269	0.74

Error= $|(d_p^* - d_p)| / d_p \times 100$.

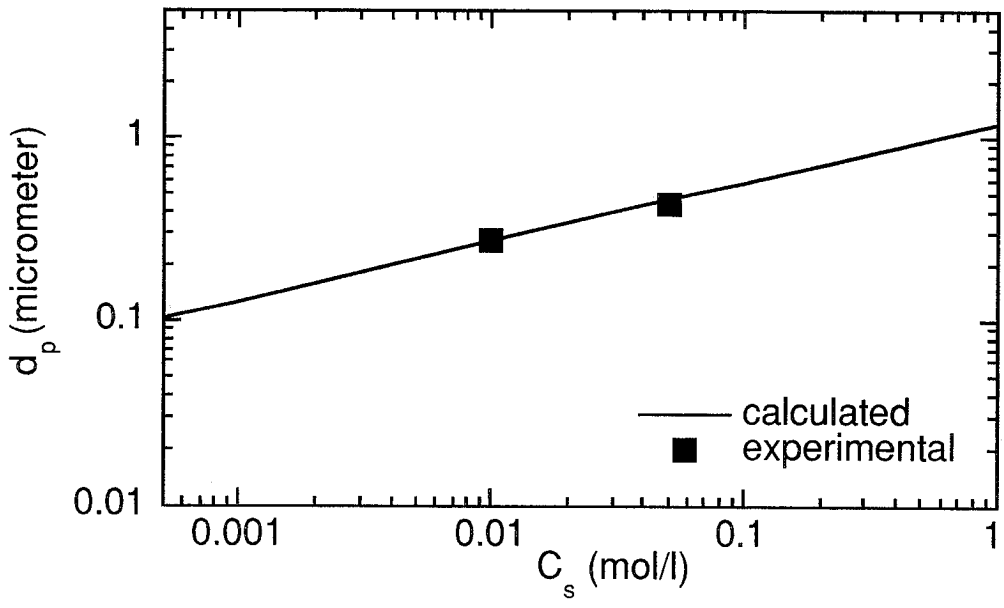

Fig. 6 Relationship between the solution concentration Cs and the average volume mean diameter of CuS particles, experimental (d_p) and calculated by eq. (2) (d_p*).

Table 1 and figure 6 show the relation between the volume mean diameter of CuS particles prepared d_p, with the solution concentration C_s. The volume mean diameter of water droplets D_d was 4.56 μm (Okuyama et al., 1997), and we assume that the droplet size distribution does not change in this study. At solution concentrations of 0.05 and 0.01 mol/l, d_p of CuS particles prepared agreed quite well with the calculated values d_p^* by eq. (2).

4 Summary

It has been demonstrated that spherical copper sulfide particles of submicron order could be formed by spray pyrolysis of the aqueous solutions. Hexagonal CuS particles of single covellite phase were formed at the molar ratio of copper nitrate and thiourea from 1:2 to 1:5 and the furnace temperature from 200 to 600°C, respectively. Above these temperature ranges, the particles contained $Cu_{1.8}S$. The morphology of the particles is mainly controlled by the residence time of the droplets or particles in the furnace and by the composition of the precursors.

5 References

Boer, K. W. (1977) *Phys. Status Solidi A,* 40, 355.

Krunks, M., Mellikov, E. and Bijakina, O., (1997) *Physica Scripta,* T69, 189.

Loferski, J. J., Shewchun, J., Mittleman, S. D., Demeo, E. A., Arnott, R., Hwang, H. L., Beauliew, R. and Chapman, G. (1979) *Sol. Energy Mater.*, 1, 157.

Nair, M. T. S., Alvarez-Garcia, G., Estrada-Gasva, C. A. and Nair, P. K. (1993) *J. Electrochem. Soc.*, 140, 212.

Nair, P. K., Nair, M. T. S., Pathirana, H. M. K., Zingaro, R. A. and Meyers, E. A., (1993) *J. Electrochem. Soc.* 140, 754.

Nascu, C., Pop, I., Ionescu, V., Indrea, E. and Bratu, I. (1997) *Mater. Lett.*, 32, 73.

Nomura, R., Miyawaki, K., Toyosaki, T. and Masuda, T. (1996) *Vapor Deposition,* 2, 174.

Okuyama, K., Lenggoro, I. W., Tagami, N., Tamaki, S. and Tohge, N. (1997) *J. Mater. Sci.*, 32, 1229.

Tohge, N., Tamaki, S. and Okuyama, K. (1995) *Jpn. J. Appl. Phys.*, 34, L207.

Vedel, J., Cowache, P. and Dachraoui, M. (1980) *Revue Phys. Appl.*, 15, 1521.

7.4　静電噴霧熱分解法による微粒子製造

1．　はじめに

電子材料、顔料、化粧品などの原料として、粒径、形態および結晶構造が制御された機能性微粒子が製造できる簡易プロセスの開発が重要となっている。微粒子の製造法のうち、連続的に、しかも迅速に製造できるプロセスとして噴霧熱分解法が広く使われている[1-2]。噴霧熱分解法による微粒子の製造プロセスでは、まず目的の固体粒子の金属塩などが溶けている原料溶液またはプリカーサーを噴霧（液滴化）し、キャリアガスによってその液滴を直接反応炉などの高温場に導入する。反応炉内では、液滴中の溶媒は蒸発し、プリカーサーが周囲のガスとの反応または熱分解などにより、目的の固体微粒子となる。このプロセスでは、最終的な粒子のサイズは発生する液滴の大きさおよび溶液濃度により決定される。噴霧熱分解法の研究では、噴霧方法として超音波噴霧法や加圧または二流体ノズルを用いるのが一般的であるが、これらの噴霧法では発生する液滴径が数μmから数10μm程度が普通である。仮に粒径が5μmの液滴から粒径が0.15μmの固体粒子を生成する場合には、噴霧溶液中に0.0008%（体積）以下の非常に低い溶質濃度が必要となる。この場合、微粒子の生成速度の低下および純度に問題が生じ、0.1μm以下の超微粒子の生成が困難になる。そこで、噴霧法としてより微小な液滴の発生が可能であると報告されている静電気力を利用した静電噴霧法の応用が注目されつつある。最近の静電噴霧法による機能性微粒子の製造について述べる。

2.　静電噴霧の原理

液体が供給される金属製細管と金属製の対向電極との間に電圧を与えると、細管の先端に出ている液体には、表面張力、電気力、または場合によって重力が作用する。これらの合力が推進力となり、液体が円錐形メニスカスとなるコーン状にに歪められる(Fig.1-a,c)。つまり、電気力が増加し、表面張力を越えると液体表面が不安定になり、場合によって液柱現象が生じる。また液柱の不安定性によって液柱が分裂し、そこから液滴が発生する。この現象を繰返し、液体の供給量に対応した適当な電気力をそのまま維持すれば、比較的均一な液滴が連続的に放出される。これが静電噴霧法の原理である[3]。

Zeleny [4] は、コーン先端より液滴が発生することを観測し、液体の帯電と表面張力との関係で液滴が発生することを考えた。その後、ある程度高い電界ではほぼ均一な液滴が発生することを示し、液滴の帯電量を予測するなどの研究が行われた。Taylor[5]が導電性の液体メニスカスにおける力のバランスの解析などの先駆的な研究を行い、その後、この円錐形メニスカスのことをよくTaylor coneと呼んでいる。

3.　静電噴霧における液滴径の制御

また、直径が100μmオーダーまたはそれ以上の大きい液滴を発生する静電噴霧も報告されているが、ここでは100μm以下で、噴霧用の細管の内径d_cより比較的小さい直径D_d（$<<d_c$）の液滴の発生を中心にして、静電噴霧における噴霧状態および液滴径の評価

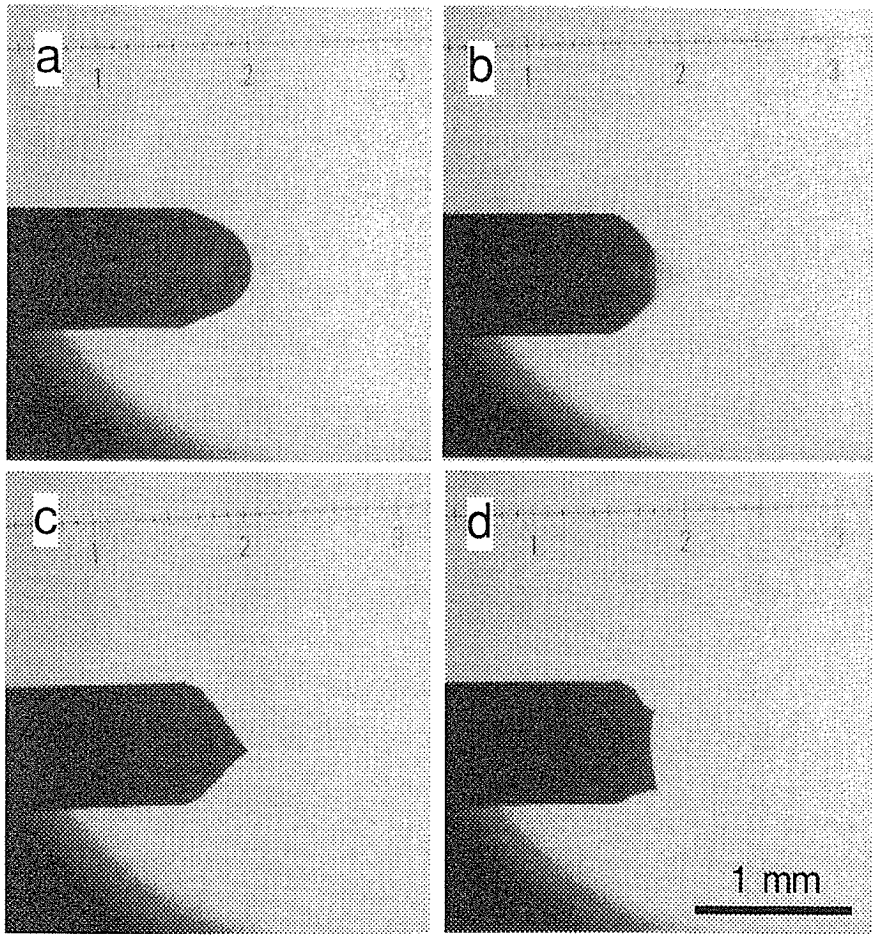

Fig.1　電圧を変化させたときの液体メニスカス
(a) dripping mode, 2.5kV, (b) pulsating mode,2.8kV,
(c) stable cone-jet made,and (d) multi-jet mode, 3.7kV.
溶液濃度＝0.0025 mol/l（ZnSプリカーサー）,供給液体流量＝0.10 ml/h.

に関する既往の研究を簡単に紹介する。

多くの報告のうち、CloupeauとPrunet-Foch[6]は、噴霧モードを詳細に区別し、連続的にコーン先端より非常に小さい安定な液柱(jet)および液滴が発生する条件が存在することを示した。この状態をCone-jetモードといい、その後の多くの研究者もこの用語を使用している。Fig.1(a)-(d)にも示したように一定の液体流量において、主に電圧によって、液体メニスカスの形態が滴下(dripping)モードから、パルス（pulsating）モード、コーンジェット（cone-jet）モード、およびコーン先端が複数に分裂したマルチジェット(multi-jet) モードまで変化する。

Smith[7]らは、液滴径と種々な液体の物性との関連性を調べた。その結果、液体の電気伝導度（導電率）が最も大きな影響を与えることを明らかにした。一般的な傾向として、より小さいな液滴を発生するには、液体の導電率を大きくし、噴霧液体の供給流量を低くすることが最も重要な条件となっている[8]。液体の流量が$4x10^{-5}$～$1x10^{3}$ml/h、液体の導

電率10^{-13}～10^{0}S/mのオーダーであれば、安定な静電噴霧が可能となることが報告されている[12]。なお電圧の極性（正／負）の違いや、交流および直流にかかわらず静電噴霧化が可能である。発生する液滴径と重要な関係があるとされるメニスカスまたはコーンの帯電、液ジェット、コーン中の流れの機構などの研究も最近報告されている[10-12]。

4． 液滴径の推算式

また､液滴径と操作条件との関連性を示す経験および非経験的な推算式 (Scaling laws) も多く報告されている[8,12-15]。ここで操作条件とは、主に液体の導電率、表面張力、粘度、密度、比誘電率などと噴霧電極の構成、液体流量、雰囲気の物性などが主にあげられる。そのうち、ここでは、噴霧液体が極性をもち（比誘電率$\varepsilon >> 1$）、導電率Kが10^{-5}S/m以上の溶液のcone-jet モードのみの場合に適応できるFernandez de la Moraら[8,12]が提案した式を簡単に述べる。彼らは、液滴径は液体の流量と物性に影響されるものの、電極の構成、電界の強度（電圧）とほぼ無関係であること示した。またcone-jetモードの形成が可能となる最小液体流量をQ_{min}をとすると、流量Q（$Q/Q_{min} < 16$）以内では単分散の液滴のみが発生する範囲となることも示した。ここで液滴径D_dは、液柱の径D_jおよび electrical relaxation length r*と同じオーダーである。それらの関係は次の式で表される。

$$Dd = G(\varepsilon)\ r^* \qquad (1)$$

$$r^* = (Q\varepsilon\varepsilon_o / K)^{1/3} \qquad (2)$$

ここでε_0は真空の比誘電率である。Gの値は、液体の粘度mまたは表面張力γにも少し影響されるが、主に液体の比誘電率εに依存する。G,εの文献からの値をTable 1に示す。つまり、液体の流量Qおよび主な物性（ε,K）が既知の値であれば発生する液滴径Ddが推測できることになる。

しかし、静電噴霧の研究は現在のところ操作条件の影響による液体コーンや噴霧状態のメカニズムを説明できる理論が確立されるには至っていない。

5． 静電噴霧の応用

発生する液滴径が数nm[16]から数mmと広い範囲で、かつ単分散性が比較的良好（幾何標準偏差σ_gが1.1 以下)な液滴が得られるので、静電噴霧法がいろいろな分野に応用されている[17]。近年では、質量分析装置のイオン源としての応用が非常に盛んになっている[18]。

5.1. 静電噴霧法による微粒子の製造

既に60年代に、静電噴霧法は、帯電金属粒子またはイオンの発生装置[19]として使用さ

Table 1. G(ε) の値[25]

ε	G(ε)	備考
~40	0.76	液柱の径を直接測定
20	0.68	液滴の aerodynamics径を測定
80	0.60~1.10	phase Doppler anemometryより水のD_dを測定
111	0.74	ホルムアミド溶液、K: ~1 S/m 、超音速インパクタよりD_dを測定
81	0.648	広範囲のKをもつ水溶液
6	1.8	ベンジルアルコールおよびセバシン酸ジブチル, K =: 2.4 ~ 4.5 x 10^{-3} S/m

Table 2. 静電噴霧法で製造される機能性微粒子の一例

微粒子 組成	噴霧溶液 溶質／溶媒	粒径 (平均、μm)
Sn, Bi	溶融体	150 - 600
Cu, Pd, Ta, Mo	溶融体	<36, - 147 (Pd)
Al_2O_3	溶融体	0.01 - 300
Sn60/Pb40, Sn, Ga , Wood's metal	溶融体	0.2 - 2
SiO_2	水ガラス／ベンゼン	30-500
ZrO_2 (-Y_2O_3)	酢酸塩／水	1.7
SnO_2	酢酸塩／ethanol	0.5-8
Y_2O_3	硝酸塩／n-propanol	0.17 - 0.29
ZnS, CdS	硝酸塩、チオ尿素／ethanol	0.06-0.15

れた。その後、液滴または粒子径は数100μm以上と大きいものの、固体粒子の生成も報告されはじめた。Table 2 に静電噴霧法で製造した機能性微粒子の一例を示す。これらの

製造法は大まかに３つのタイプに分類できる。

(Type-A)原料そのものまたは金属を細管中で高温に加熱し、溶融状態にして静電噴霧化させる。この場合、冷却または凝固過程を経てから粒子が生成され、対向電極板などに粒子が付着する。溶融体の表面張力が高いため、コーンの形成および静電噴霧を行うには数10kVと比較的高い直流電圧が必要となる。また径がサブミクロンから数100 μmの範囲で、ほぼ球形の粒子の生成が可能である。

(Type-B) キャリアガスを使用せず、噴霧部の細管より発生した比較的大きい液滴を直接液体中に導入し、液中で反応などをさせて、粒子を生成する研究も行われている。

（Type-C、静電噴霧熱分解法）噴霧部より溶液の液滴を発生させキャリアガスにより高温場に導入し、溶媒を蒸発させることにより、反応または熱分解を経る場合である。まず安定な溶液のコーンや噴霧状態を形成できる溶液の選択が重要な問題になる。この場合、表面張力が特に低いなど溶液の物性によりType-Aに比べて比較的低い電圧で静電噴霧が可能となり、粒径もほとんどサブミクロンまたはそれ以下の機能性微粒子が生成される。反応部における液滴の蒸発過程によって、球形粒子の他に中空粒子が生成する。

5.2 静電噴霧熱分解法による金属硫化物微粒子の製造

ここでは、著者らの金属硫化物微粒子（硫化カドミウム CdSおよび硫化亜鉛 ZnS ）の製造実験[20,21]について述べる。原料溶液としては硝酸カドミウム ($Cd(NO_3)_2$)または硝酸亜鉛 ($Zn(NO_3)_2$)とチオ尿素 ($(NH_2)_2CS$)を常温下で溶媒であるエタノールに溶かしたものを原料溶液とした。

Fig.2に著者らが用いた静電噴霧熱分解法による微粒子製造装置のフローシートを示す。主に、本装置は試料溶液を液滴にする静電噴霧発生部、粒子が生成される反応部、生成粒子の電気移動度分布を測定する測定部、および粒子を捕集する捕集部より構成されている。測定部には凝縮核計数器 (Condensation Nucleus Counter, CNC)と微分型静電分級器 (Differential Mobility Analyzer, DMA)を用いた。最初の研究[20]では、生成する粒子濃度を高くするために、液体供給電極を4本の金属細管、対向電極をポーラスディスク型金属製の板から構成された静電噴霧発生部を用いた(Fig.2-a)。

静電噴霧で発生した帯電液滴は、高い電気移動度をもっているので壁などへの沈着の問題が生じる。そこで、噴霧チャンバーから出る液滴の個数濃度を上げるために、改良されたチャンバー[21]では、Am-241より放射されるα線を用いてイオン化された雰囲気によって帯電液滴を中和した。

反応部は、内径15mm、長さ100および200mmのガラス製円筒とそれを囲む加熱部からなっている。キャリアガスとして不活性ガスであるN_2ガスを用いた。また、捕集器で回収した微粒子の結晶性の評価は、X線回折法により行い、粒子径及び粒子形状はDMA-CNCおよび電子顕微鏡写真により観察した。生成した粒子径および粒子形状などについ

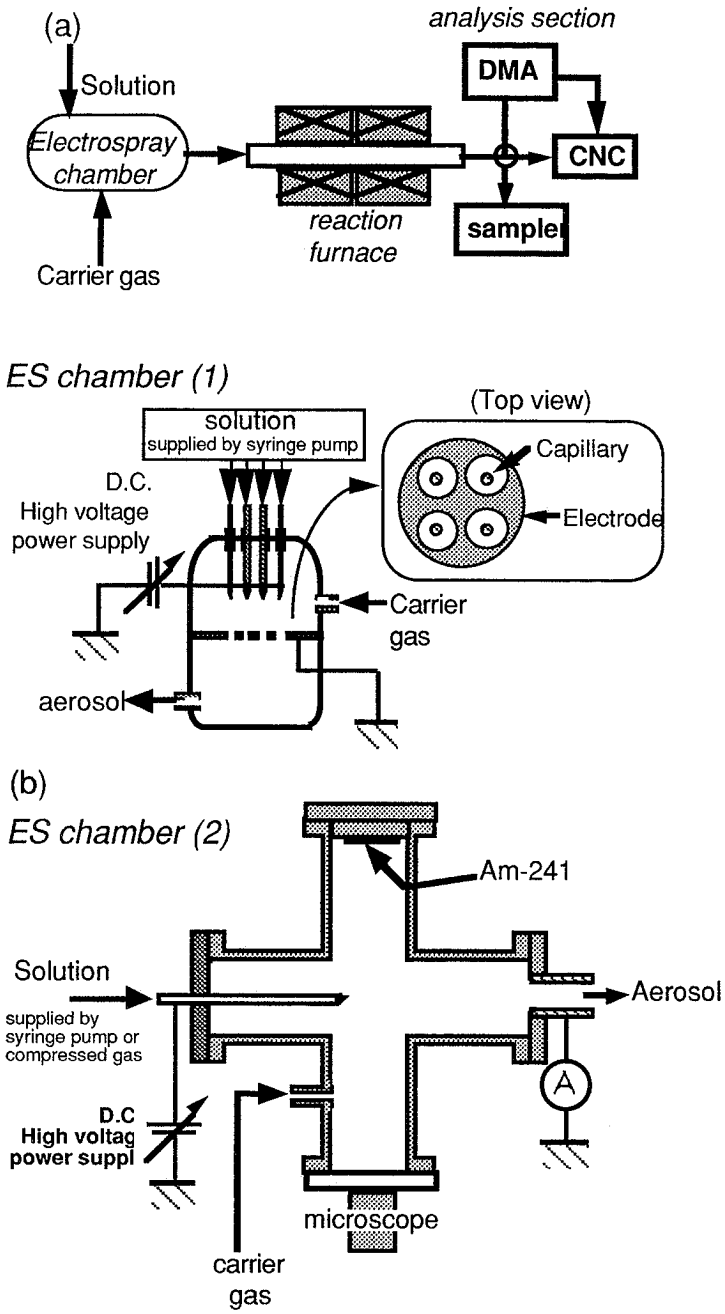

Fig.2　(a) 静電噴霧熱分解法による微粒子製造装置及び噴霧チャンバー（1）の詳細, (b) 噴霧チャンバー（2）の詳細

て従来利用してきた超音波噴霧熱分解法[22]により生成した微粒子との比較を行った。

噴霧する溶液の濃度は10^{-3}～10^{-1}mol/lオーダーの範囲で変化させた。これによって、溶液の導電率は10^{-4}～10^{-1}S/mと三桁にわたって変化し、安定なcone-jetモードを形成できる流量が0.05～0.15ml/hであった。Fig.3に、同じ濃度の噴霧溶液を用いて、超音波および静電噴霧熱分解法で生成されたCdS微粒子のSEM写真(a)、ZnS微粒子のTEM写真(b)を示す。いずれの場合も、超音波噴霧熱分解法（US）で得られた凝集粒子の径より、静電

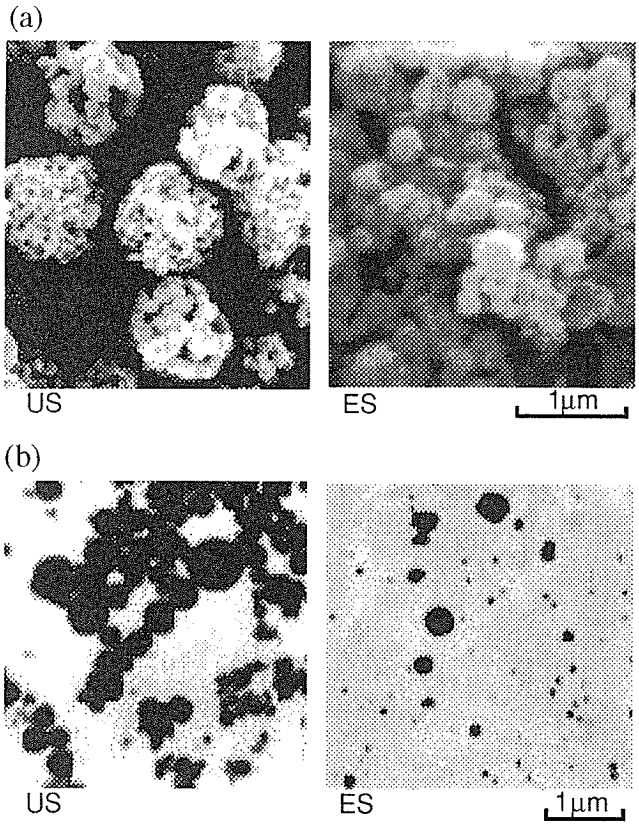

Fig.3 (a)CdSおよび(b)ZnS微粒子のSEM/TEM写真（溶液濃度は0.05mol /l)

噴霧熱分解法（ES）で得られた凝集粒子の径がかなり小さく、0.1 μm 以下の超微粒子が生成可能であることがわかった。

蒸気圧が高く、蒸発しやすい溶液を使用したため、発生する液滴径を直接測定するのが困難であるので、Scaling-lawsの適用により液滴径の推算を試みた[21]。まず、溶液の比誘電率εおよび表面張力γとして、溶媒であるエタノールの値を用いた。εは24.3およびγは0.02275N/mであるので、式（1,2）におけるGの値は約0.60となる。また、噴霧溶液流量が既知の値であるので、式（1,2）を用いて発生する液滴の径が推算できた。Fig. 4-aには、Scaling-lawsによって計算された液滴径の大きさの範囲を示す。流量の変化にそれほど依存せず、溶液濃度C_sが高くなると導電率Kも増加し、液滴径が小さくなることがわかる。溶液濃度C_s=0.0025 mol/lでは665±50nmとなり、C_s=0.2mol/lでは163±13nmとなる。

また噴霧熱分解法において、生成される微粒子の粒径 d_p は、1個の液滴 より 1 個の微粒子（密度 ρ）が生成されると仮定すると、液滴の粒径 D_d と溶液の濃度 C_s により、

$$d_p^3 = (M D_d^3 C_s) / 1000 r \qquad (3)$$

で求められる。ZnS粒子の生成の場合は、M = 97.46 およびρ = 4.09 g/cm^{3}であるので、式（3）は次式となる。

$$d_p = 0.288 D_d C_s^{1/3} \qquad (4)$$

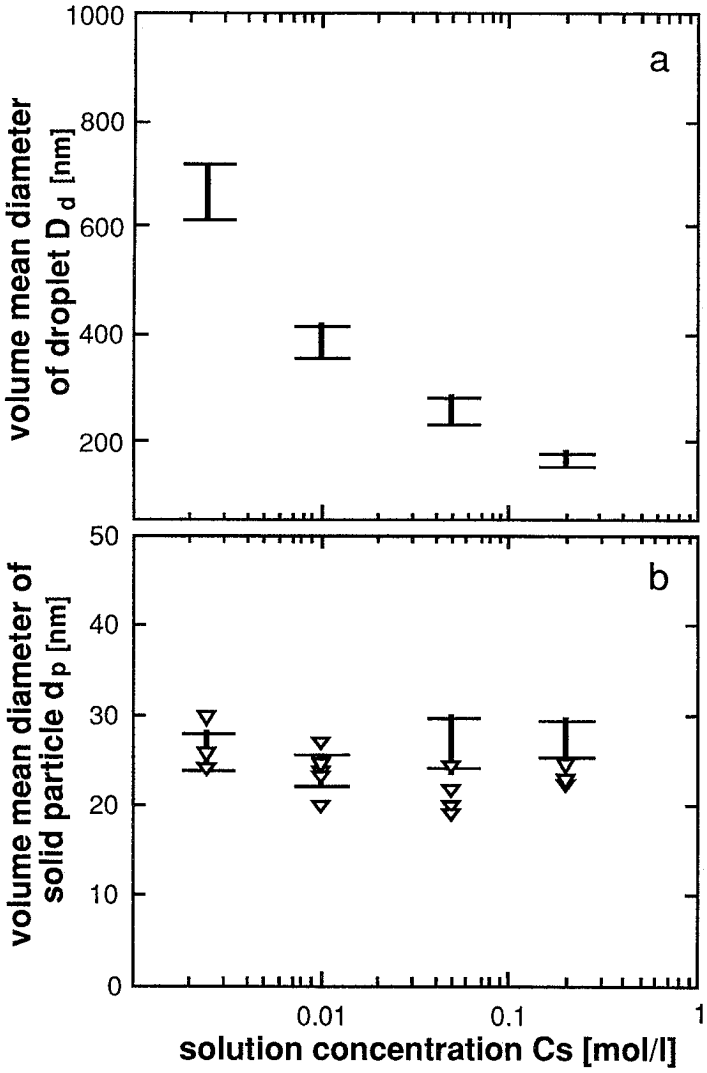

Fig.4 (a) 各溶液濃度（ZnSプリカーサー）におけるScaling Laws [G (ε) =0.6] より推算された液滴径D_dの範囲. (b) (a) のD_dより転換されるZnS粒子径の範囲.
プロット（▽）はDMACNCより測定した実験値

ただし、この式には、蒸発などによる液滴表面での核発生、成長および破裂などが生じていない緩やかな蒸発による粒子の生成の場合に適用できる。

Fig.4-bでは、Fig.4-aで得られた液滴径D_dより式(4)を用いて計算された粒子径d_pの範囲を示す。特に溶液濃度C_sが低い場合において、DMA-CNCで得られた実験値（プロット▽）と、かなり良好な結果を示した。これによりScaling-laws[19]は、静電噴霧熱分解法における生成粒子の径をある程度推測できることがわかった。また今後、主な操作条件である流量および導電率を検討すれば10nm 程度の超微粒子の生成がより容易に行われることが期待される。

6. おわりに

微小な液滴の発生が可能である静電噴霧、静電噴霧法による機能性微粒子の製造を中心に述べた。生成した液滴および粒子径が他の噴霧法より小さくなるという良い結果の一方、特に静電噴霧熱分解法では生産速度が低いという課題がまだ残っている。この問題の解決も含めて、粒径が0.1 μm 以下の超微粒子の製造を目的とする研究が少ないので、今後微粒子材料の機能性などと関連させながら、静電噴霧の理論および実験的な研究の展開が大いに期待される。

引用文献

1. Gurav, A., Kodas, T., Pluym, T. and Xiong, Y. (1993) Aerosol Sci. Tech., 19, 411-452
2. Meshing, G. L., Zhang, S.C. and Jayanthi, G. (1993) J. Am. Ceram. Soc., 76, 2707-2726
3. Lenggoro, I. W.、奥山喜久夫、微粒化、, 6 (1997) 15-20
4. Zeleny, J., Phys. Rev., 3 (1914) 69-91; Proc. Camb. Phil. Soc., 18 (1915) 71-83; J., Phys. Rev., 10 (1917) 1-6
5. Taylor, G.I., Proc. Roy. Soc. London, A280 (1964) 383-397
6. Cloupeau, M. and Prunet-Foch, B., J. Electrostatics, 22, (1989) 135-159; J. Electrostatics, 25 (1990) 165-184; J. Aerosol Sci., 25 (1994) 1021-1036
7. Smith, D. P. H., IEEE Trans. Ind. Appl., IA-22 (1986) 527-535
8. Rosell-Llompart, J. and Fernandes de la Mora, J., J.Aerosol Sci., 25 (1994) 1093-1120
9. Grace, J.M. and Meesters, G.M.H., J. Aerosol Sci., 25 (1994) 1005-1020
10. Hayati, I., Bailey, A. I. and Tadros, Th. F., Nature, 319 (1986) 41-43
11. Fernandez de la Mora, J., J. Fluid Mech., 243 (1992) 561-574
12. Fernandez de la Mora, J. and Loscertales, I. G. , J. Fluid Mech.,260 (1994) 155-184
13. 森康夫、土方邦夫、長崎孝夫、日本機械学会論文集、47 (1985) 1881-1890
14. 山口学、松井章、村上英樹、片山俊、化学工学論文集、21 (1995) 357-364
15 Ganan-Calvo, A. M., Davila, J. and Barrero, A., J. Aerosol Sci., 28 (1997) 249-275
16. Benassayag, G., Sudraud, P. and Jouffrey, B., Ultramicroscopy, 16 (1985) 1-8
17. Michelson, D.: Electrostatic Atomization, Hilger, New York (1990)
18. Fenn, J. B., Mann, M., Meng, C. K., Wong, S. F. and Whitehouse, C. M., Science 246 (1989) 64-71
19. Mahoney, J. F., Yahiku, A. Y., Daley, H. L., Moore, R. D. and Perel, J., J. Appl. Phys., 40 (1969) 5101-5106
20. 奥山喜久夫、I. W. Lenggoro、田上敬一、玉城真吉、 峠 登、粉体工学会誌、33 (1996) 192-198
21. Lenggoro, I. W., Okuyama, K., Fernandez de la Mora, J. and Tohge, N., J. Aerosol. Sci., 投稿中
22. Okuyama, K., Lenggoro, I. W., Tagami, N., Tamaki, S. and Tohge, N., J. Mat. Sci., 32 (1997) 1229-1237

7.5 Effect of electrostatic properties of spray solution on the nanometer-sized metal sulfide particles preparing by the electrospray pyrolysis

Effect of electrostatic properties of spray solution on the nanometer-sized metal sulfide particles preparing by the electrospray pyrolysis

1 Introduction

Spray-pyrolysis is a representative droplet-to-particle conversion process. With considerable advantages such as low cost and simplicity, this technique has been applied to the preparation of a variety of functional material particles and thin films (Gurav et al., 1993; Messing et al., 1993). In this spray pyrolysis technique, aqueous solutions of metal salts are usually used as spray solutions and the droplets are subsequently pyrolyzed to become solid particles. The average size of the final solid particle can be roughly determined from the droplet size and the solute concentration of the solution sprayed. Most authors have used various typical atomizers such as twin fluid or ultrasonic nebulizer to generate the droplets. These atomizers can produce droplets of an average size in the range of several microns. For a typical initial droplet diameter of 5 μm in diameter to dry into a particle with diameter of 0.1 μm, the initial volume fraction of dissolved involatile solute must be less than 0.0008 %. In practice, these low concentrations of the solution may lead to a low particle generation rate and may affect the purity of the particles as the final products. In the other words, the preparation of ultrafine material particles below 0.1 μm via a spray pyrolysis method is still a problem.

Continuing a series of studies on the production of functional fine particles of

metal sulfide (Tohge et al., 1995; Tamaki et al., 1995, 1996) by an ultrasonic spray pyrolysis, we have succeeded in producing size-controlled zinc sulfide (ZnS) and cadmium sulfide (CdS) particles by changing the solution concentrations (Okuyama et al., 1997). In those studies, an ultrasonic nebulizer which could generate droplets of 4.56 μm in average diameter was used and 0.2~1.5 μm ZnS or CdS fine particles were prepared by varying the solution concentrations from 0.001 to 0.3 mol/l.

The electrospray technique has been studied as a method which can produce ultrafine droplets. In this method, a meniscus of spray solution at the end of the capillary tube becomes conical when charged to a high voltage (several kV) with respect to a counter electrode. The droplets are stably formed by the continuous breakup of a jet extending from this liquid cone, generally called a "Taylor cone" (Taylor, 1964). A variety of experimental studies have shown that the diameter of such jets and drops may be controlled from nanometer (Benassayag et al., 1995) up to hundreds of micrometers (Jones and Thong, 1971) mostly through the electrical conductivity of the liquid or the flow rate (e.g., Smith, 1986; Rossel-Llompart and Fernandez de la Mora, 1994; Ganan-Calvo et al., 1997). Recently, Chen et al. (1995) reported the production of monodispersed droplets in the range of 40 nm to 1.8 μm using sucrose solutions with different electrical conductivities ranging from 1.56×10^{-3} to 8×10^{-1} S/m.

Electrospray has recently become quite familiar in the analytical chemistry area as an ion generation method for mass spectrometry (Fenn et al., 1989). There are some reports on particle productions using the applications of electrospray (e.g., Bollini et al., 1975; Mahoney et al., 1987; Levi et al., 1988) and the electrospray pyrolysis (Slamovich and Lange, 1990; Park and Burlitch; 1992; Rullison and Flagan, 1994a). As a preliminary study, Okuyama et al. (1996) have also reported that ultrafine ZnS and CdS particles below 0.1 μm in diameter could be made by an electrospray pyrolysis method. In that study, however, the spray functioning mode could not be

fully determined as a function of spray liquid flow rate or applied voltage. Also, the precise influences of the concentration or the physical properties of the solutions on the size of generated solid particles remains unclear.

In this study we control the spray liquid flow rate, the applied voltage and the solute concentration, and make sure that we operate under stable spray conditions in so-called cone-jet mode (Cloupeau and Prunet-Foch, 1989, 1990, 1994). The particles generated are measured by a differential mobility analyzer and a condensation nucleus counter system, and their sizes are compared with those expected after drying from available scaling laws. Also by sampling the particles, the suitability of electrospray pyrolysis to generate nanometer-sized spherical ZnS fine particle is investigated.

2 Experimental apparatus and procedure

Figure 1 (a) shows the experimental system used for the investigation of the effect of experimental conditions on the physical characteristics of obtained ZnS fine particles. This system consisted of the following sections: (i) an electrospray source, (ii) a reaction furnace, and (iii) an analysis section; a differential mobility analyzer (DMA, TSI model 3071), a condensation nucleus counter (CNC, TSI model 3020) and a handmade thermophoretic sampler.

In earlier studies on the preparation of ZnS and CdS particles using ultrasonic spray pyrolysis, water was used as solvent. Meanwhile, the main difficulty encountered in electrically spraying water solutions lies in the large surface tension of this liquid, that requires very high applied voltages for the establishment of a stable spray. If the surface tension of the liquid is sufficiently large, as in the case of pure water, the necessary applied voltage may be higher than the electrical breakdown threshold of the surrounding gaseous medium, usually air, and corona discharge would follow (e.g., Smith, 1986). An alternative way to solve this problem going back to Zeleny (1915) is to flow a sheath gas with relatively high electrical breakdown

threshold to prevent or delay the onset of corona discharge. Examples of such suppressing gases are SF_6 or CO_2 (Tang and Gomez, 1994; Rullison and Flagan, 1994a, 1994b; Chen et al., 1995).

In this study nitrogen was used as a sheath gas to avoid oxidation of the Zn in the final product. Ethanol was chosen as the solvent to dissolve the solute containing zinc nitrate ($Zn(NO_3)_2$) and thiourea ($SC(NH_2)_2$) as a source of Zn and S, respectively. The molar ratio of Zn : S was kept constant at 1:2. Ethanol solvent had a good solubility to the solutes. And because of the low surface tension of ethanol, a stable cone of the solutions could be formed at a voltage below the electrical breakdown threshold of nitrogen.

As described in equation 1, thiourea and zinc nitrate form a complex in the solution. Then the droplets containing the complex are pyrolyzed to synthesize directly ZnS particles at a furnace temperature around 600°C which is necessary to drive the reaction (Okuyama et al., 1997).

$$Zn(NO_3)_2 + (NH_2)_2SC \rightarrow Zn(SC(NH_2)_2)_2(NO_3)_2 \rightarrow ZnS \qquad (1)$$

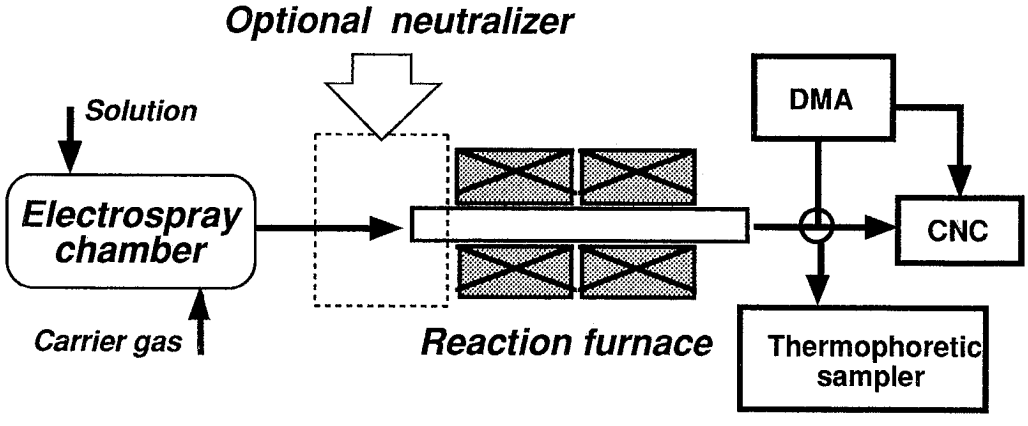

Fig.1 Experimental apparatus of electrospray pyrolysis
(a) Schematic of the overall system.

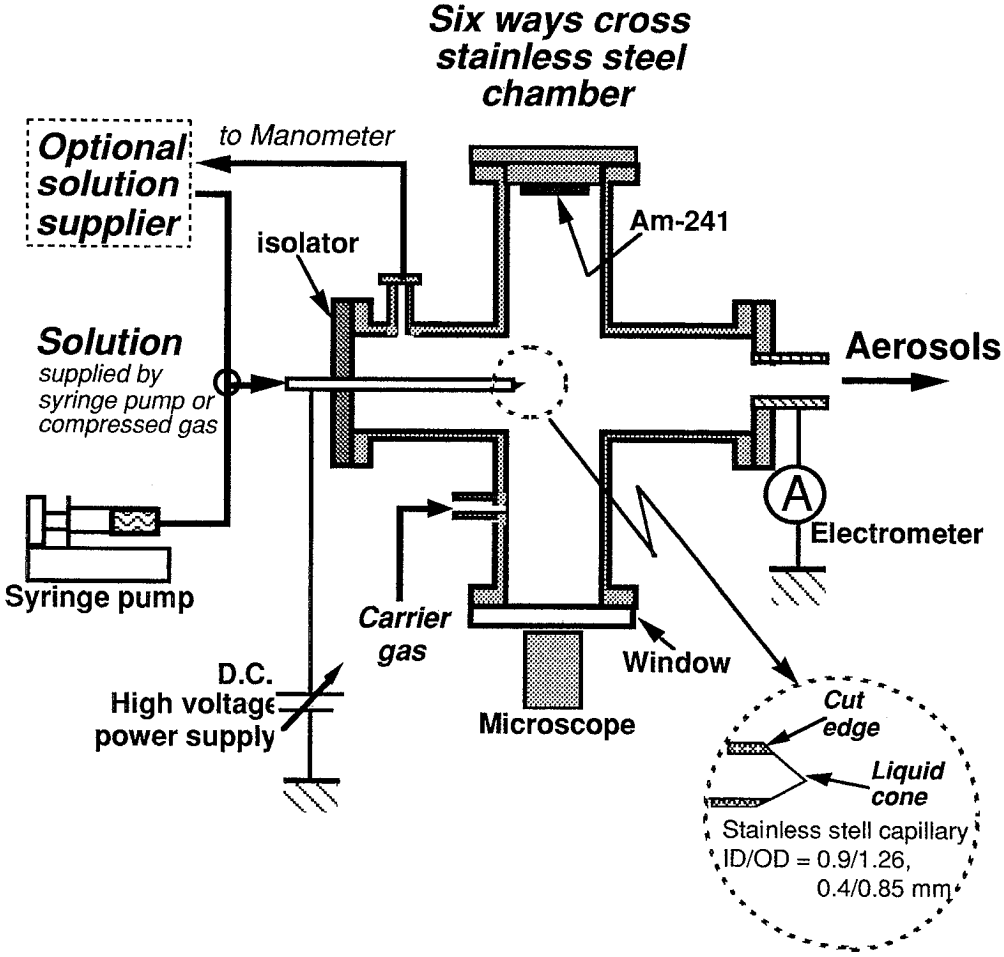

Fig.1 Experimental apparatus of electrospray pyrolysis
(b) Electrospray chamber

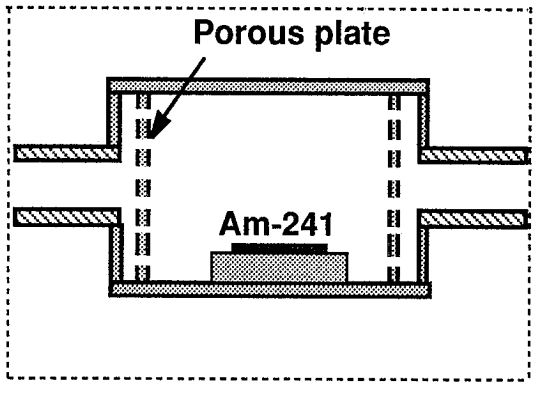

Fig.1 Experimental apparatus of electrospray pyrolysis
(c) Optional neutralizer

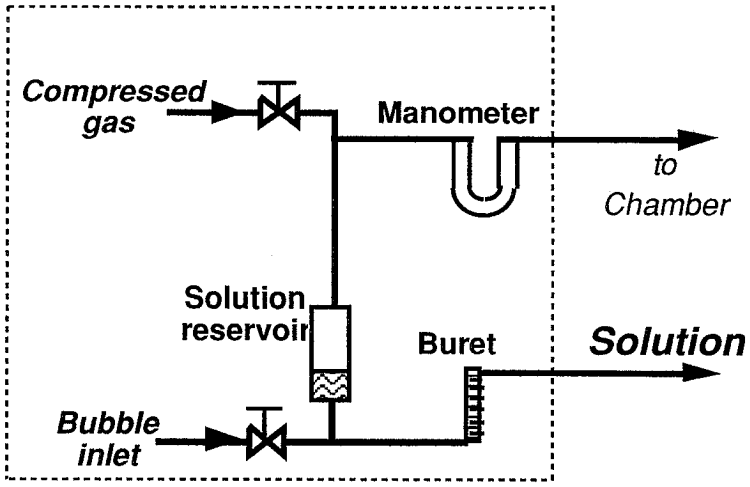

Fig. 1 Experimental apparatus of electrospray pyrolysis
(d) Optional solution supplier

Nitrogen is used as a suitable inert carrier gas, because air or CO_2 would lead to the formation of ZnO as well as ZnS. Flow rate was kept constant at 1.0 l/min.

Table 1 shows the physical properties of the solvent and solutions used. Four different solution concentrations C_s were prepared as spray liquids. Increasing C_s by two decades did not change substantially the density ρ and viscosity μ of the liquid, but increased its electrical conductivity K by about 35 times as seen from the comparison of the highest C_s with the lowest C_s, and by 1600 times with respect to the unseeded solvent. The most important physical property of the solution controlling both the stabilility of the electrospray (Cloupeau and Prunet-Foch, 1989; Tang and Gomez, 1996) and the droplet size is known to be the liquid electrical conductivity K. This study thus focused on this parameter among the liquid physical properties. Notably, the value K around 0.2 S/m is fairly large in relation to typical literature values. The electrical conductivity of the solutions was measured by a conductivity meter (Toko Chemical Inc., TX-90) at 25°C, the liquid density and viscosity were measured by an Ostwald type pycnometer and a viscometer, respectively.

Table 1 Physical properties of solvent and solutions

C_s [mol/l]	ρ [kg/m^3]	μ mPa.s	K [S/m]
0	788.9	1.207	1.20×10^{-4}
0.0025	789.6	1.220	5.62×10^{-3}
0.01	791.5	1.243	2.01×10^{-2}
0.05	801.4	1.365	6.53×10^{-2}
0.20	838.8	1.822	1.92×10^{-1}

The liquid was sprayed inside a six ways cross stainless steel chamber (Fig.1 (b)). Two of the opposing sides were used for supplying the spraying liquid and sampling the generated aerosols. Positive and negative D.C. high voltage sources (Matsusada Co. Ltd., HER-10R3) were connected to the stainless steel capillaries. Two such capillaries were used, having inner/outer diameters: 0.90/1.20 and 0.40/0.88 mm. These are referred as the "large" and the "small" capillaries, respectively. Each capillary tip was tapered down to nearly zero thickness. The liquid was supplied to the capillary either through a programmable syringe pump (Harvard Apparatus, Model 55) fixing a constant flow rate, or by introducing compressed nitrogen above the sample liquid inside a vertical syringe (Fig.1 (d)). The flow rate of solution was calibrated by measuring the moving velocity of a gas bubble injected into the solution line through a buret.

Expecting to prevent the evaporation of solvent at the cone, an attempt was made to saturate the nitrogen gas with ethanol vapor by passing it through an ethanol reservoir. A precipitate, however, still appeared at the capillary tip after running times of tens of minutes at solution concentrations ranging from 0.05 to 0.2 mol/l.

At the opposing side of the spray capillary, a stainless steel tube having inner

diameter of 5 mm was placed as a sampling tube. The distance from the sampling tube to the capillary was adjustable, but was kept at 40 mm for most runs. This sampling tube was grounded through an electrometer (Keithley, model 485) for measuring the electric current brought by the droplets that were deposited onto the sampling tube and the chamber wall. This allowed monitoring the stability of the electrospray. The noise level of the electrometer was maintained as low as 1.0 nA. The spray capillary electrode and sampling tube were set horizontally to facilitate the connection of the spray chamber to a furnace or a DMA - CNC system (Fig.1 (a)). Another pair of opposing sides of the chamber are windows for monitoring the meniscus shape at the capillary tip through a 30X microscope set at one side and a continuous light source at the other.

The droplets generated in an electrosprays are always highly charged. Due to their high electrical mobility, the droplets tend to have high deposition rates onto the walls, which decreases their overall throughput efficiency. To reduce their electrical mobility and to produce finer aerosols by evaporation without Rayleigh disintegration, it is necessary to neutralize of the droplet. Electrical neutralizations of electrosprayed droplets through a source of ions of the opposite polarity has been reported by Meester et al. (1993) prior patent cited by Tang and Gomez (1994). Clopeau (1994) suggested four possible neutralization methods; a unipolar type corona discharge, electrospray of volatile liquids, thermoelectric emission, and flames. Recently, the applications of a radioactive bipolar ion source as the neutralizer for electrospray drops was reported by Lewis et al. (1994), Chen et al. (1995) with two Po-210 (370 MBq) and Rullison and Flagan (1994b) with one Po-210 (185 MBq).

Because of the simple setting and the ability of stable ion generation, an α-ray radioactive source was used in our device. Am-241 (2.22 MBq) was placed at several millimeters-frontward at the upper part of the tip of a liquid cone where the droplets were approximately ejected from the jet. The neutralization of the droplets could be

made, because the chamber was filled with bipolar ions from Am-241. The distance between the capillary tip and the neutralizer was kept at around 45 mm, above the range of α-ray from Am-241 (40 mm).

To test the effectiveness of the neutralizer, the CNC was placed at the outlet of the spray chamber by counting the total generated particles. From the measurement, the number concentration of generated particles increased from order of 10^2 or 10^3 up to 10^6 particles/ cm^3. This increasing tendency was also obtained when a neutralizer with Am-241 was located between the spray chamber and the furnace, as descibed in figure 1(c). Since the neutralization of particles could greatly improve the throughput efficiency of the generated particles, the Am-421 source was installed in all subsequent experiments.

The droplets generated were introduced from the spray chamber into a reaction furnace using nitrogen carrier gas. In order to reduce the loss of particles, a relatively short tubular furnace was used; a quartz glass tube of 20 mm inner diameter and 200 mm long which consisted of two independently-controlled heating-zones 10 cm long. The residence time inside the furnace was estimated to be 1.5 s for 1.0 l/min of carrier gas flow. All experiments were made at atmospheric pressure and room temperature.

The use of a DMA-CNC system for the size analysis of electrosprayed particles has been reported earlier (Lewis et al., 1994; Rullison and Flagan, 1994 a, 1994b; Chen et al., 1995). Without using the neutralizer, de Juan and Fernandez de la Mora (1997) also used DMA to measure their involative liquid sprays before introducing those droplets into an aerodynamic size spectrometer (API's Aerosizer).

Here, a DMA and a CNC are placed at the outlet of the furnace. The size of the solution droplets generated is further reduced by the evaporation process and, finally, the size distributions of the resulting ZnS particles were analyzed on-line. The sheath air in the DMA is set to 10 l/min and the flow ratio of aerosol to sheath air is kept at 0.1. A thermophoretic sampler with a 150-mesh brass grid is placed at the outlet of the furnace. Some transmission electron microscopy (TEM) photographs were obtained to

verify and support the data obtained from the DMA-CNC system.

3 Experimental results

3.1 Determination of the stability domain of the cone-jet

Before measuring the particle size distributions, one must distinguish and control the regime at which the liquid cone and the spray operate. A different spray mode may lead to quite different drops size distributions for a given solution (e.g., Cloupeau and Prunet-Foch, 1989). Figure .2 shows typical curves of the electric current versus the applied voltage of (a) ethanol and (b) 0.0025 mol/l solution performed without a neutralizer (Am-241) using the apparatus shown in figure 1. Flow rates fed by a syringe pump to the small capillary were kept constant at (a) 0.20 ml/h and (b) 0.08 ml/h. First, the applied positive voltage was increased gradually, and then reduced after the liquid meniscus at the capillary tip passed some spray modes. When the applied voltage was lower (character a at figure 2), the liquid on the capillary tip was changed from a meniscus to a dripping mode (Fig. 3 (a)). Increases in the frequency of the dripping and the current were observed with increasing applied voltage and it was referred to as the pulsating mode (Fig. 3 (b)). The shapes of liquid meniscus are alternating between cusp-like and approximately hemispherical. Increasing the voltage further increases the pulsating frequency, until the measured current increases drastically when the liquid meniscus formed a stable cone, a Taylor cone (Fig. 3(c)),

(caption of the figure depicted in the next page)

Fig.2 Typical current versus applied voltage curve of ethanol (**a**) and 0.0025 mol/l solution (**b**). Characters a, b, c, d indicate the formation of different liquid meniscus as described in fig. 3. Flow rates Q were 0.20 (**a**) and 0.08 ml/h (**b**). The measurements were performed at small capillary and positive applied voltage, without a neutralizer (Am-241) using the apparatus showed in fig. 1.

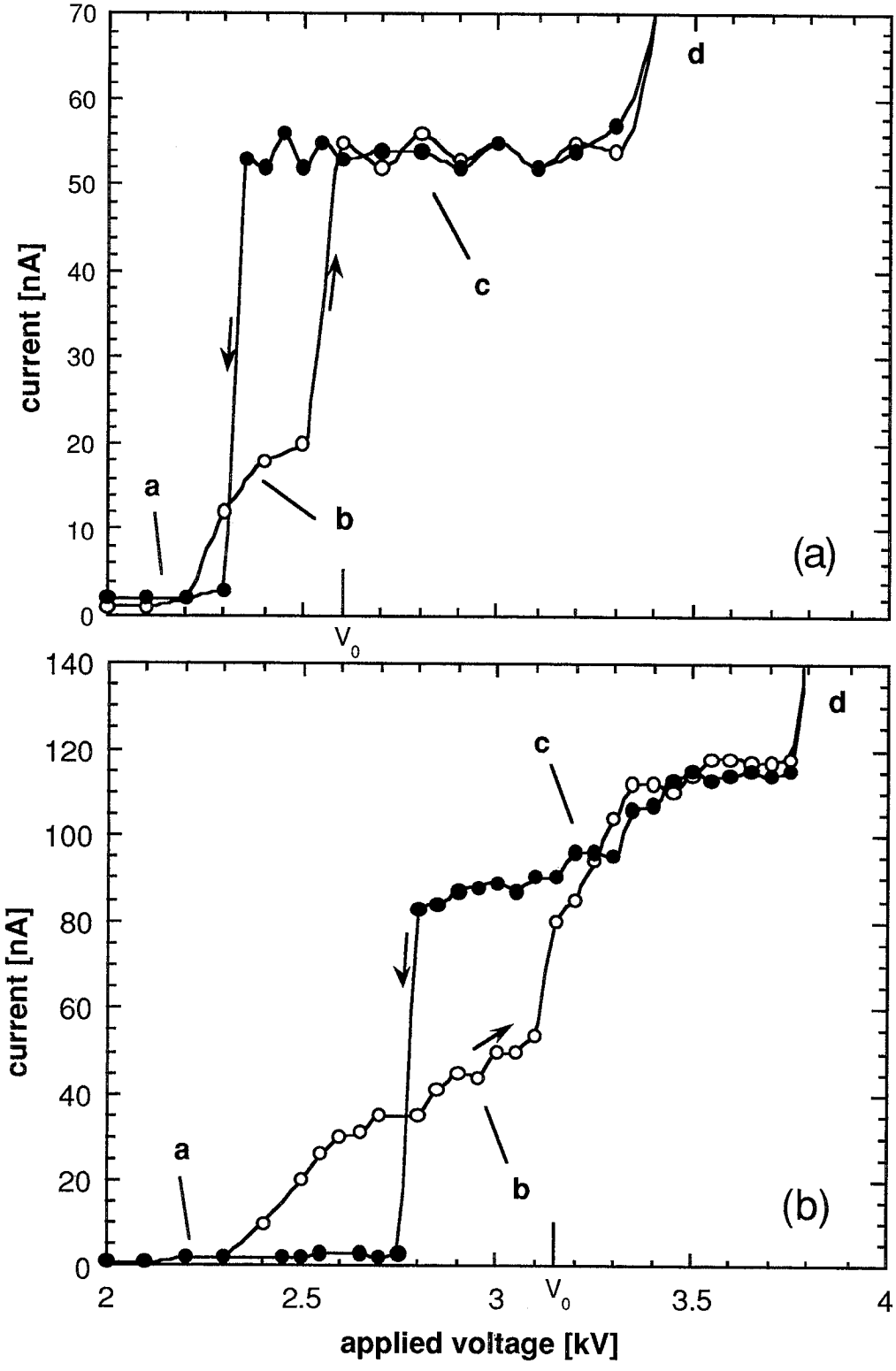
current [nA]
70
60
50
40
30
20
10
0
a
b
c
d
(a)
V_0
current [nA]
140
120
100
80
60
40
20
0
a
b
c
d
(b)
2
2.5
3
V_0
3.5
4
applied voltage [kV]

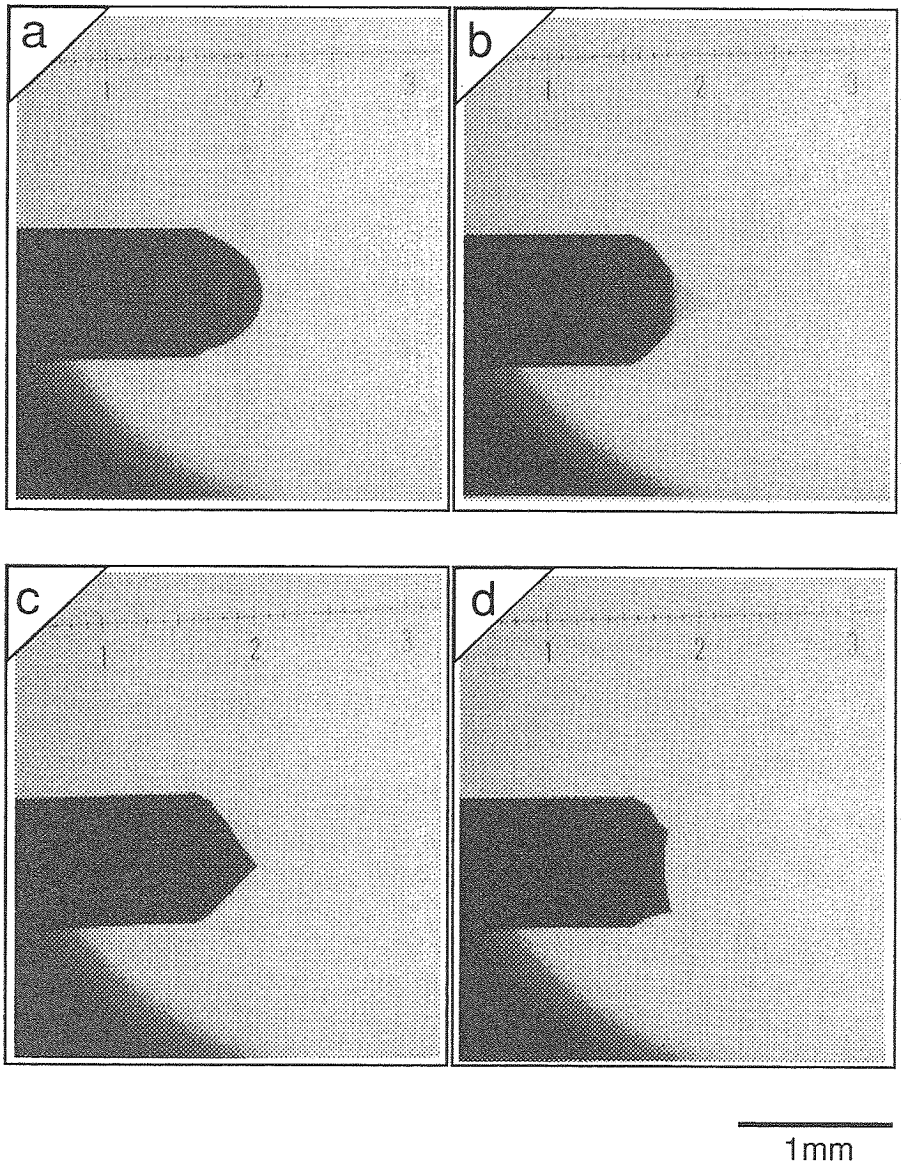

Fig.3 Photographs of the variants of liquid meniscus at capillary tip. (**a**) dripping mode, (**b**) pulsating mode, (**c**) stable cone-jet mode, and (**d**) multi-jet mode.

at a certain critical voltage. The formation of a stable liquid cone, in so-called cone-jet mode (Cloupeau and Prunet-Foch, 1989) was accomplished in a certain voltage range. When increasing the voltage at constant liquid flow rate, the volume of the liquid cone decreased and the cone angle increased. Figure 2 (a) shows that the electric current of ethanol was lower, due to its lower electrical conductivity, and did not change much with increasing voltage in the cone-jet mode, compared with the curve of 0.0025 mol/l solution (Fig.2(b)). At subsequent higher voltage, the currents and the cone suddenly became unstable and multi jets were frequently formed at the tip of the capillary (fig.3(d)). In the reverse-way, when reducing the voltage, the liquid meniscus (the cone) was formed similar to the modes in increasing-voltage, but there was a hysteresis loop in the cone-jet mode. Figure 2 was globally similar to that depicted in the voltage-current characteristic reported in other papers (Smith, 1986; Chen et al., 1995).

For a given solution concentration C_s, a stable cone-jet could be established only within a certain domain of flow rate Q and applied voltage V, $Q_{min}(V) < Q < Q_{max}(V)$, which was defined a stable cone-jet domain. Q_{min} and Q_{max} are the minimum and maximum flow rates within the stability domain. This domain was affected by C_s (electrical conductivity K), shifting toward smaller flow rate as C_s increased. The capillary size was found to affect the stable cone-jet domain of the electrospray as reported by Cloupeau and Prunet-Foch, 1989; Tang and Gomez, 1996. While Q_{max} was almost similar, Q_{min} increased as the capillary diameter increases. This may be due to larger evaporation of larger surface area of the cones of the large capillary which led to a higher rate of solvent evaporation. Considering $Q_{jet} = Q_{feed} - Q_{evap.}$, where Q_{jet} is the flow rate Q pushed through the jet, Q_{feed} is Q fed to the capillary and $Q_{evap.}$ is Q of the evaporated materials, for the constant Q_{jet}, $Q_{evap.}$ is larger for the case of the large capillary and Q_{feed} is also larger than the small capillary case. Consequently, the use of large capillary caused a narrowing of the stable cone-jet

domain of the electrospray.

The polarity also was found to affect the stable cone-jet domain. Negative voltage required higher flow rates, both Q_{min} and Q_{max}, than those of the positive polarity. However, corona discharge was frequently observed at a high voltage or at a high flow rate in the negative mode. The fact that spraying at positive polarity is more stable than at negative has been known at least since Zeleny's work.

In the high C_s, the first mode to appear is the cone-jet mode occasionally (Cloupeau and Prunet-Foch, 1994). As mentioned before, at C_s = 0.05 and particularly at 0.2 mol/l solutions, the salt precipitated on the capillary tip after several tens of minutes of operation time, even when the carrier gas was saturated with ethanol. This made the sampling of the particles difficult, since more than one hour is needed to obtain a suitable quantity of sample.

Due to differences in electrode geometry and liquid properties such as electrical conductivity, permitivity, viscosity, density, surface tension and vapor pressure, the range of liquid flow rates where we could form a stable spray was relatively narrow (Rossel-Llompart and Fernandez de la Mora, 1994; Cloupeau and Prunet-Foch, 1989; Chen et al., 1995). For instance, in the case of C_s = 0.0025 mol/l spraying at small capillary and positive voltage, Q_{min} was 0.09 and Q_{max} was about 0.20 ml/h. The narrowest range, i.e., the smallest ratio Q_{max} / Q_{min} was found at C_s = 0.2 mol/l, with Q_{min} = 0.05 ml/h and Q_{max} = 0.08 ml/h. No stable spray could be formed at any voltage in our system below 0.05 ml/h.

Since it was well known that lower flow rates of spray liquids generate smaller electrospray droplets, an attempt was made in this study to maintain Q near the minimum value Q_{min}. The fact is that the cone was most easily controlled and the fluctuation of the current was smallest near Q_{min} at a certain applied voltage V(Q).

3.2. Size distribution of ZnS particles

Using the DMA - CNC system, particle size distributions were measured at furnace temperature of 600 °C and at a liquid flow rate Q near or at the minimum value Q_{min} in each case. Figure 4 shows the influence of applied voltage and the liquid mode of electrospray on size distributions. In this example, the solution with concentration C_s = 0.01 mol/l was used and the flow rate Q was set at 0.10 ml/h. The particle size distribution function expressed by f (ln d_p) is

$$f(\ln d_p) = (Dn / D\ln(d_p)) / N \qquad (2)$$

and the data was relaxed with the method adopted from Adachi et al. (1990). Dn is the number concentration in the size (d_p) range, and N is the total particle number concentration. All the figures show a geometrical standard deviations σ_g of about 1.3. Figure 4 (a) shows the results for the pulsating mode with an associated volume mean diameter d_p of 32.6 nm. The particle size distributions for the cone-jet modes are showed in figure 4 (b) (3.15 and 3.5 kV), and the volume mean diameters d_p are finer than that in the pulsating mode. This is because in the pulsating mode two or more different shapes of liquid are involved and switching between them introduces different and larger breakup volumes (Cloupeau and Prunet-Foch, 1988, 1989; Chen *et al.*, 1995).

The effect of applied voltage on size distribution at the cone-jet mode is also shown in figure 4 (b). Droplet size was reported to be nearly independent of the applied voltage for almost liquids of somewhat high electrical conductivity and low flow rate (Rossel-Llompart and Fernandez de la Mora, 1994). On the other hand, Tang and Gomez (1996) also have reported on electrosprays of heptane at their relatively large flow rates (4 ~ 28 ml/h), that the droplet size decreased monotonically with the increase of the applied voltage. Figure 4 (b) shows that the volume mean diameter of obtained particles slightly increased with increasing applied voltage. Among the literature, this tendency is similar to the results recently reported by

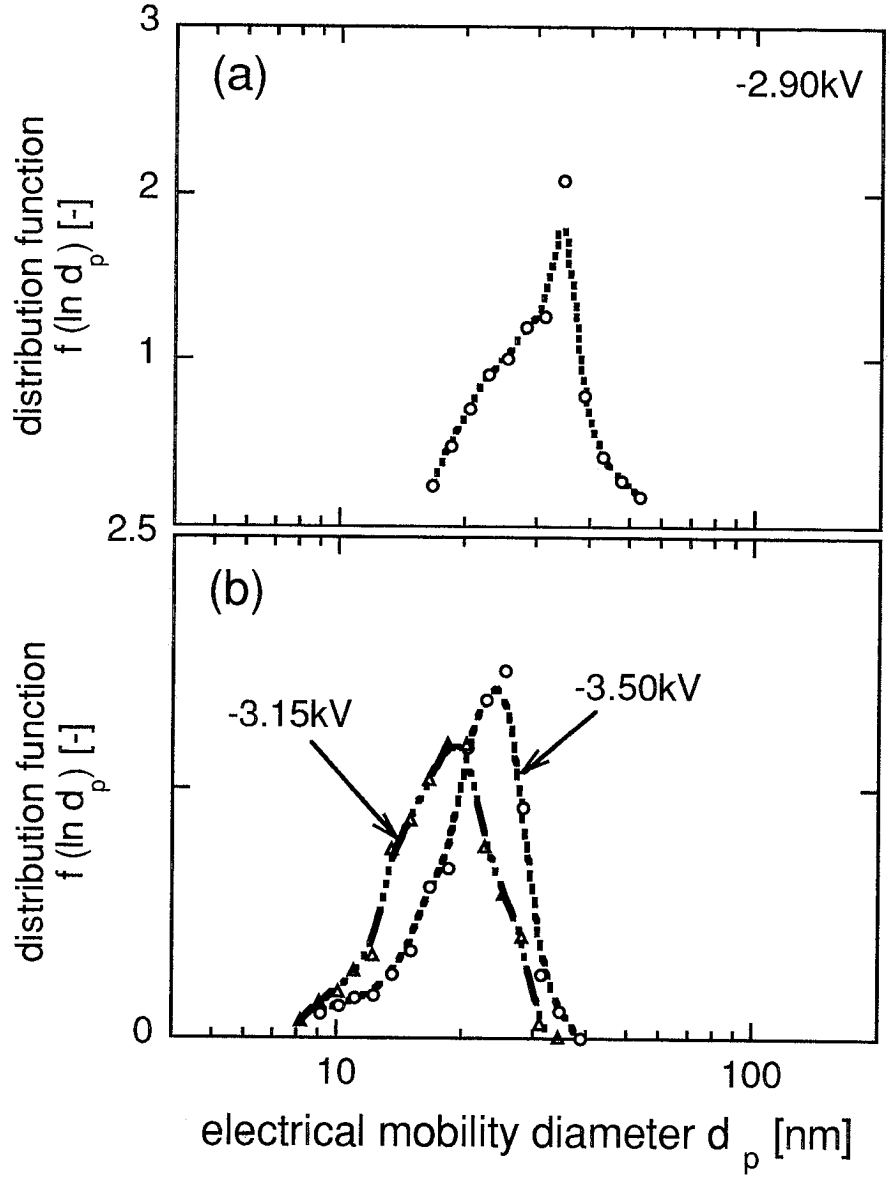

Fig.4 Measured particle size ditributions at (a) pulsating mode (2.90 kV) and (b) stable cone-jet mode: 3.15 and 3.50 kV, for the case of the solution concentration Cs = 0.01 mol/l and the flow rate was 0.06 ml/h.

Rulison and Flagan (1994).

Again, this may be due in part to solvent evaporation occuring at the cone. Since the droplet size is determined by Q_{jet}, while $Q_{feed} = Q_{jet} + Q_{evap.}$, for a constant Q_{feed}, the higher voltage forms smaller liquid cone (e.g., smaller $Q_{evap.}$), so Q_{jet} becames larger.

By varying the concentration of spray solutions C_s, figures 5 and 6 show the size distributions of particles generated at the cone-jet mode with small capillary at positive and negative voltage, respectively. The flow rates were set to near their minimum value Q_{min} where the most stable liquid cone could be obtained. In all of the cases showed, variations in C_s almost have no influence on the volume mean diameter in the distributions. The particles obtained in the case of large capillary (not shown) also suggested the insensitivity of the size distribution on the solution concentration.

The result of electrosprayed particle size distribution obtained with different polarities of applied voltage has not been reported in the literature in the past, while the result of the insensitivity of the particle sizes on the capillary size is in a good agreement with the general tendency in electrosprays (e.g., Rossel-Llompart and Fernandez de la Mora, 1994; Tang and Gomez, 1996).

The present results show the generation of ZnS particles with d_p ranging from 20 to 30 nm. In contrast, Rulison and Flagan (1994b) reported that the addition of solute to the solution made smaller solid particles since it also increased the electrical conductivity K which reduced the droplet size. These differences will be discussed in section 4.

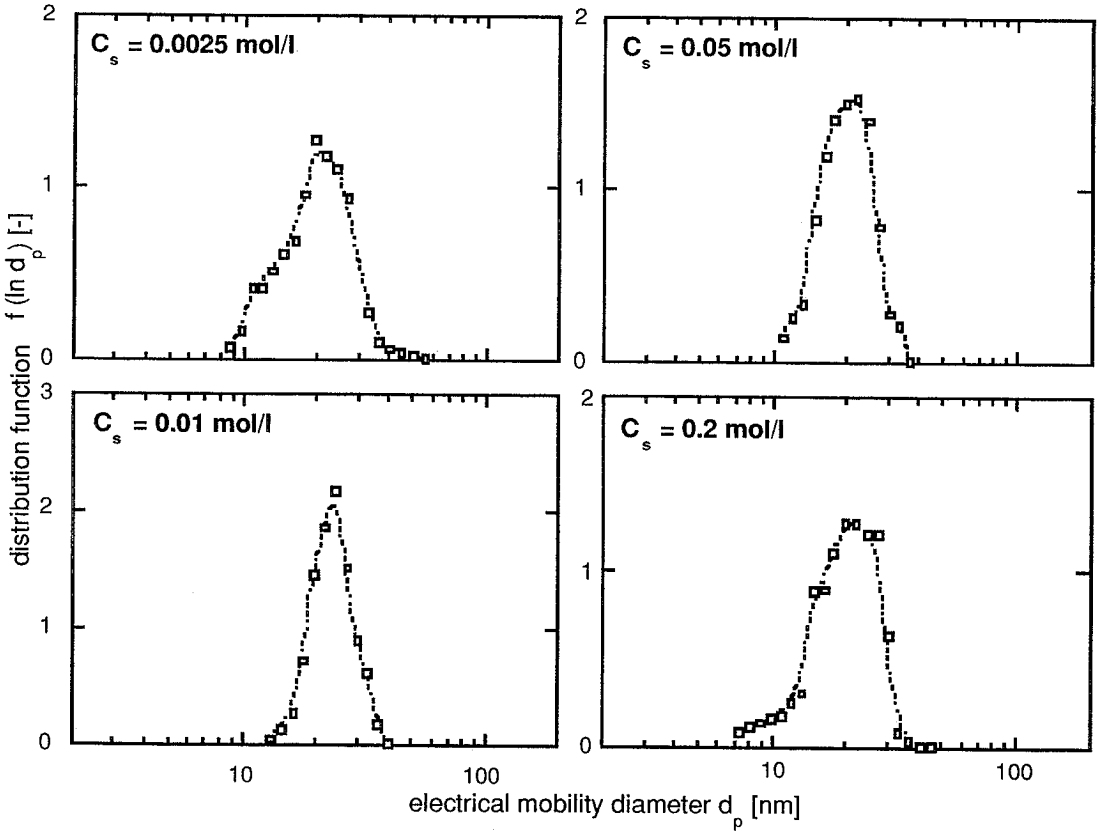

Fig.5 Variant of measured particle size ditributions as a function of solution concentration Cs in mol/l. The flow rates were set near minimum values for each Cs, sprayed used small capillary and at positive applied voltage.

3.3. Photographs of ZnS particles

ZnS particles prepared by an ultrasonic spray pyrolysis were somewhat dense and spherical and had a smooth surface (Tohge *et al.*, 1996). Figure 7 shows TEM photographs of ZnS particles prepared by using small capillary and positive polarity at solution concentration of 0.01 mol/l and the flow rate of 0.10 ml/h. The shapes of the particles were spherical, and their size distributions were similar to those of figure 5. The similar TEM photograph (not showed in this thesis) results were also obtained by varying other parameters such as capillary size, polarity of applied voltage and

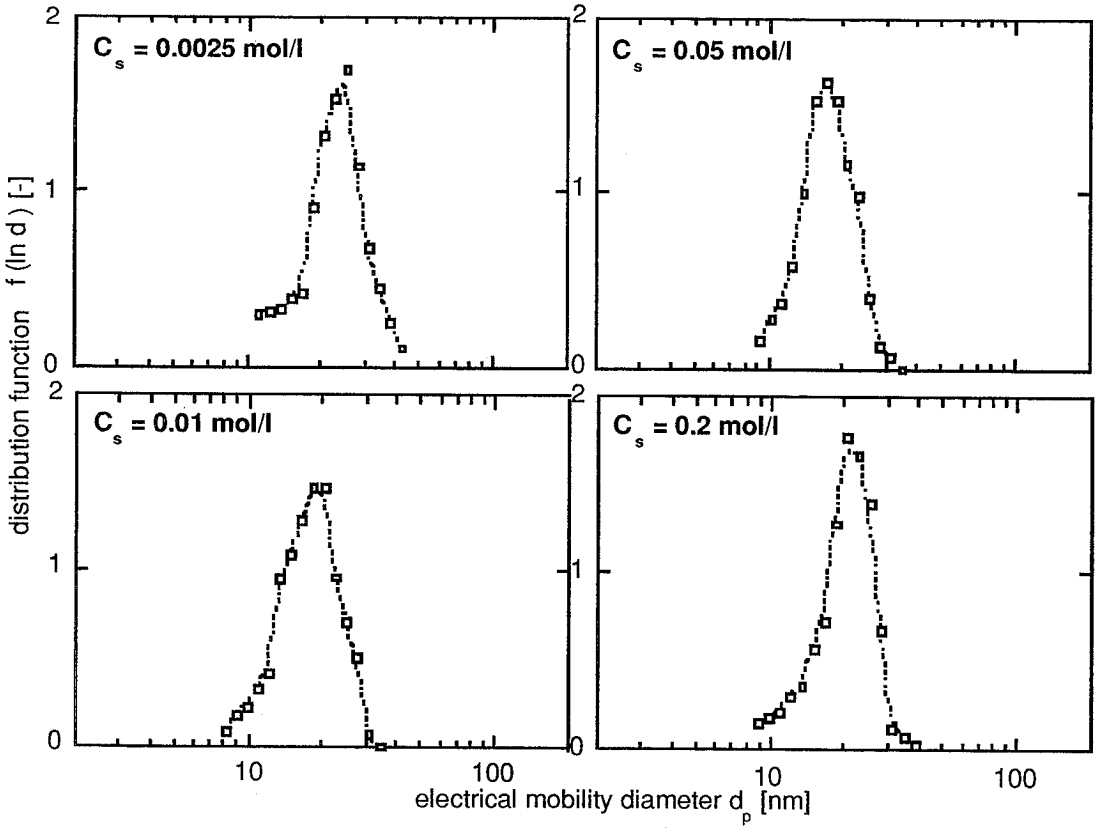

Fig.6 Variant of measured particle size ditributions as a function of solution concentration Cs in mol/l. The flow rates were set near the minimum values for each Cs. The liquid were sprayed from the small capillary and at negative voltage.

solution concentrations. In other words, the TEM photographs could verify the mobility diameter data measured by the DMA-CNC.

4 Discussion

4.1 Prediction of droplet diameter

Figure 8 shows the relation among the volume mean particle diameter d_p, the electrical conductivity of solution K, and the volume mean droplet diameter D_d as

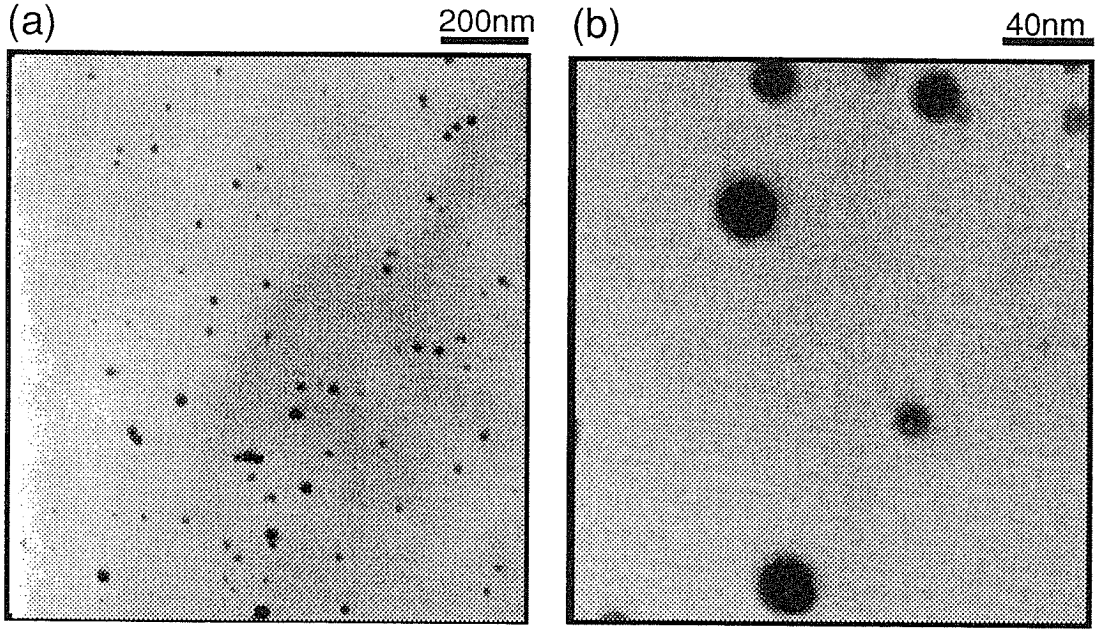

Fig.7 TEM photographs of ZnS particles prepared from Cs = 0.01 solutions over a period of 2 h. The flow rate was 0.06 ml/h. Magnification of (a) 50000 x and (b) 250000 x.

functions of solution concentration C_s. d_p was infered from the mobility diameter distributions, shown in the part in figures 4, 5, 6 that measured by the DMA-CNC at the cone-jet mode with the flow rates set near Q_{min}. The droplet diameter D_d was predicted using equation (3(a)) derived from the mass balance between the droplet and the final solid particle d_p, by assuming that one droplet changed into one dense spherical particle during the spray pyrolysis without the disruption of the droplet.

$$d_p^3 = (M D_d^3 C_s) / 1000 \rho_p \qquad (3\ a)$$

where, M and ρ_p are molecular weight and theoretical density of solid particle, and C_s is solution concentration in mol/l. For ZnS with M = 97.46 and ρ_p = 4.09 g/cm^3 equation 3 (a) can be written as:

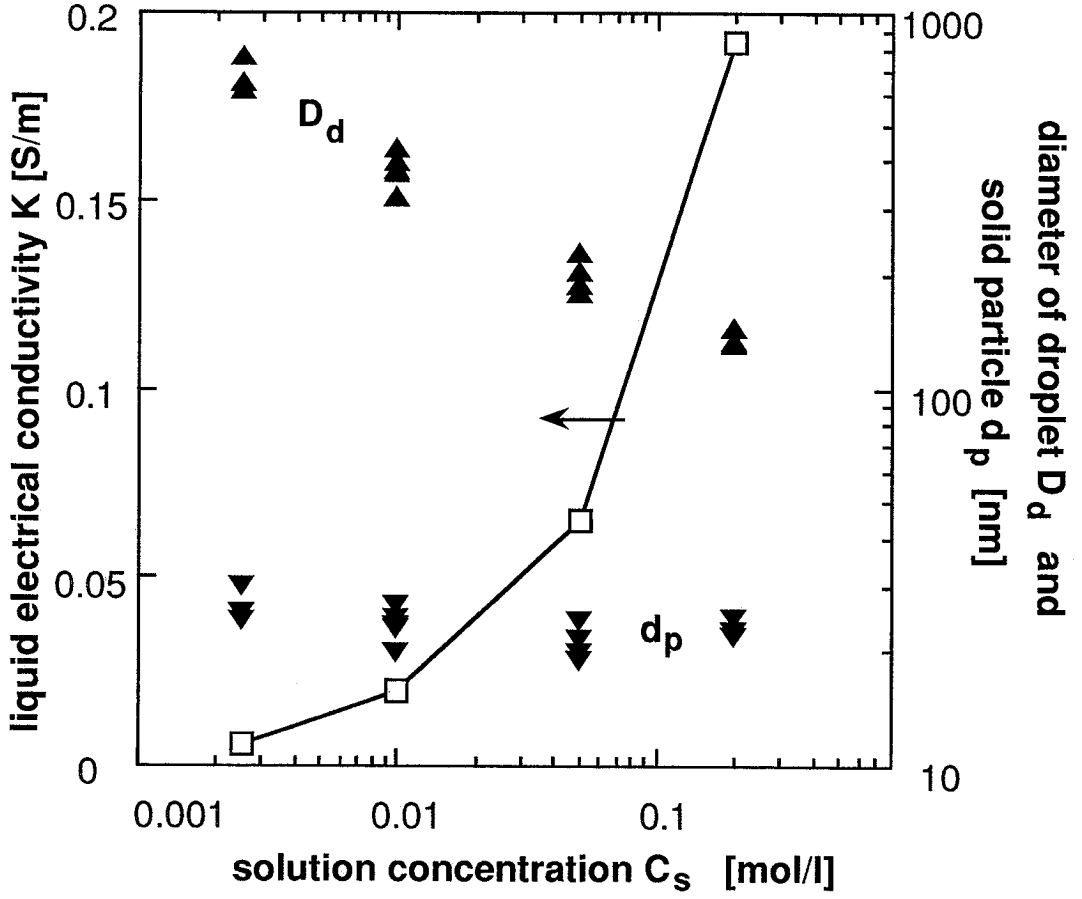

Fig.8 Measured volume mean particle diameter d_p converted from the size distribution with the predicted droplet diameter D_d as a function of the solution concentration C_s and their electrical conductivity K.

$$d_p = 0.288\, D_d\, C_s^{1/3} \qquad (3\,b)$$

Figure 8 supports the strong dependence of the droplet size on the electrical conductivity of the spray solution K. The volume mean droplet diameter D_d ranged from 140 to 580 nm, and decreased with increasing K. The increased solution concentration brought precipitated particles whose size was a larger fraction of the

droplet size, but it also brought higher K which reduces the droplet size. In this study, the overall effect made the solid particle size in a narrow range of 20 to 30 nm.

4.2 Size evaluation of droplet and particle based on scaling laws

The scaling laws based on the studies of Fernandez de la Mora and Loscertales (1994) were applied to evaluate the size of the droplets generated in our system. They reported that the droplet diameters were nearly independent of external electrostatic variables (electrode geometries and voltages), but dependent mostly of flow rate and liquid properties. When the flow rate ratio of Q / Q_{min} takes values not too large (typically smaller than 16), the droplets were generated mainly in a single size, whose initial diameter D_d^* scales with the electrical relaxation length r* of the cone jet. The following equations can be given for the case of polar liquid with electrical permitivity $e > 6$ (see also de Juan and Fernandes de la Mora, 1997) and electrical conductivity K of typically larger than 10^{-5} S/m.

$$D_d^* = G(\varepsilon)r^* \tag{4a}$$

$$r^* = (Q\varepsilon\varepsilon_o / K)^{1/3} \tag{4b}$$

where Q is the flow rate pushed through the jet and ε_o is the electrical permitivity of vacuum. The value of G depends mainly on ε, but is also influenced by the following viscosity variable (Rosell-Llompart and Fernandes de la Mora, 1994):

$$\Pi(\mu) = ((\rho\gamma^2\varepsilon\varepsilon_o / K)^{1/3}) / \mu \tag{5}$$

where g is the surface tension of the liquid. $\Pi(\mu)$ was useful to find the importance of viscous effect on the jet breakup. Particularly when dealing with the diameter of the "satellite" droplets which depend steeply on $\Pi(\mu)$ for values of this parameter below 0.06, but appear to level off above $\Pi(\mu) = 0.15$. Table 3 shows that $\Pi(\mu)$ of the present solutions ranges between 0.4 and 2.

Table 2 Values of G(ε) in previous studies.

Sources	ε	G(ε)	
Fernandez de la Mora and Loscertales (1993)	~40	0.76	*1
Rosell-Llompart and Fernandez de la Mora (1994)	20	0.68	*2
Fernandez de la Mora (1995)	80	0.60 ~ 1.10	*3
Loscertales and Fernandez de la Mora (1995)	111	0.74	*4
de Juan and Fernandez de la Mora (1997)	81	0.648	*5
	6	1.8	*6

Note:

*1 : supported by optical determination of jet diameters

*2 : based on aerodynamics measurements of droplet diameter.

*3 : D_d of water have been obtained by a phase Doppler anemometry

*4 : Formadide solution K= ~ 1 S/m, D_d has been obtained by a hypersonic impactor.

*5 : droplets of water in a wide range of K, rearranged the data of Chen et al. (1995).

*6 : Benzyl Alcohol and Dibutyl Sebacate Acid, K : 2.4 ~ 4.5 x 10^{-3} S/m.

Table 3 Properties and calculation results for the case of spraying at small capillary and positive polarity

C_s [mol/l]	Q ml/hr	d_p nm	D_d nm	η -	Π -	r* nm	D_d* nm (G=0.60)	Δ %	D_d* nm (G=0.75)	Δ %
0.0025	0.10	22.8	583.6	5.02	2.050	1021.0	612.6	4.98	765.8	31.2
0.01	0.07	21.9	353.1	7.95	1.317	592.6	355.6	0.69	444.5	25.9
0.05	0.06	23.4	220.7	13.35	0.813	380.1	228.1	3.32	285.1	29.2
0.20	0.05	23.8	141.6	21.38	0.432	249.7	149.8	5.84	187.3	32.3

Note:

D_d* is "D_d" described in equation (3), where D_d is described in equation (2).

$\Delta = 100 \times | D_d - D_d^* | / D_d$

Available data on G were compiled from the literature and were showed in table 2, while the physical and electrostatic properties of our solutions were showed in table 1. Since the electrical permitivity ε and the surface tension γ were not measured, these properties of the solutions were assumed to be equal to those of pure ethanol with γ of 0.02275 N/m and ε of 24.3. $G(\varepsilon)$ also appeared to be a constant independent of the dimensionless flow rate parameter η,

$$\eta = (\rho Q K/(\gamma \varepsilon \varepsilon_o))^{1/2} \qquad (6)$$

below a certain flow rate at which a change in the breakup pattern (Rosell-Llompart and Fernandes de la Mora, 1994). In the present prediction, considered the value of ε to be 24.3, G was assumed to be between 0.60 and 0.75. Notice, however, the values of η at the high solution concentrations C_s = 0.05 and 0.2 mol/l were calculated to be 15±2 and 24±3 as shown in table 3. These values were several times larger than those found previously for more polar liquids as reported by Fernandez de la Mora and his colleagues. Since they proposed that the first jet bifurcation where only the primary droplets generated required the flow rate near Q_{min} and corresponding roughly to the criterion η to be around 1.

Since the alcoholic solutions used were volatile, the amount of material might be evaporated from the liquid cone surface during spraying. As a result, the total flow rate of the liquid ejected from the jet (Q in equation 4) would be differed from that supplied to the spray capillary and the concentration of the solution inside the cone was changed, so the physical properties also would be changed during spraying.

For instance, table 4 also shows the calculated data obtained from the experimental conditions described in figure 5, i.e., small capillary and positive polarity. Compared with D_d which calculated from equation (3), the values of D_d* calculated by the scaling laws (equation (4)) seems agree well when $G(\varepsilon)$ was 0.60.

The experimental data in points of figures 9a and b are replotted from figure 8. The bars showed in figure 9 (a) indicated the range of D_d* when $G(\varepsilon)$ was fixed at

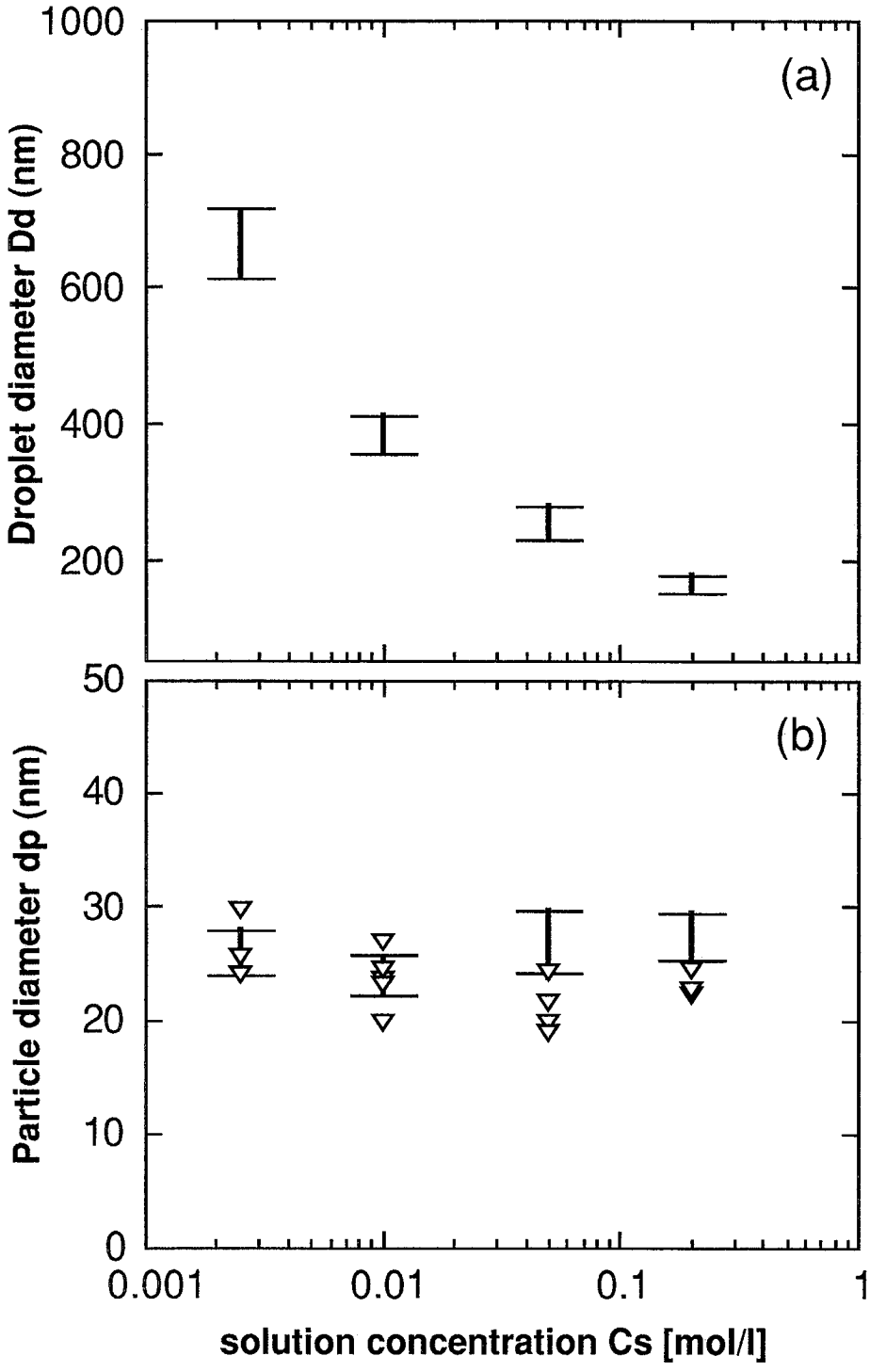
1000
800
600
400
200
50
40
30
20
10
0
(a)
(b)
Droplet diameter Dd (nm)
Particle diameter dp (nm)
0.001
0.01
0.1
1
solution concentration Cs [mol/l]

(caption of the figure depicted in the previous page)
Fig.9(a) Range of droplet diameter predicted by the scaling laws (G = 0.6) for each solution concentration Cs. (b) Range of particle diameter which converted from the droplet diameter of fig. a. The points are re-plotted from fig. 8.

0.60. D_d^* was computed at the flow rates used at a given solution concentration C_s where the other solution properties were fixed constant. The bars shown in figure 9(b) were the values of the volume mean diameter of solid particle d_p converted using equation (3) from D_d^* of figure 9(a). As shown in these figures, the scaling laws also predicted the generation of the droplet ranged from 665±50 nm for the case of C_s=0.0025 mol/l to 163±13 nm for the case of C_s=0.2 mol/l. Then the converted volume mean particle diameters were predicted to be between 20 and 30 nm. The slight overprediction found at the higher C_s is most likely due to evaporation, which makes $Q_{jet} < Q_{feed}$. Our calculation of D_d^* was based on Q_{feed}, since we have no means to measure directly the flow rate through the jet. These narrow predicted ranges also supported the size distributions obtained from the DMA-CNC and the results of TEM pictures.

On the whole, it seemed that the scaling laws are suitable for the prediction of the droplet size, mainly by adopting the value of 0.6 for G in the present condition. Especially for the case of C_s=0.0025 mol/l, the agreement was quite good and errors were below 6%. The error is $(d_{p1} - d_{p2}) / d_{p2} \times 100$, where subscripts 1 and 2 indicate the volume mean diameters of solid particles d_p predicted by the scaling laws and that obtained by the DMA-CNC, respectively. The less accuracy of the scaling laws at the higher C_s can be avoided by spraying the solution using finer capillary, since the evaporation can be minimized using smaller capillary. Although it is difficult to vary flow rate Q without significantly changing K or other physical properties at a given solution concentration, the application of the scaling laws is attractive.

In this study, only unimodal size distributions were found, probably because we operate near the minimum flow rate Q_{min}. At higher Q, a bifurcation phenomenon tends to occur, leading to bimodal particle size distributions are frequently obtained (Rosell-Llompart and Fernandez de la Mora, 1994; de Juan and Fernandez de la Mora, 1997). Another reason is the sampling loss by the deposition of the droplets onto the wall or the limitation of the efficiency of the devices. The measured size range of the DMA is 5~200 nm and the efficiency of the CNC is down to 50% at 5 nm.

We conclude that submicron solution droplets and nanometer-sized particles may be produced during the preparation of ZnS particles by electrospray pyrolysis. And it should be feasible to apply the method to the preparation of various materials.

5 Summary

The electrospray pyrolysis technique was applied to the synthesis of nanometer sized zinc sulfide particles. Electrospray could atomize a spray solution containing zinc nitrate and thiourea with ethyl alcohol as the solvent under a variety of experimental conditions such as: solution concentrations between 0.0025 and 0.2 mol/l, electrical conductivites between 10^{-4} and 10^{-1} S/m, flow rates of about 0.10 ml/h, charging polarity, and the geometry of spray capillary. The use of an α-ray radioactive source with bipolar ions to neutralize the highly charged droplet could greatly improve the throughput efficiency of the generated particles. The preparation of nanometer-sized spherical ZnS particles was presented and verified by the results obtained from the DMA-CNC system and TEM photographs. The dependence of the size of the droplets or particles on the physical properties of the spray solution was studied. Generation of submicron droplets and the converted solid particles having diameter between 20 to 40 nm, were indicated by the prediction using scaling laws.

6 References

Adachi, M., Okuyama, K., Kousaka, Y., Moon, S. W. and Seinfeld, J. H. (1990) *Aerosol Sci. Tech.*, 12, 225.

Aguirre-de-Carcer, I. and Fernandez de la Mora, J. (1995) *J. Colloid Interface Sci.*, 171, 512

Benassayag, G., Sudraud, P. and Jouffrey, B. (1985) *Ultramicroscopy*, 16, 1.

Bollini, R., Sample, S. B., Seigal, S. D. and Boarman, J. W. (1975) *J. Colloid Interface Sci.*, 51, 272.

Chen, D. R., Pui, D. Y. H. and Kaufman, S. L. (1995) *J. Aerosol Sci.*, 26, 963.

Cloupeau, M. and Prunet-Foch, B. (1989) *J. Electrostatics*, 22, 135.

Cloupeau, M. and Prunet-Foch, B. (1990) *J. Electrostatics*, 25, 165.

Cloupeau, M. and Prunet-Foch, B. (1994) *J. Aerosol Sci.*, 25, 1021.

Cloupeau, M. (1994) *J. Aerosol Sci.*, 25, 1143.

de Juan, L. and Fernandez de la Mora, J. (1997) *J. Colloid Interface Sci.*, 186, 280.

Fenn, J. B., Mann, M., Meng, C. K., Wong, S. F. and Whitehouse, C. M. (1989) *Science*, 246, 64.

Fernandez de la Mora, J. and Loscertales, I. G. (1994) *J. Fluid Mech.*, 260, 155.

Ganan-Calvo, A. M., Davila, J. and Barrero, A. (1997) *J. Aerosol Sci.*, 28, 249.

Gurav, A., Kodas, T., Pluym, T. and Xiong, Y. (1993) *Aerosol Sci. Tech.*, 19, 411.

Jones, A. R. and Thong, K. C. (1971) *J. Phys. D: Appl. Phys.* 4, 1159.

Levi, C. G., Jayaram, V., Valencia, J. J. and Mehrabian, R. (1988) *J. Mater. Res.*, 3, 969.

Mahoney, J. F., Taylor S. and Perel, J. (1987) *IEEE Trans. Ind. Appl.*, IA-23, 197.

Meesters, G. M. H., Vercoulen, P. H. W., Marijnissen, J. C. M. and Scarlett, B. (1992) *J. Aerosol Sci.*, 23, 37.

Meshing, G. L., Zhang, S.C. and Jayanthi, G. (1993) *J. Am. Ceram. Soc.*, 76, 2707

Okuyama, K., Lenggoro, I. W., Tagami, N., Tamaki, S. and Tohge, N. (1996) *J.*

Soc. Powder Technol., Jpn., 33, 192.

Okuyama, K., Lenggoro, I. W., Tagami, N., Tamaki, S. and Tohge, N. (1997) *J. Mater. Sci.*, 32 , 1229.

Park, D. G. and Burlitch, J. M. (1992) *Chem. Mater.*, 4, 500.

Rosell-Llompart, J. and Fernandes de la Mora, J. (1994) *J. Aerosol Sci.*, 25, 1093.

Rulison, A.J. and Flagan, R.C. (1994a) *J. Amer. Ceram. Soc.*, 77, 3244.

Rulison, A.J. and Flagan, R.C. (1994b) *J. Colloid Interface Sci.*, 167, 135.

Slamovich, E. B. and Lange, F. F. (1990) *J. Am. Ceram. Soc.*, 73, 3368.

Smith, D. P. H. (1986) *IEEE Trans. Ind. Appl.*, IA-22, 527.

Tamaki, S., Tohge, N. and Okuyama, K. (1995) *J. Mater. Sci. Lett.*, 14, 1388.

Tamaki, S., Tohge, N., Tagami, K. and Okuyama, K. (1996) *J. Ceramic Soc. Japan*, 104, 137.

Tang, K. and Gomez, A. (1994) *J. Aerosol Sci.*, 25, 1237.

Tang, K. and Gomez, A. (1996) *J. Colloid Interface Sci.*, 184, 500.

Taylor, G. I. (1964) *Proc. Roy. Soc. London*, A280, 383.

Tohge, N., Tamaki, S. and Okuyama, K. (1995) *Jpn. J. Appl. Phys.*, 34-2, L207.

Lewis, K. C., Dohmeler, D. M., Jorgensen, J. W., Kaufman, S. L., Zarrin, F. and Dorman, F. D. (1994) *Anal. Chem.*, 66, 2285.

Zeleny, J. (1915) *Proc. Camb. Phil. Soc.*, 18, 71.